Archive

LWR FUEL PERFORMANCE ANALYSIS
Fuel Cracking and Relocation

by
J.T. Maki and J.E. Meyer

Energy Laboratory Report No: MIT-EL 78-038

October, 1978

LWR FUEL PERFORMANCE ANALYSIS

Fuel Cracking and Relocation

by

J.T. Maki and J.E. Meyer

Energy Laboratory
and
Department of Nuclear Engineering

Massachusetts Institute of Technology
Cambridge, Massachusetts 02139

Final Report for Research Project

sponsored by

Northeast Utilities Service Co.
Yankee Atomic Electric Co.

under the
MIT Energy Laboratory Electric Utility Program

Energy Laboratory Report No. MIT-EL 78-038

October, 1978

TABLE OF CONTENTS

LIST OF FIGURES

SUMMARY

It is expected that virtually all fuel pellets in a pressurized water reactor (PWR) are cracked during power operation. This report provides quantitative estimates of the thermal effects of cracking for a case of interest (relatively new fuel in the Maine Yankee Reactor). The method to account for cracking has been previously developed by others.

Results show that it is important to account for cracking. The equivalent temperature that represents heat stored in a fuel rod operating at 40 kW/m is 892°C for the cracked pellet versus 1016°C for a no-crack calculation, a decrease of 124 K.

Methods used in this study were designed to isolate cracking as a single effect for a representative case. The method used for obtaining fuel rod outside surface temperature as a function of linear heat generation rate for this representative case is felt to be especially suited for use in this and other isolated effect studies.

1. INTRODUCTION

1.1 Objective

During normal power changes in light water reactors, thermal stresses within the fuel rod cause the uranium dioxide fuel pellets to crack. Associated with cracking is relocation, defined as the geometry changes of the fuel pellet by displacement of the cracked pieces. Pellet cracking and relocation has several important mechanical and thermal consequences. This report primarily gives a quantitative comparison of those thermal effects for cracked and uncracked fuel pellets at the beginning of life. Even though all ceramic fuel pellets crack, calculations for uncracked pellets permit making esimates of the cracking contribution to fuel behavior. The estimates can also be used to indicate the nature of errors in fuel rod modeling codes in which the cracking/relocation effects are neglected.

1.2 Cracking Scenario

During the first rise to power, a temperature gradient within the fuel rod causes the center of the pellet to expand more than the cooler periphery. Thermo-elastic deformation proceeds until the fracture stress of the pellet is exceeded. For typical light water reactors, the fracture stress of the fuel is reached at a linear heat generation rate of about 5 kW/m. Once the fracture stress is exceeded, sudden jumping of the pellet pieces occurs upon cracking (Ref. 1). With increasing power, further relocation results from thermo-elastic deformation of each cracked pellet piece. If cladding contact is made, the crack void in the bulk of the fuel is under compressive forces and accommodates some fraction of the pellet thermal expansion. After the crack void is consumed, radial expansion is approximately equal to the free thermal expansion of the pellet.

1.3 Crack Patterns

Photomacrographs display distinctive crack patterns that seem different for fast than for thermal reactor fuel (Refs. 2 and 3). After cooldown, fast reactor fuel exhibits radial cracking from the central void to the periphery. Light water power reactor fuel displays an

irregular crack pattern. It is apparent, therefore, that findings concerning cracking from fast reactor research may not be applicable for light water power reactor cases (see also Sec. 1.7).

1.4 Major Thermal Effects of Cracking

Due to nonperfect radial cracking, the fuel to cladding gap width will be circumferentially nonuniform. The gap width may vary between that calculated for a non-cracked operating fuel rod and essentially zero. Relocation of the pellet pieces into the gap causes improved heat transfer between fuel and cladding. The effective fuel to cladding gap conductance corresponds to a value reflecting both contact and open gap conductance. However, cracking also causes fuel to fuel gaps to open within the fuel pellet. Some of these gaps are oriented so as to degrade heat conduction, counteracting at least some of the effect of improved heat transfer at the pellet surface. Estimates of the magnitude of change resulting from both these effects are given later in this report.

1.5 Effects of Cracking on Fission Gas Release

One possible mode of fission gas release concerns gases formed in the columnar grain growth region of the pellet. Such gases diffuse to the center of the pellet and are contained under pressure by the plastic central region. When the fuel is cooled, thermal stresses crack the pellet and the gas is released (Ref. 4). Another postulated mechanism is that gas is released from all free surfaces of the fuel pellet. When pellet cracking occurs, the free surface area increases by an order of magnitude. Thus, pellet cracking apparently plays a significant role in fission gas release (Ref. 5). At least at the time of preparation of the MATPRO Version 09 report, the state-of-the-art was represented by quoting an Argonne National Laboratory quarterly report and indicating that the effects of fuel cracking on gas release are not well documented (Ref. 6, p. 146). Such effects will be omitted from the remainder of this report as well.

1.6 Major Mechanical Effects of Cracking

There have been a number of fuel rod failures by clad cracking during plant up-power maneuvers. It is thought that physical features, which characterize such failures, include:

- as the power level is increased, the thermal expansion of the fuel pellet is larger than the expansion of the clad;
- if the fuel/clad gap is nearly closed at the start of the maneuver, then contact forces between pellet and clad can develop as the power is increased (pellet-clad mechanical interaction, PCMI);
- fission products from the pellet (such as iodine and/or cesium), possibly freshly released, are available for chemical attack on the clad (pellet-clad chemical interaction, PCCI);
- the combined effect of clad stresses from PCMI and local corrosive action from PCCI can lead to clad failure from stress corrosion cracking (SCC); and
- SSC failures require the action of both a corrosive environment and a sufficiently high stress for a sufficiently long period of time.

If the reactor is brought to power very slowly, it is thought that PCMI forces are reduced. This action is called "conditioning" the fuel. Existing fuel vendor conditioning recommendations can mandate power ascensions as long as one or two days (rather than few hour startups that could otherwise be employed). High costs of power to replace that lost during the long startups and load dispatching plant readiness considerations emphasize the importance of eliminating overconservatisms in the conditioning recommendations.

Fuel cracking and relocation can influence the SCC situation in several ways. Edges of broken pieces which contact the clad can provide locations for highly concentrated PCMI forces to act (and perhaps also to break protective clad oxide layers). The cracks themselves may act as routes by which fission products can reach the clad. Finally, the broken pieces of the fuel may not fit together easily during the pellet compaction caused by the PCMI forces. But the compaction could be accomplished by smaller PCMI forces if very local creep deformations of the fuel occur. Thus the time dependent compaction of cracked and

relocated fuel could play a role in fuel pellet conditioning. Time dependent compaction information is not now available. It has also been omitted from the present study.

1.7 Crack Healing

During steady state reactor operation, healing* of cracks may occur simultaneously with grain growth if the pellet exceeds 1400°C (approximately the onset of equiaxed grain growth) (Refs. 7,8,9 and 10). Typical light water reactor fuel rarely exceeds this temperature and thus, healing essentially does not occur. Fast reactor fuel often exceeds 1700°C (the onset of columnar grain growth) whereby extensive healing occurs. Healing and columnar grain formations contribute to the crack pattern differences noted in Sec. 1.3.

* Healing is used to describe a re-establishment of solid material where previously a cracked surface existed. The local creep deformation of Sec. 1.6, on the other hand, could occur with a change in shape which does not affect the existence of the cracked surface.

2. THERMAL CALCULATIONS NOT DEPENDENT ON CRACKING

The computational procedures used in the comparative study of cracked/uncracked fuel pellets are presented in this and the next two chapters. This chapter deals with thermal calculations needed for both cracked and uncracked fuel pellets.

2.1 Outline of Computer Calculations

Before describing the cracked and uncracked fuel model calculations in detail, an overview of the computational method is presented. Serving as a general outline for this and the following two chapters, Figure 2-1 presents a simplified flow chart of the computer program developed for this study.

The computer program is initialized by reading in the input data whereby the cladding temperature profile, thermal strain, and stored heat are computed. Not evident by the diagram is that a branch exists after the cladding stored heat calculation is made. Each model (cracked/uncracked) has its own computational procedure for the fuel pellet temperature profile calculations and fuel stored heat calculation. Regardless of model, however, an iterative process for computing the fuel pellet temperature profile is utilized. An initial guess of the gap width (the cold gap width) is made whereby the pellet temperatures are calculated, followed by the fuel thermal strain calculation which gives the new hot gap width. The above procedure is repeated until the hot gap converges within 0.05 μm where the iterative process is stopped. Following this, each model undergoes the same fuel rod equivalent temperature calculation.

2.2 Cladding Temperature Profile

Beginning with the steady-state heat conduction equation

$$-\nabla(k_c \nabla T) = q''' \tag{2-1}$$

where q''' = rate of heat deposition per unit volume;
k_c = cladding thermal conductivity; and
T = temperature,

a relation for the cladding temperature profile may be derived.

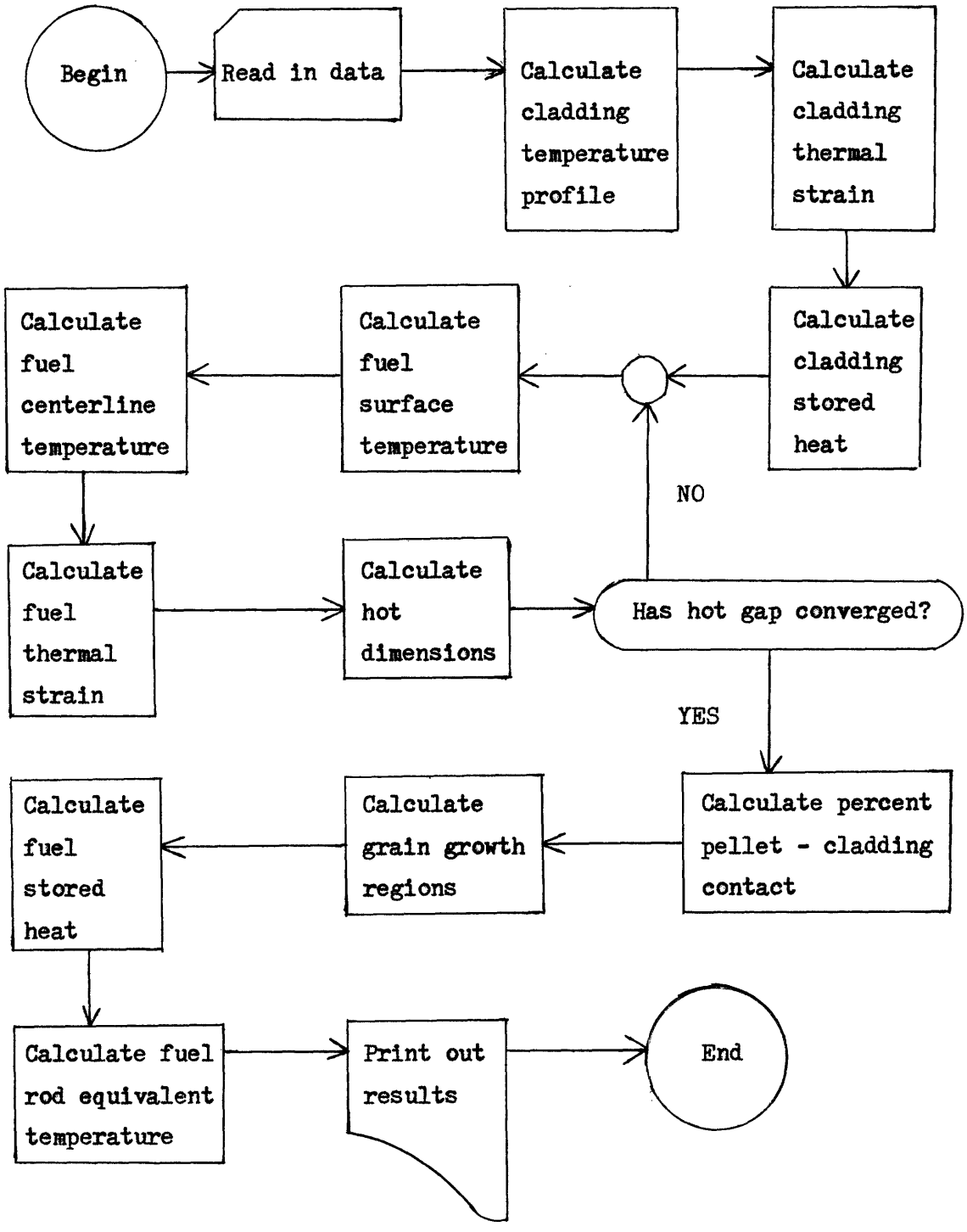

Figure 2-1. Flow chart for comparative study computer program.

If internal heat deposition in the clad is neglected, Eq. (2-1) may be manipulated to give

$$\int_{T}^{T_o} k_c dT = \frac{-q'}{2\pi} \ln\left(\frac{r_o}{r}\right) \qquad (2\text{-}2)$$

where T_o = outside cladding temperature;

r_o = outside radius of cladding;

T = temperature at radius r;

and q' = linear heat generation rate (LHGR) of the fuel rod.

With a relation for the thermal conductivity of Zircaloy-4 given in Appendix B, the left side of Eq. (2-2) is evaluated to yield a second order expression in temperature. Solving the quadratic equation gives

$$T(r) = -1.015\text{x}10^{5} \{ 1.3959\text{x}10^{-2} - [1.9485\text{x}10^{-4} + 1.9704\text{x}10^{-5}(1.3959\text{x}10^{-2}T_o + 4.9261\text{x}10^{-6}T_o^{\,2} + \frac{q'}{2\pi} \ln\left(\frac{r_o}{r}\right))]^{\frac{1}{2}} \} \qquad (2\text{-}3)$$

where

$T(r)$ = temperature of cladding at radius r in °C;

T_o = outside cladding temperature in °C;

and

q' = LHGR in kW/m.

2.3 Cladding Thermal Strain

The average cladding thermal strain is calculated from the equation

$$\bar{\varepsilon}_c = \frac{2}{r_o^2 - r_1^2} \int_{r_1}^{r_o} (\varepsilon_T)_c \, r \, dr \qquad (2\text{-}4)$$

where $\bar{\varepsilon}_c$ = average cladding thermal strain;

$(\varepsilon_T)_c$ = cladding thermal strain at radius r (given in Appendix B);

r_1 = hot inside cladding radius;

and r_o = hot outside cladding radius.

To perform the above integration, the trapezoidal rule is employed, using twenty five equally spaced mesh intervals of size M where

$$M = \frac{r_o - r_1}{25} \quad . \tag{2-5}$$

The calculation of the average thermal strain requires hot dimensions which are determined by

$$r_{hot} = r_{cold}(1 + \bar{\varepsilon}_c) \quad . \tag{2-6}$$

Since the hot dimensions and the average thermal strain are dependent upon one another, an iterative approach is taken in which the hot inside cladding radius converges within 0.5 μm.

2.4 Cladding Stored Heat

The cladding stored heat is defined by the equation*

$$SH_c = \int_{r_1}^{r_o} \Delta H_c \rho_c 2\pi r \, dr \tag{2-7}$$

* Note that either cold dimensions and cold density or hot dimensions and hot local density should be employed in this calculation. However, the temperature profiles utilized in the computation are based upon hot dimensions. Therefore hot dimensions are combined, for simplicity, with cold density in Eqs. (2-7) and (2-9). It is felt that only slight error arises from this practice.

where SH_c = cladding stored heat;

ρ_c = density of Zircaloy-4 = 6550 kg/m^3

and ΔH_c = enthalpy change of cladding at radius r (given in Appendix B).

Utilizing the trapezoidal method with 25 trapezoids, an explicit solution to Eq. (2-7) is obtained. The value for the stored heat is used in the equivalent fuel rod temperature calculation.

2.5 Fuel Thermal Strain

The average fuel thermal strain calculation is similar to that for the cladding thermal strain. For the fuel pellet

$$\bar{\varepsilon}_f = \frac{2}{r_2^2} \int_o^{r_2} (\varepsilon_T)_f \, r \, dr \qquad (2\text{-}8)$$

where $\bar{\varepsilon}_f$ = average fuel thermal strain;

$(\varepsilon_T)_f$ = fuel thermal strain at radius r (given in Appendix B);

and r_2 = hot fuel pellet radius.

Fifty equally spaced mesh intervals are employed in the trapezoidal method to solve the above integral. The fuel thermal strain is determined for each iteration of the fuel temperature profile calculation until hot gap width convergence is reached.

2.6 Fuel Stored Heat

The fuel stored heat calculation is also similar to that for the cladding.* For the fuel

$$SH_f = \int_o^{r_2} \Delta H_f \, D\rho_f \, 2\pi r \, dr \qquad (2\text{-}9)$$

* See footnote accompanying Eq. (2-7).

where SH_f = fuel stored heat;
D = fractional theoretical density
ρ_f = fuel density = 10 980 kg/m^3
r_2 = hot fuel pellet radius
and ΔH_f = enthalpy change of fuel at radius r (given in Appendix B).

Again, fifty trapezoids are used to numerically solve this integral.

2.7 Fuel Rod Equivalent Temperature

The actual stored heat of a fuel rod may be equated to the stored heat if the rod were at some constant temperature. That constant temperature may then be defined as the fuel rod equivalent temperature, T_{eq}. In physical terms, T_{eq} is the temperature that would be reached by the fuel rod if all internal heating and external cooling were instantaneously stopped. In mathematical terms

$$SH_f + SH_c = (SH_f)_{eq} + (SH_c)_{eq} \tag{2-10}$$

At constant temperature, the stored heat equations become

$$(SH_f)_{eq} = D\rho_f \, \Delta H_f(T_{eq}) \, \pi r_2^2 \tag{2-11}$$

$$(SH_c)_{eq} = \rho_c \, \Delta H_c(T_{eq}) \, \pi(r_o^2 - r_1^2) \tag{2-12}$$

It should be noted that the stored heat from the fill gas has been deleted from consideration because it is insignificant compared to that of the fuel and cladding. Rearranging Eq. (2-10),

$$f(T_{eq}) = (SH_f)_{eq} + (SH_c)_{eq} - SH_f - SH_c = 0 \tag{2-13}$$

where T_{eq} = fuel rod equivalent temperature, as yet unknown.

The root of Eq. (2-13), T_{eq}, may be found by using Newton's method of slope intercept. The slope intercept is determined by

$$T_I = T_s - \frac{f(T_s)}{f'(T_s)} \tag{2-14}$$

where T_I = slope intercept temperature;

T_s = temperature where the slope is evaluated;

$f(T_s)$ = value of the function f at T_s;

$f'(T_s)$ = the derivative of the function f, evaluated at T_s;

and where the derivative of the function f is

$$f'(T) = D\ \rho_f (C_p(T))_f\ \pi r_2^2 + \rho_c (C_p(T))_c\ \pi (r_o^2 - r_1^2) \tag{2-15}$$

where $(C_p)_f$ = constant pressure specific heat capacity of UO_2 (given in Appendix B)

and $(C_p)_c$ = constant pressure specific heat capacity of the cladding (given in Appendix B).

Beginning with an initial guess for T_s (fuel pellet surface temperature), T_I is calculated by Eq. (2-14) and replaces T_s for another calculation. Through this successive iteration, the fuel rod equivalent temperature is determined when T_I converges upon itself within 0.05°C where

$$T_{eq} = T_I \quad .$$

3. THERMAL CALCULATIONS FOR UNCRACKED FUEL PELLETS

This chapter contains the computational methods used for uncracked UO_2 pellets employed in the comparative thermal effects study.

3.1 Pellet Surface Temperature and Gap Conductance

Solving the steady-state heat conduction equation for the gap yields an equation for the pellet surface temperature

$$T_2 = T_1 + \frac{q'}{2\pi r_2 h_g} \tag{3-1}$$

where T_2 = pellet surface temperature

T_1 = inside cladding temperature

q' = LHGR

r_2 = hot fuel pellet radius

and h_g = gap conductance.

The gap conductance is determined by

$$h_g = \frac{k_g}{\delta+\delta'} \tag{3-2}$$

where k_g = thermal conductivity of fill gas (100% helium given in Appendix B);

δ = hot radial gap width;

and δ' = root mean square cladding-fuel surface roughness.

3.2 Pellet Temperature Profile

The fuel temperature profile (based on constant volumetric heat deposition rate) is calculated from the following equation

$$\int_o^T k\,dT = \int_o^{T_2} k\,dT + \frac{1}{PF}\left\{\frac{q'}{4\pi}\left[1 - \left(\frac{r}{r_2}\right)^2\right]\right\} \tag{3-3}$$

where $\int_o^T k\,dT$ = conductivity integral for 95% theoretical density fuel (given in Appendix B);

PF = porosity factor (given in Appendix B);

and T = temperature at radius r.

The temperature of the fuel pellet at radius r may be determined by equating the value of the conductivity integral (a function of r) to its corresponding temperature. This is accomplished by fitting second order equations to the conductivity integral. The pellet temperature profile is then computed from equations of the form:

$$T(r) = A + Bx + Cx^2 \qquad (3\text{-}4)$$

where $x = \int_o^T k\,dT$ in kW/m

and A, B, C = constants.

The constants A, B, and C are presented in Table 3-1. The accuracy of the above fit to the conductivity integral for $250 \leq T \leq 2800°C$ is ±0.4°C. This error is deemed insignificant compared to the overall assumptions made in the study.

Table 3-1

Constants for Temperature of Conductivity Integral Equation (Eq. 3-4)

Range	A	B	C
$T \leq 585°C$ ($x \leq 3.441$)	26.68	72.42	26.08
$585 < T \leq 1000°C$ ($3.441 < x \leq 4.814$)	126.7	12.82	35.01
$1000 < T \leq 1405°C$ ($4.814 < x \leq 5.866$)	40.26	46.48	31.75
$1405 < T \leq 1800°C$ ($5.866 < x \leq 6.783$)	-630.9	274.13	12.43
$1800 < T \leq 2205°C$ ($6.783 < x \leq 7.723$)	-1750.15	604.12	-11.91
$T \geq 2205°C$ ($x \geq 7.723$)	-2589.9	822.27	-26.08

4. THERMAL CALCULATIONS FOR CRACKED FUEL PELLETS

This chapter deals with the computational methods used for cracked pellet thermal effects.

4.1 Pellet Surface Temperature and Gap Conductance

As in Section 3, the pellet surface temperature may be determined by

$$T_2 = T_1 + \frac{q'}{2\pi r_2 h_g} \quad , \tag{4-1}$$

However, the gap conductance for a cracked fuel pellet takes the form (Ref. 11)

$$h_g = (1-F)h_o + F\, h_c \tag{4-2}$$

where h_o = zero contact pressure conductance = $\frac{k_g}{\delta+\delta'}$;

h_c = contact conductance = $\frac{k_g}{\delta'}$;

k_g = thermal conductivity of fill gas (given in Appendix B);

and F = fraction of pellet circumference lying against the cladding.

Two models for the fraction of circumferential cracked pellet contact were investigated. The Kjaerheim & Rolstad model (Ref. 12) may be expressed as

$$F = 0.3 + 0.7[0.2]^{(50\ \delta/r_2)} \tag{4-3}$$

where δ = hot radial gap width in mm;

and r_2 = hot fuel pellet radius in mm.

The FRAP-S model is given below for fuels with burnups less than 0.6 MWd/kgU (Ref. 11).

$$F = 0.3 + [100(\frac{100\delta}{r_2})^4 + 1.429]^{-1} \tag{4-4}$$

and for burnups greater than 0.6 MWd/kgU

$$F = 0.3 + [A(\frac{100\delta}{r_2})^B + 1.429]^{-1} \quad (4\text{-}5)$$

where $A = 100\text{-}98\ F_b$;

$B = 4\text{-}0.5\ F_b$;

$F_b = 1\text{-}[(x\text{-}0.6)^4 + 1]^{-1}$;

and x = burnup in MWd/kgU.

It should be noted that the burnup factor F_b, and thus, the fraction of pellet-clad contact, F, reaches an asymptotic limit near 10 MWd/kgU burnup.

Figure 4-1 presents the Kjaerheim & Rolstad model and the FRAP-S model for burnups under 0.6 MWd/kgU and for 10 MWD/kgU. Only at larger ratios of δ/r_2 does the Kjaerheim & Rolstad model predict a larger fraction of pellet contact than the FRAP-S model (regardless of burnup). With increasing burnup, the FRAP-S model predicts a larger fraction of pellet contact for all ratios of δ/r_2. Due to the accumulation of gaseous fission products at the grain boundaries in the fuel, the fuel pellet tends to crack more and thus causes greater contact with the cladding.

Noting that the FRAP-S model is more conservative in the usual operating range of δ/r_2 than the Kjaerheim & Rolstad model, and that the FRAP-S model is capable of including burnup considerations, the FRAP-S model was chosen for incorporation into the study.

4.2 Pellet Temperature Profile

The cracked fuel pellet temperature profile is calculated from the steady state heat conduction equation

$$-\nabla(k\nabla T) = q''' \quad (4\text{-}6)$$

which can be put into the form

$$\frac{dT}{dr} = \frac{-q'r}{2\pi r_2^2 k} \quad . \quad (4\text{-}7)$$

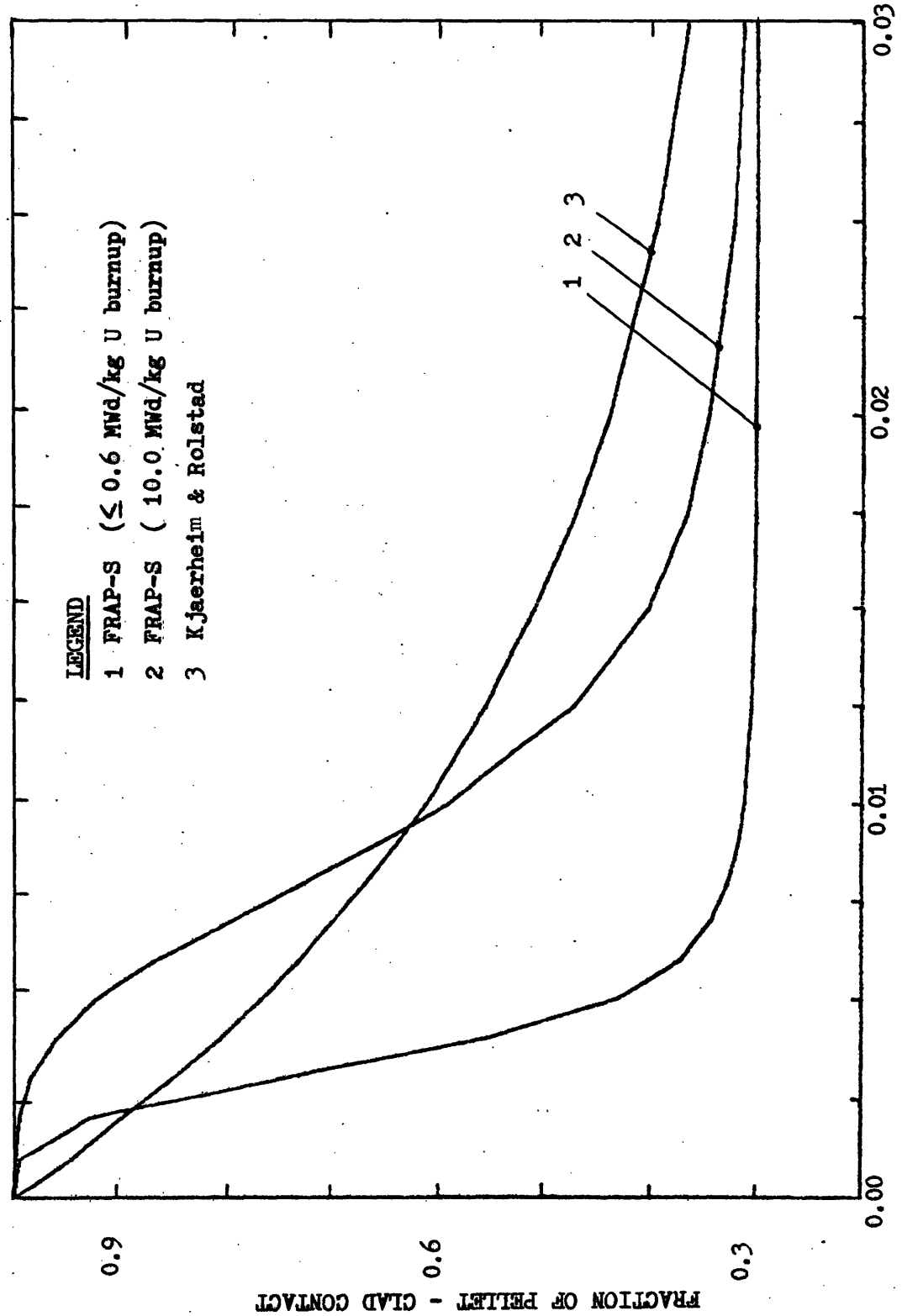

Figure 4-1. Comparison of circumferential pellet - clad contact models.

Using a finite difference method

$$\frac{dT}{dr} = \frac{T(r_n) - T(r_n - \Delta r)}{\Delta r} \quad , \tag{4-8}$$

Eq. (4-7) is rearranged to

$$T_{n+1} = T_n + \frac{q' r_n \Delta r}{2\pi r_2^2 (k_f)_n} \tag{4-9}$$

where T_n = fuel pellet temperature at radius r_n;

n = index with range $2 \leq n \leq 52$;

$\Delta r = r_2/50$ = radial increment;

q' = LHGR;

and $(k_f)_n = UO_2$ thermal conductivity at radius r_n.

Beginning at the surface of the pellet, the temperature at the first radial increment is computed using a temperature T_2 obtained from gap calculations. Equation (4-9) is then used successively to step toward the center of the pellet and obtain the temperature profile of the fuel.

The cracked pellet temperature profile is calculated in 50 radial increments. Comparison of uncracked pellet centerline temperatures calculated from the conductivity integral and from the finite difference equation (also using 50 radial increments) displayed a maximum deviation of 0.1°C. From these calculations it can be assumed that 50 increments would produce sufficient accuracy for the cracked pellet temperature calculations.

To account for the reduction in heat transfer due to cracks in the fuel, an effective UO_2 thermal conductivity is employed in Eq. (4-9). The effective UO_2 thermal conductivity is (Ref. 12)

$$k_e = k_f \left[\frac{\delta \cdot 10^{-3} - 3.175 \times 10^{-2}}{r_2 (0.077 \frac{k_g}{k_f} + 0.015)} + 1 \right]^{-1} \tag{4-10}$$

where k_f - UO_2 thermal conductivity (given in Appendix B);

k_g = fill gas conductivity (given in Appendix B);

δ = hot radial gap width in μm;

and r_2 = hot fuel pellet radius in mm.

5. ILLUSTRATIVE EXAMPLE

This chapter presents the results of the computer calculations for cracked/uncracked fuel pellets with a nominal cold radial gap width of 95 μm. This and other dimensions are based on the nominal fuel rod dimensions for the Maine Yankee reactor (see also Appendix C). Calculations were also made for initial radial gap widths of 75 and 115 μm and are presented in Appendix A. The 75 and 115 μm radial gap widths are estimates which correspond to the extreme tolerances expected in the determination of the nominal gap width (Ref. 13).

Note that the calculations of this chapter have been performed for linear heat generation rates (LHGR) between zero and 60 kW/m. The local peak LHGR for Maine Yankee is 35.8 kW/m. In addition, occurrences such as columnar grain growth and central hole formation occur when temperatures rise above ∿1700°C. Therefore, portions of the plots above approximately 40 kW/m should be regarded as mathematical extrapolations from the lower LHGR results. These portions are included for the purposes of illustrating how the calculations behave, but may be significantly in error because of the neglect of some significant high temperature phenomena.

5.1 Fuel Pellet Surface Temperature

Figure 5-1 shows the fuel surface temperature as a function of LHGR for a cracked and uncracked pellet. The uncracked pellet consistently shows a higher temperature than the cracked pellet with a maximum difference of about 210°C at 40 kW/m. This effect is due to the fact that the cracked pellet relocates into the gap, resulting in improved gap conductance and a lower fuel surface temperature.

The uncracked fuel surface temperature decreases with increasing LHGR above 45 kW/m. Beyond this LHGR, the pellet core becomes hotter where thermal strains expand the pellet into the gap and improved gap conductance results in a lower surface temperature. Within 60 kW/m, the cracked fuel pellet does not exhibit this effect.

The surface temperature for uncracked fuel displays a concave downward function of LHGR, while the cracked pellet displays a nearly linear function. For both cases, a kink exists at 25 kW/m in the

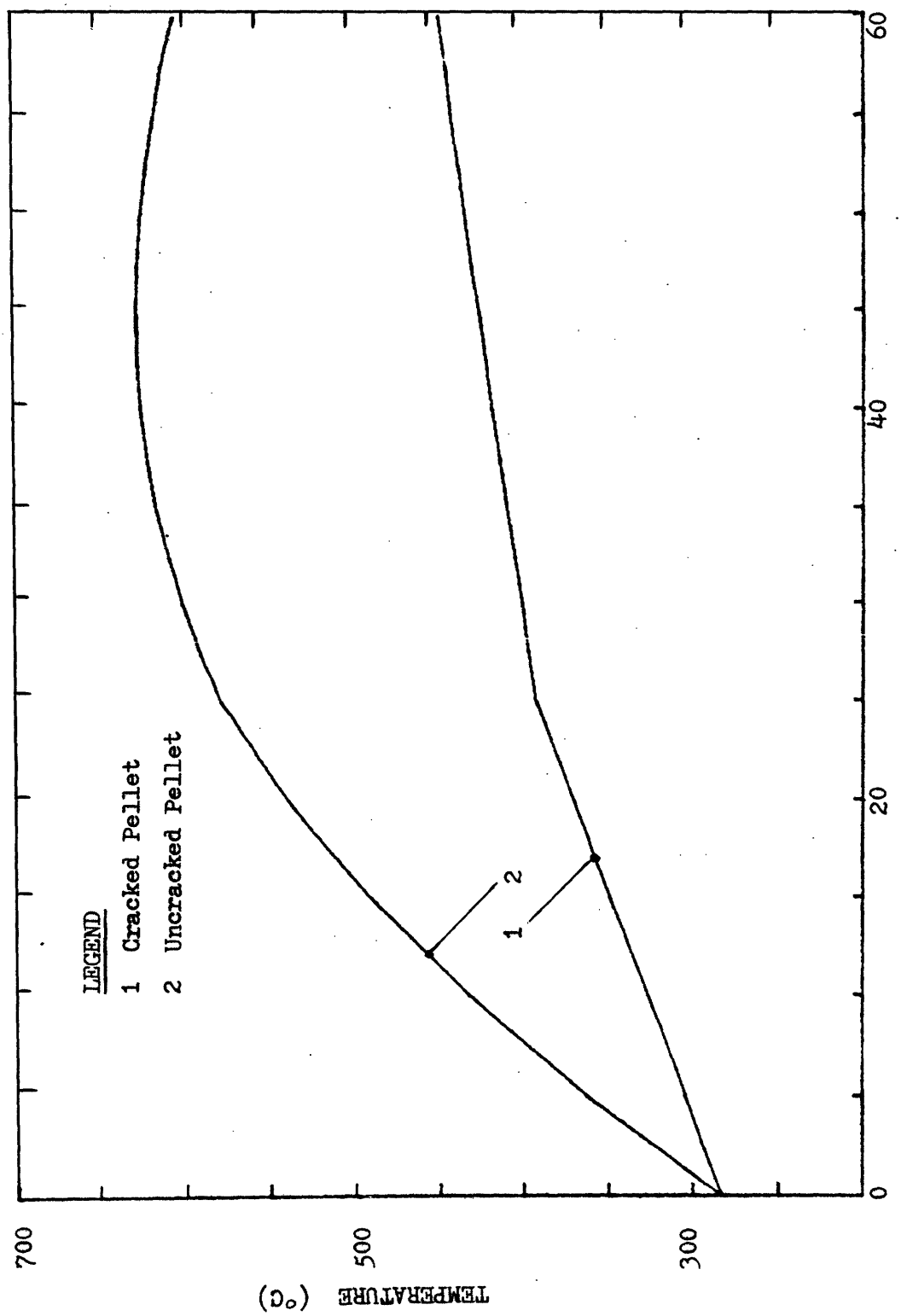

Figure 5-1. Comparison of cracked/uncracked fuel pellet surface temperature (cold radial gap width = 95 um).

surface temperature plot. This kink corresponds to the LHGR at which the outside cladding temperature changes from an increasing function of LHGR to a constant temperature at the onset of nucleate boiling (see Appendix C for further details on the determination of the outside cladding temperatures).

The general shape of the surface temperature curves remains unchanged with different gap sizes. However, with increasing initial gap size, the uncracked pellet surface temperature increases at all linear heat generation rates. The differences between the cracked/uncracked pellet surface temperatures also increases with increasing cold gap size. The maximum difference occurs at higher temperatures for larger cold gap widths. Remaining within 1°C of themselves, the surface temperature of the cracked pellets is unaffected by cold gap sizes up to linear heat generation rates of 40 kW/m. The largest calculated difference is 6.5°C (at 60 kW/m for the two extreme cold gap widths).

5.2 Fuel Pellet Centerline Temperature

Figure 5.2 shows the fuel centerline temperature as a function of LHGR for a cracked and an uncracked pellet. For all linear heat generation rates, the cracked pellet exhibits a lower centerline temperature. With increasing LHGR, the difference in temperature between the cracked and uncracked pellets increases. At 30 kW/m this difference is only 20°C, while at 60 kW/m the difference increases to about 130°C.

With increasing cold gap size, the centerline temperature for uncracked and cracked pellets increases for all linear heat generation rates. Only for the larger cold radial gap width of 115 μm does the cracked pellet centerline temperature exceed that of the uncracked pellet. That is, from 10 kW/m up to 45 kW/m the cracked pellet centerline temperature is higher than that for the uncracked pellet with a maximum difference of about 40°C at 24 kW/m. Beyond 45 kW/m, the uncracked pellet temperature is higher with a centerline difference of about 60°C at 60 kW/m.

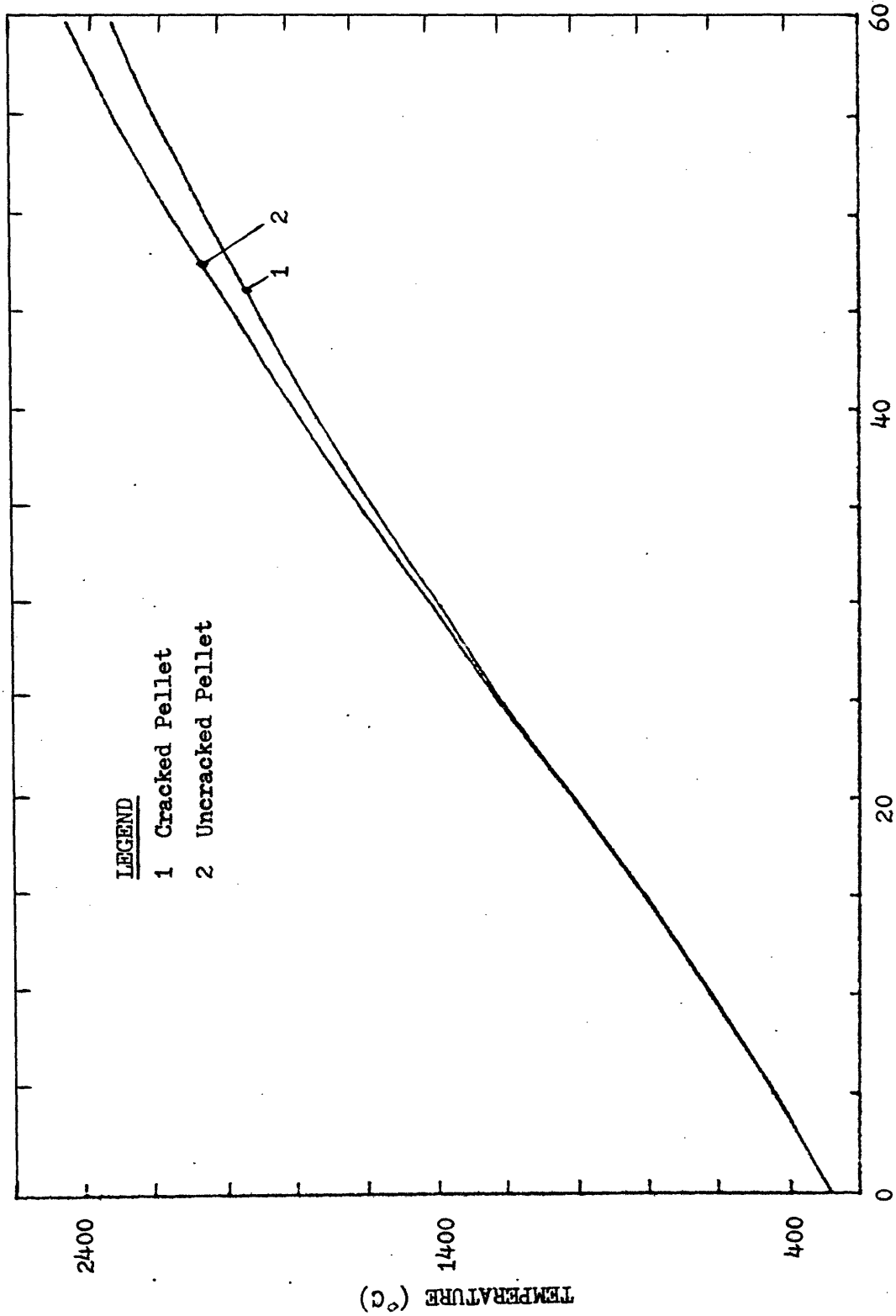

Figure 5-2. Comparison of cracked/uncracked fuel pellet centerline temperature (cold radial gap width = 95 μm).

5.3 Fuel Rod Equivalent Temperature

The fuel rod equivalent temperature as a function of LHGR for cracked/uncracked pellets is presented in Fig. 5-3. For all linear heat generation rates, the uncracked pellet displays a higher equivalent temperature. At 30 kW/m, the difference is 104°C, at 60 kW/m the equivalent temperature difference increases to 170°C.

As the cold gap size increases, the equivalent fuel rod temperature increases for both the uncracked/cracked cases. The relative difference between the equivalent temperatures for the two cases is unaffected by the cold gap size at each LHGR.

5.4 Fractional Radius for Grain Growth

A temperature for equiaxed grain growth, 1400°C, and a temperature for columnar grain growth, 1700°C, were arbitrarily chosen. However, these temperatures are within the range of those determined by other investigators (Ref. 14). In addition, a fixed temperature for grain growth in UO_2 is a gross assumption in itself because grain growth is a function of burnup, fuel stoichiometry, and duration of irradiation. The 1400°C and 1700°C grain growth temperatures do serve to indicate the extent of microstructural change (including crack healing) regions, however.

Crack healing occurs simultaneously with grain growth. At the lower pellet temperatures (within a grain growth regime), the time at a steady state operating temperature may not be long enough to allow for the diffusionally controlled grain growth and healing processes to occur. However, higher fuel temperatures (as found in fast reactor fuel) do allow equiaxed grain growth, columnar grain growth, and healing to occur quite extensively during normal reactor operating cycles.

Figure 5-4 presents the fractional radii for grain growth in cracked and uncracked fuel pellets. For this consideration, a fractional radius of 1.0 is defined as the surface of the fuel pellet. Consistent with the higher temperature profile for the uncracked pellet, grain growth occurs throughout more of the uncracked pellet than for the cracked pellet at all linear heat generation rates. Crack healing may be expected to begin at the pellet center at about 30 kW/m. At 40 kW/m, about 21% of the cracked pellet is within the grain growth/heaing regime, while at 60 kW/m, 41% of the pellet is in this range.

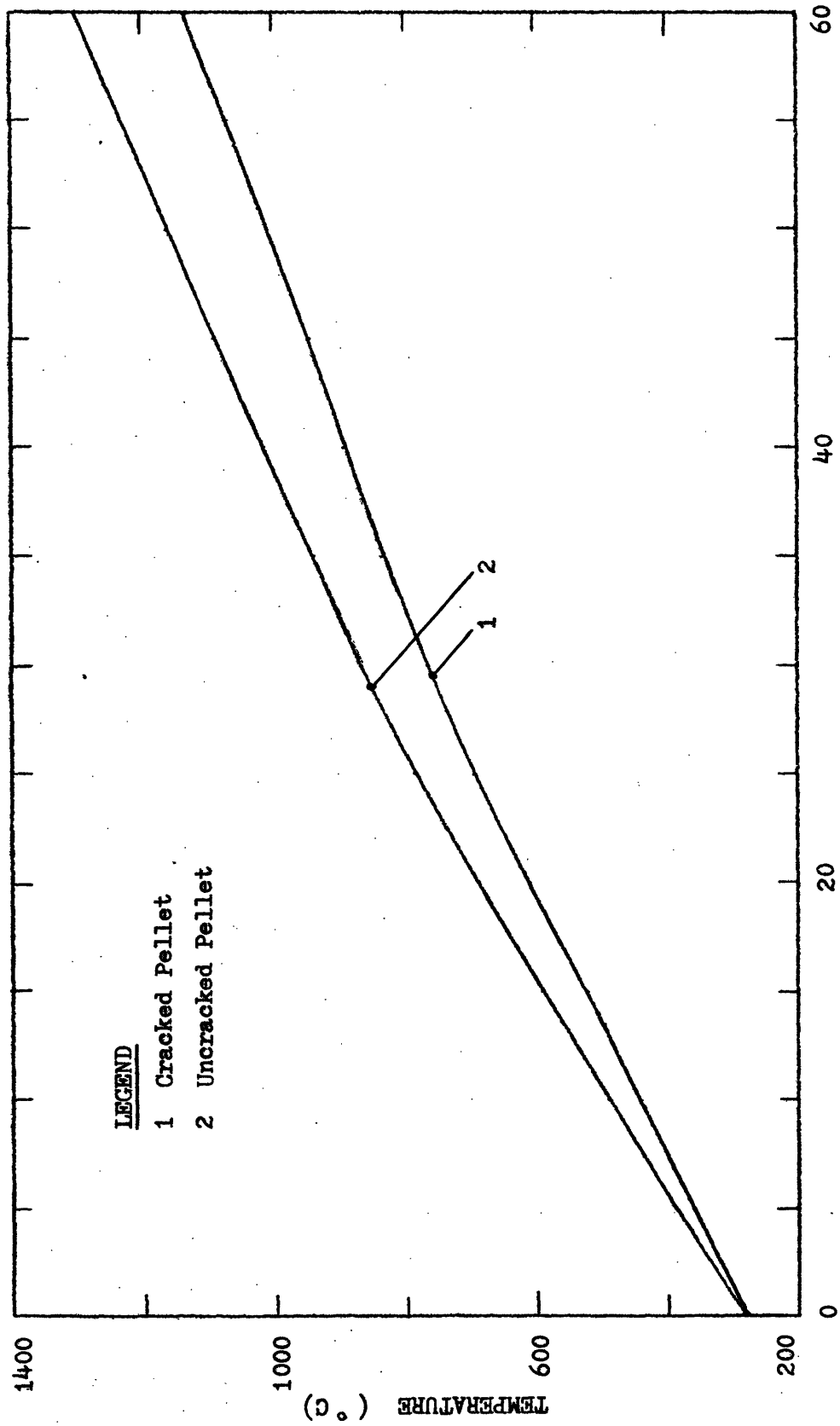

Figure 5-3. Comparison of cracked/uncracked fuel rod equivalent temperature (cold radial gap width = 95 μm).

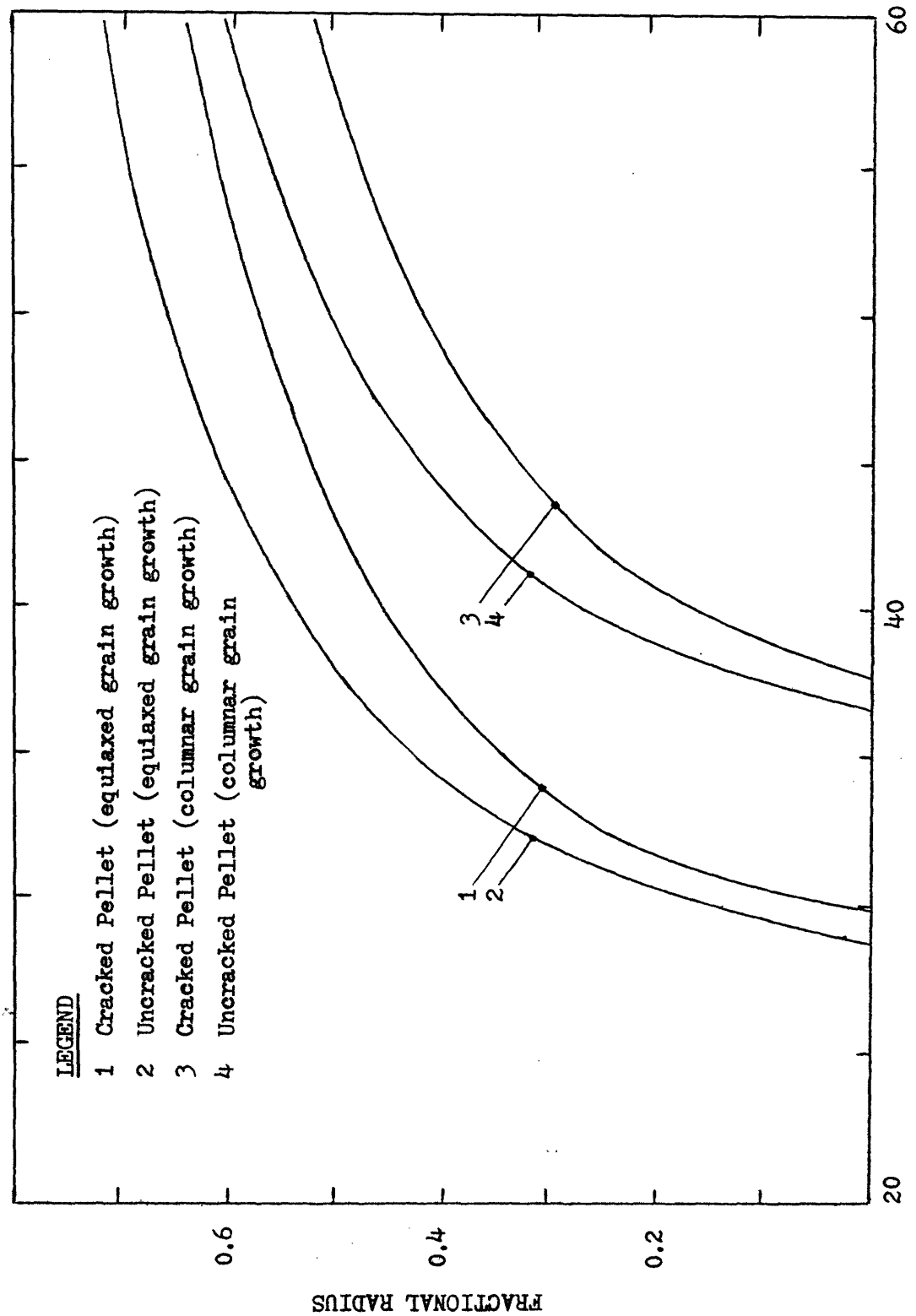

Figure 5-4. Comparison of cracked/uncracked fuel pellet fractional radius for the onset of grain growth (cold radial gap width = 95 μm).

With increasing cold gap size, a lower LHGR is required to initiate grain growth, and more of the pellet is within the grain growth area at each LHGR. This is consistent with the higher temperature profiles for larger initial gap pellets.

Only at the larger cold radial gap width of 115 μm does the cracked pellet initiate grain growth at a lower LHGR than the uncracked pellet. This effect reflects the fact that the cracked pellet has a higher central temperature profile over the lower range of linear heat generation rates than the uncracked pellet.

5.5 Gap Closure

Figure 5-5 displays the percentage of gap closure for uncracked and cracked fuel pellets. The gap width considered here is an undisturbed gap, where the fuel pellet is treated as uniformly circular and free from pellet piece relocation. Regardless of the cold gap size, the uncracked pellet achieved greater gap closure than the cracked pellet for all linear heat generation rates. Even though the cracked pellet relocates into the gap, the improved heat transfer results in a lower average pellet temperature and lower thermal strain. Thus, from reduced thermal expansion, the cracked pellet has a larger undisturbed hot gap width than the uncracked pellet at all linear heat generation rates.

For both cracked and uncracked cases, the percentage of gap closure decreases with increasing cold gap size at each LHGR. Even though the larger cold gap pellets have higher temperature profiles, and larger absolute changes in pellet size, thermal expansion alone cannot proportionally close up the original gap as that of a smaller cold gap pellet.

5.6 Pellet - Clad Contact

The uncracked pellet model assumes a perfectly circular pellet. Thus, only with 100% gap closure, where the gap width equals the pellet-cladding surface roughness, does pellet-clad contact exist. Up to 60 kW/m, pellet to cladding contact was not reached under the conditions employed in this report for uncracked pellets.

Figure 5-6 presents the calculated circumferential pellet-cladding contact for cracked pellets. With increasing LHGR, the fraction of contact increases. This is to be expected since the amount of contact

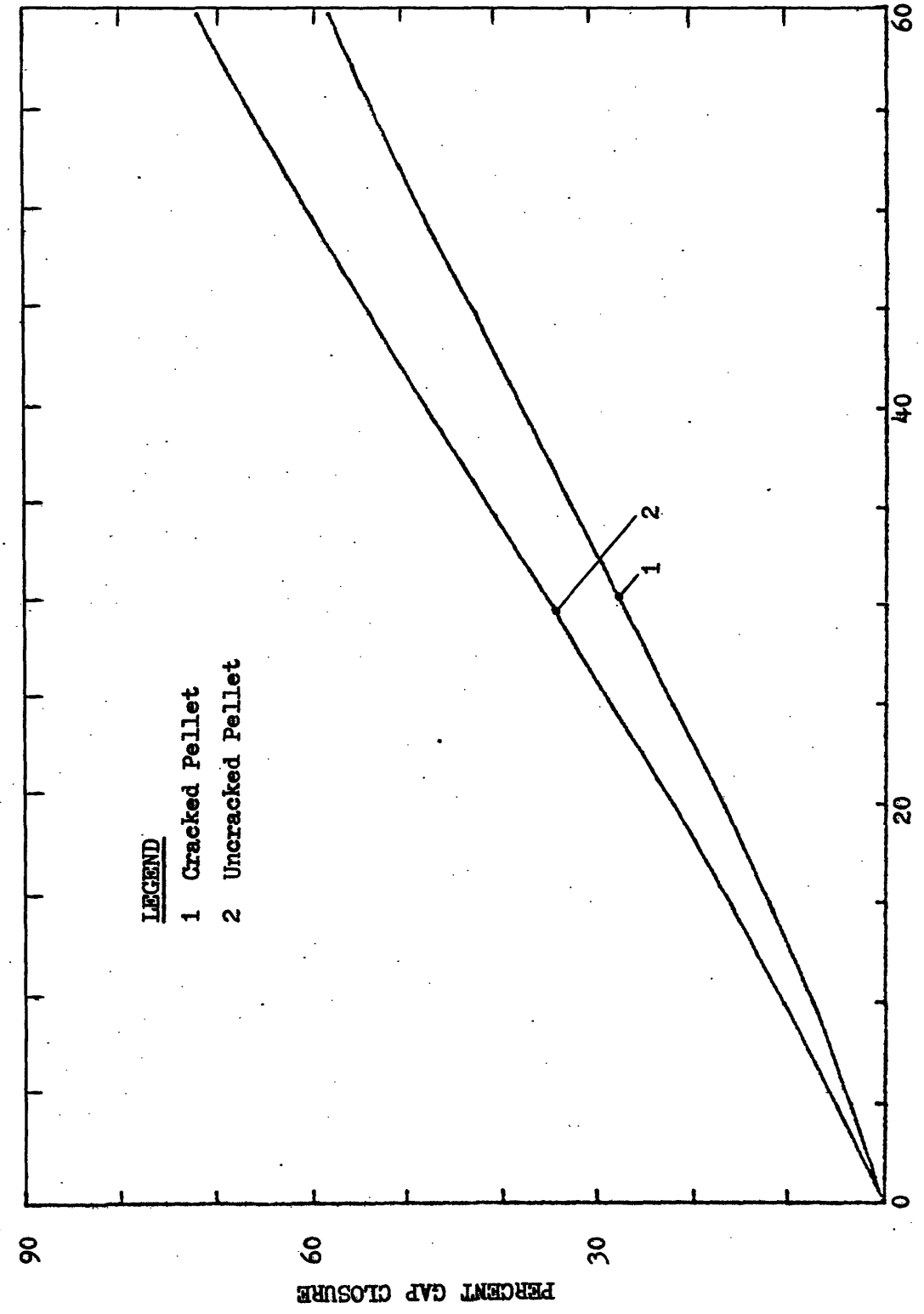

Figure 5-5. Comparison of cracked/uncracked fuel gap closure (cold radial gap width = 95 μm).

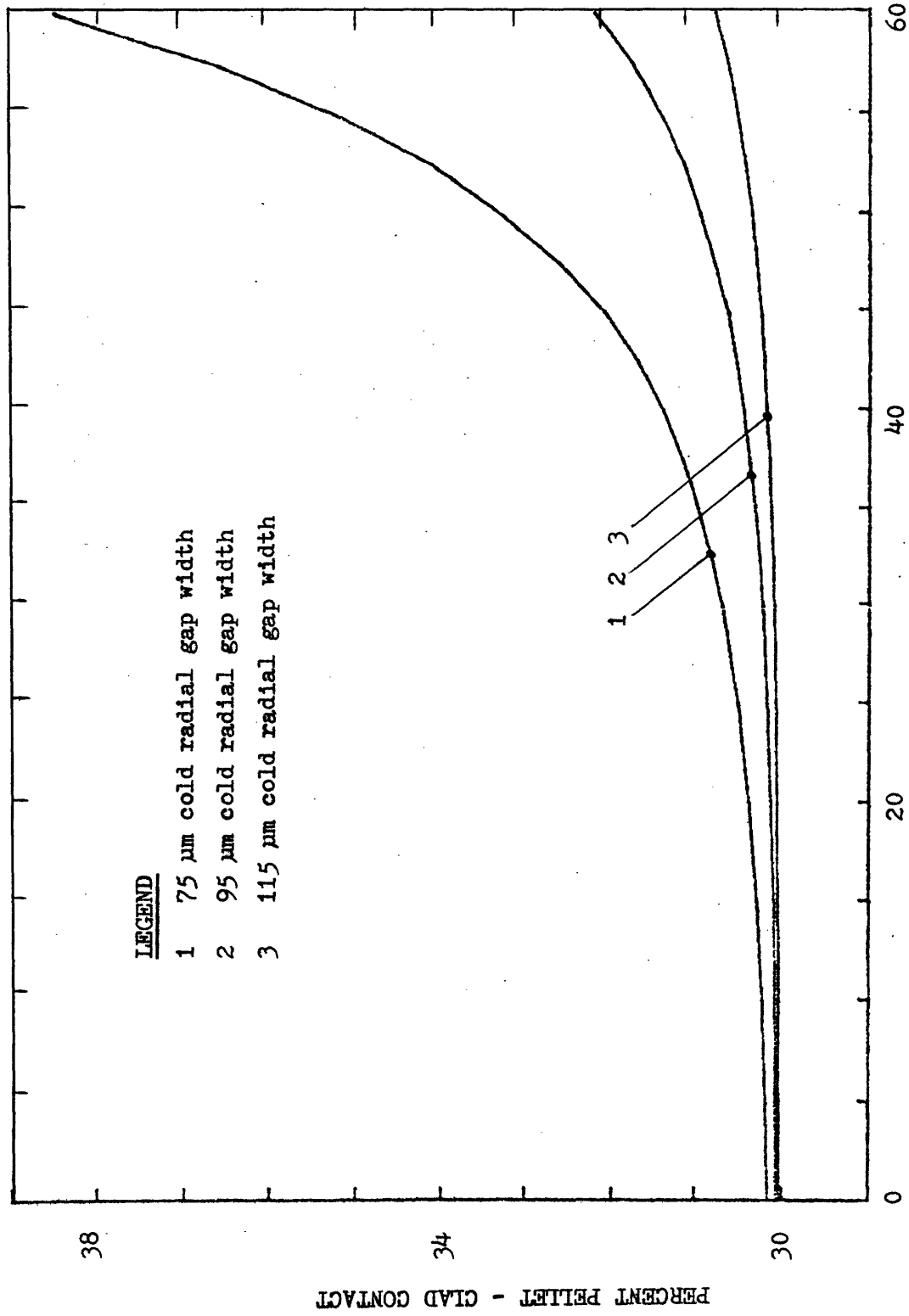

Figure 5-6. Circumferential pellet - cladding contact behavior for cracked fuel pellets.

is a function of the hot gap width. With higher linear heat generation rates, the hot gap becomes smaller which results in more contact. Also, with larger cold gap pellets, the hot gap width is larger which results in less pellet-clad contact at each LHGR.

6. EXPERIMENTAL EVALUATION

Beginning of life experimental fuel performance data was obtained from an instrumented fuel assembly irradiated at the Halden Heavy Boiling Water Reactor (Ref. 11). The fuel rods in this assembly are typical of pressurized light water reactor design in dimensions and materials (see Appendix D). Utilizing the models described in this report, calculated pellet centerline temperatures are compared to the Halden experimental data in Fig. 6-1.

The comparisons indicate that, for these experiments, only slight differences exist between the uncracked (non-relocation affected gap conductance, solid pellet thermal conductivity) and cracked (relocation affected gap conductance, cracked pellet thermal conductivity) model predictions. Both models produce reasonable pellet centerline temperatures for the third and fourth power cycles. However, when pellet piece relocation is considered in the gap conductance and a solid pellet thermal conductivity is assumed, the model drastically underestimates the centerline temperature for all power cycles. This indicates that a model incorporating pellet piece relocation in the gap conductance must also consider the crack induced heat transfer barriers within the fuel pellet to obtain reasonable results.

As displayed in Fig. 6-1, experimental evidence indicates that thermal stabilization of a fuel rod is obtained approximately after the third power cycle (Refs. 2 and 11). This asymtopic effect may result because the internal thermal stresses which cause the major amount of pellet cracking are essentially relieved during the heatup-cooldown phases of cycling, and because further pellet piece relocation is inhibited by pellet-clad contact interference. Even though the model utilized in this study for cracked pellet-clad contact does not explicitly incorporate cycling effects, the model correlates quite well to fuel rods thermally conditioned by power cycling.

Extrapolating a best fit curve through the third and fourth power ramp experimental data points, an estimated difference of 50°C exists between the cracked pellet model prediction and the experimentally determined centerline temperature at 40 kW/m. Assuming the same proportional difference in the Maine Yankee calculations, a 55°C discrepancy would result between the cracked pellet model and actual beginning of life pellet centerline temperature at 40 kW/m, with the calculated temperatures being higher.

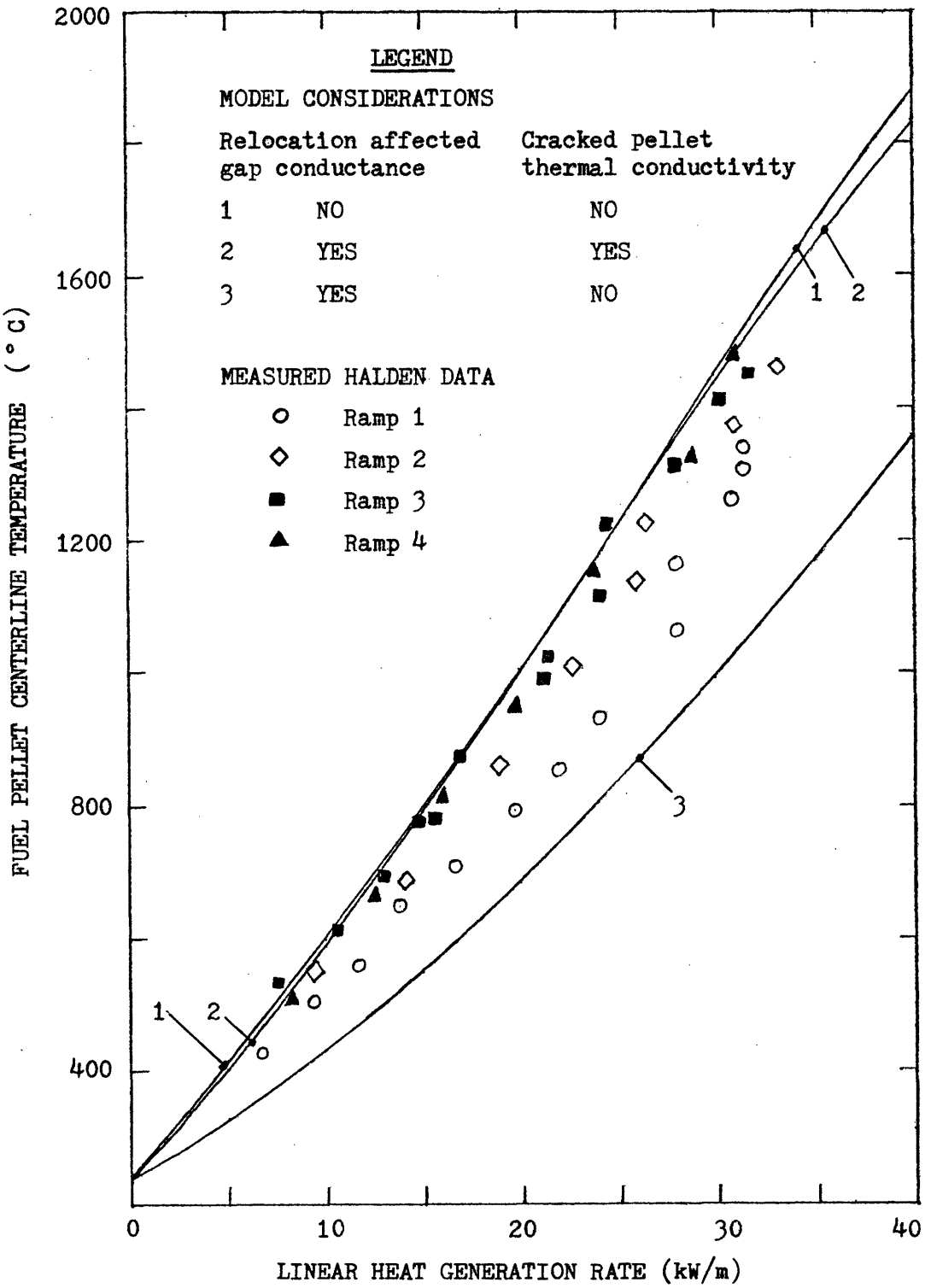

Figure 6-1. Comparison of computational models to Halden experimental fuel rod data (experimental data from ref. 11).

7. CONCLUSIONS

This chapter presents the conclusions from this study based upon Maine Yankee light water reactor fuel under steady-state, beginning of life operation.

7.1 Relocation Into Gap

Once the fuel pellet cracks, a fraction of the fuel pieces lie against the cladding. This contact results in better heat transfer conditions than for an assumed uncracked pellet which has not relocated into the gap. When compared to an uncracked pellet under the same operating conditions, the cracked fuel pellet exhibits a lower surface temperature. This difference may be as much as 210°C at 40 kW/m.

7.2 Reduced Fuel Thermal Conductivity

Some of the cracks within the fuel pellets form heat barriers and degrade overall heat transfer conditions. To account for this heat transfer degradation, an effective fuel thermal conductivity is used which essentially serves to reduce the normal UO_2 thermal conductivity. Generally, the adverse thermal effects of internal cracks are countered by the crack induced relocations into the gap. Only for large cold gap widths does the cracked pellet centerline temperature exceed that of the uncracked pellet. At 35 kW/m with an initial radial gap size of 115 μm, the cracked fuel centerline temperature exceeds that of an uncracked pellet by about 40°C. Regardless of initial gap size, the effects of internal cracks are diminished by the relocation improved gap conductance. Thus, cracked pellets always display a cooler outer temperature distribution resulting in a lower average thermal strain, less undisturbed gap closure, and less stored heat than for an uncracked fuel pellet.

7.3 Fuel Rod Equivalent Temperature

Due to the cooler outer temperature profile which results in less stored heat, the cracked fuel pellet always exhibits a lower fuel rod equivalent temperature than the uncracked pellet. At any particular LHGR, the difference between the equivalent temperatures for cracked/uncracked pellets is approximately the same for any initial gap width.

During a LOCA, the cladding and the fuel will equilibrate to roughly the same temperature since the heat transfer to coolant is poor and the heat deposition rate is low. The lower equivalent temperature indicates less severe LOCA conditions. Thus, the stored heat of an uncracked pellet at 30 kW/m will produce the same equivalent temperature as a cracked pellet at 37.5 kW/m.

7.4 Crack Healing

Significant crack healing is expected when extensive grain growth has occurred. Only at 35 kW/m does 10% of a fuel pellet with a nominal initial gap width reach into the grain growth regime (fuel temperature greater than 1400°C). Under normal reactor operating conditions, LWR fuel pellets seldom exceed this LHGR. Thus, extensive crack healing is not expected in typical light water reactor fuel.

APPENDIX A

ADDITIONAL FIGURES FROM FUEL PELLET THERMAL CALCULATIONS

This appendix presents the figures for cracked/uncracked fuel pellet thermal effects at initial radial gap widths of 75 and 115 μm. These two gap widths were chosen as the extreme tolerances for the determination of the nominal cold gap width. The figure captions should be self-explanatory, but if further explanation is required, refer to Chapter 5.

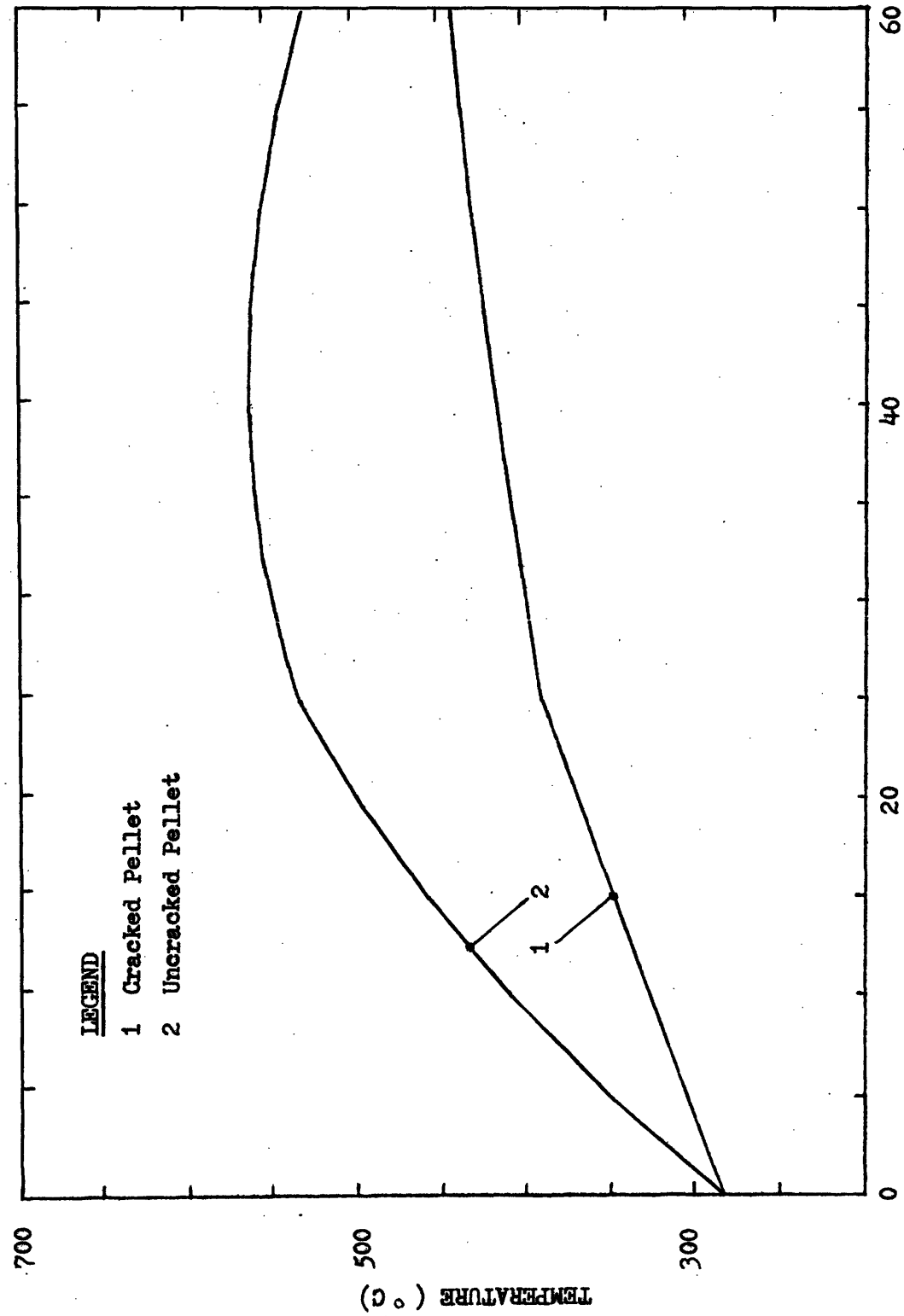

Figure A-1. Comparison of cracked/uncracked fuel pellet surface temperature (cold radial gap width = 75 μm).

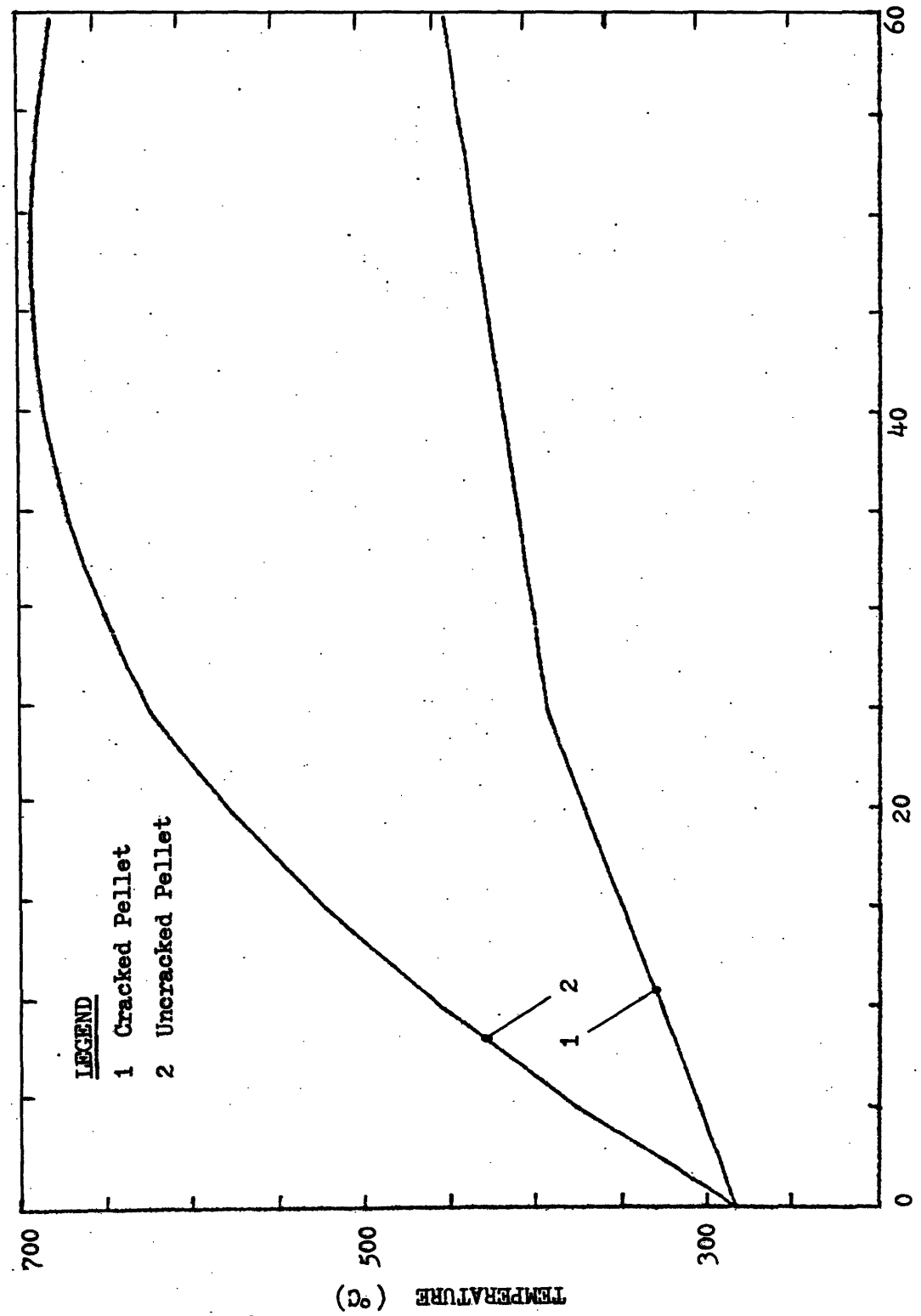

Figure A-2. Comparison of cracked/uncracked fuel pellet surface temperature (cold radial gap width = 115 μm).

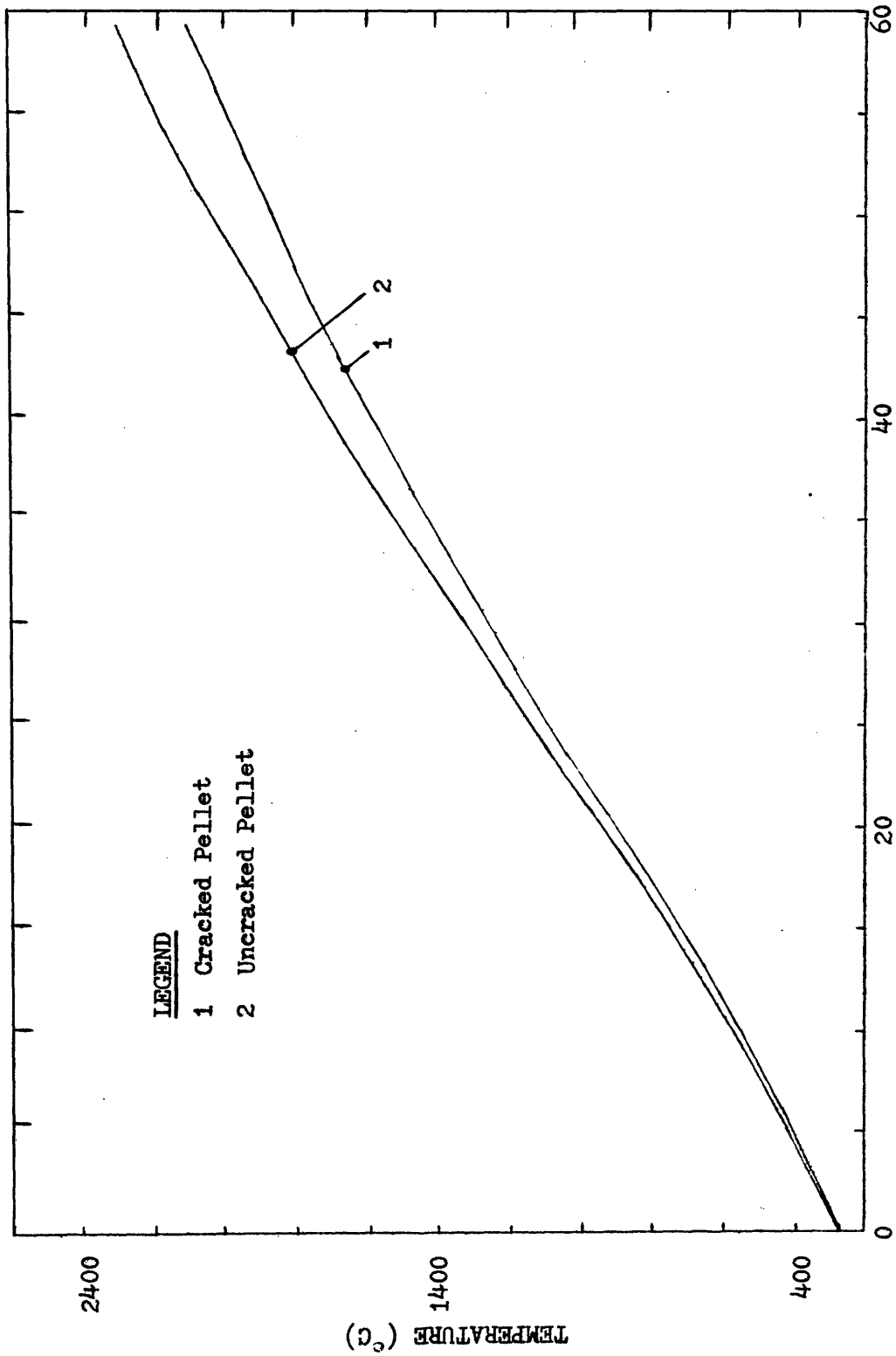

Figure A-3. Comparison of cracked/uncracked fuel pellet centerline temperature (cold radial gap width = 75 μm).

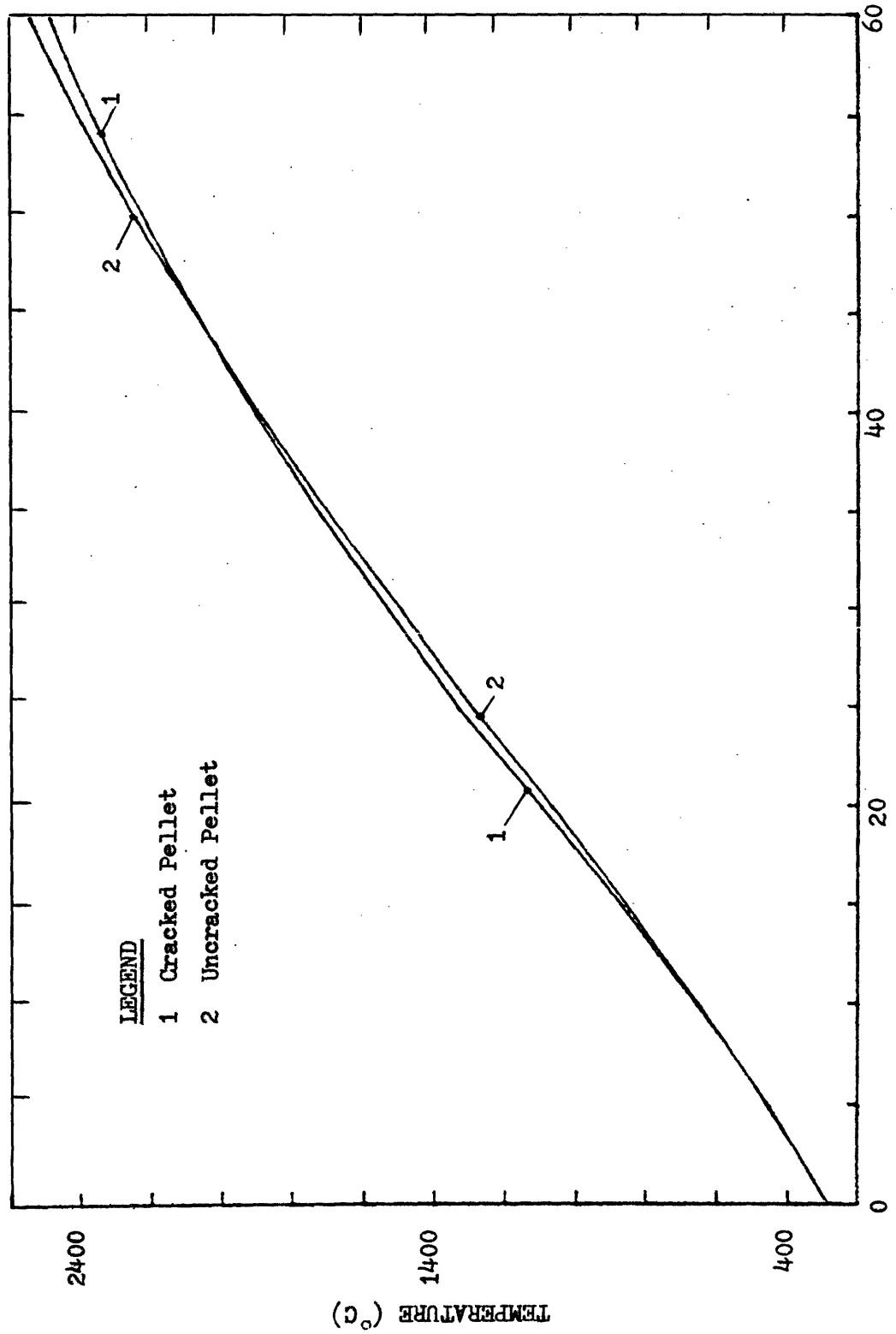

Figure A-4. Comparison of cracked/uncracked fuel pellet centerline temperature (cold radial gap width = 115 μm).

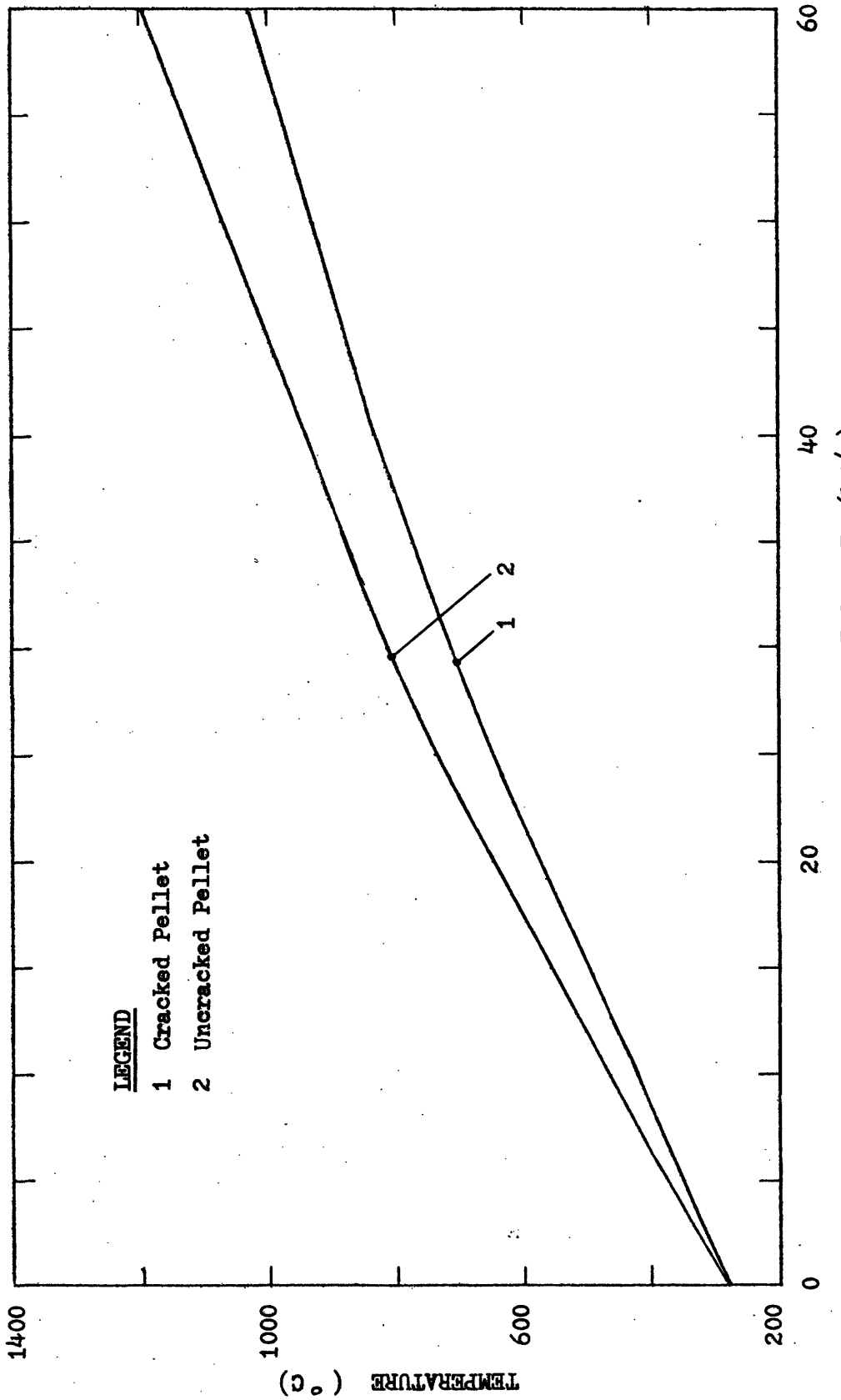

Figure A-5. Comparison of cracked/uncracked fuel rod equivalent temperature (cold radial gap width = 75 μm).

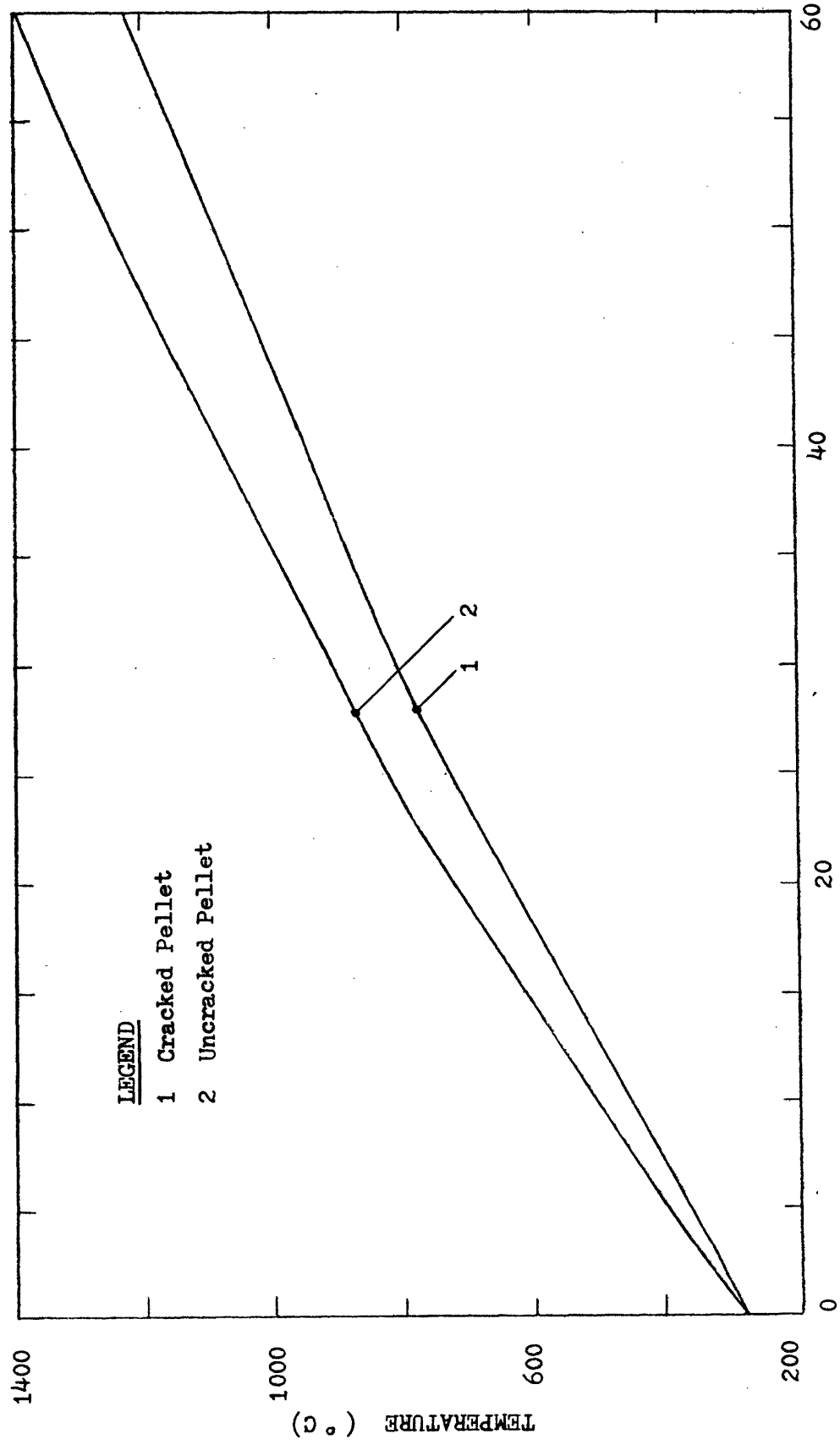

Figure A-6. Comparison of cracked/uncracked fuel rod equivalent temperature (cold radial gap width = 115 μm).

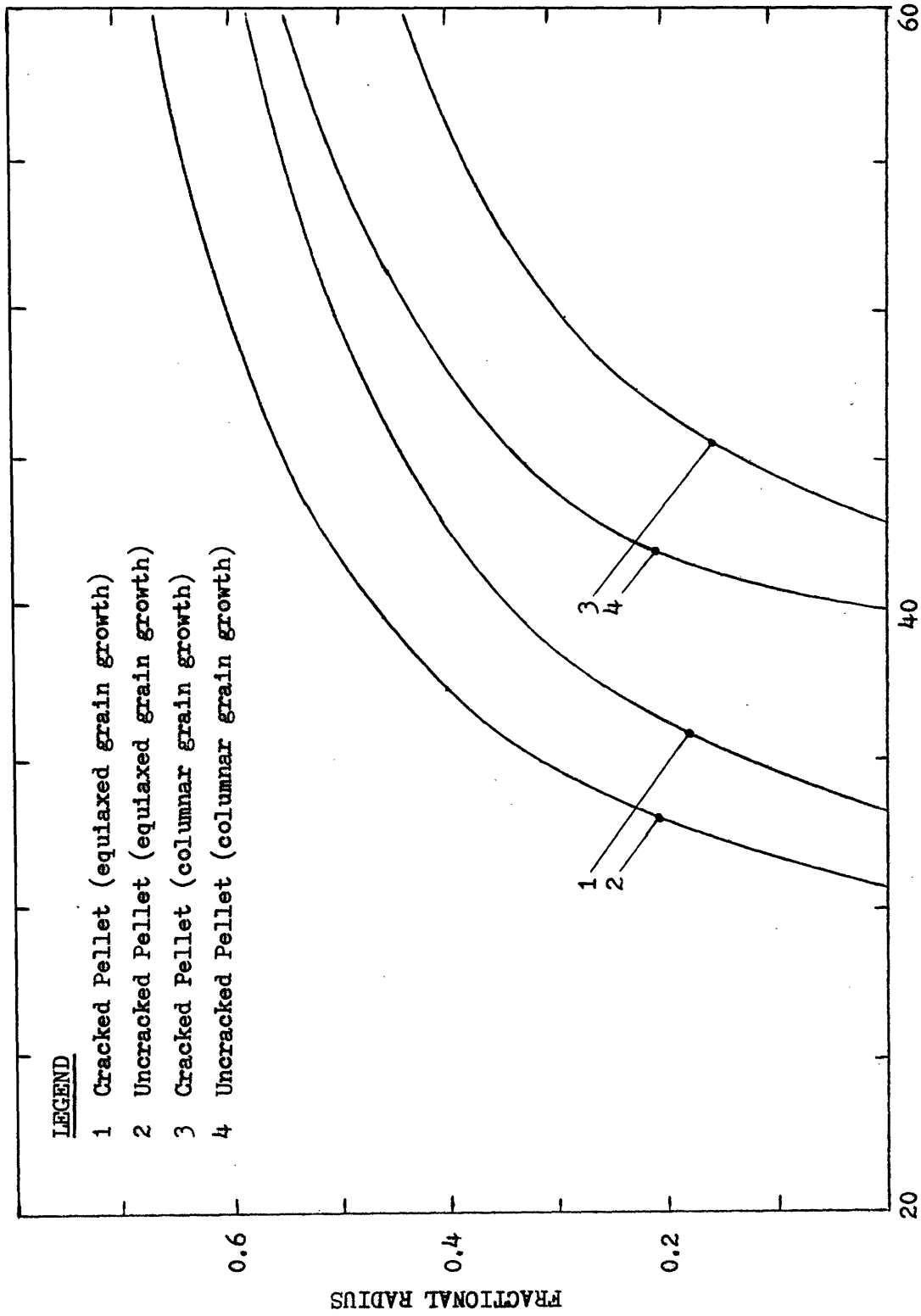

Figure A-7. Comparison of cracked/uncracked fuel pellet fractional radius for the onset of grain growth (cold radial gap width = 75 μm).

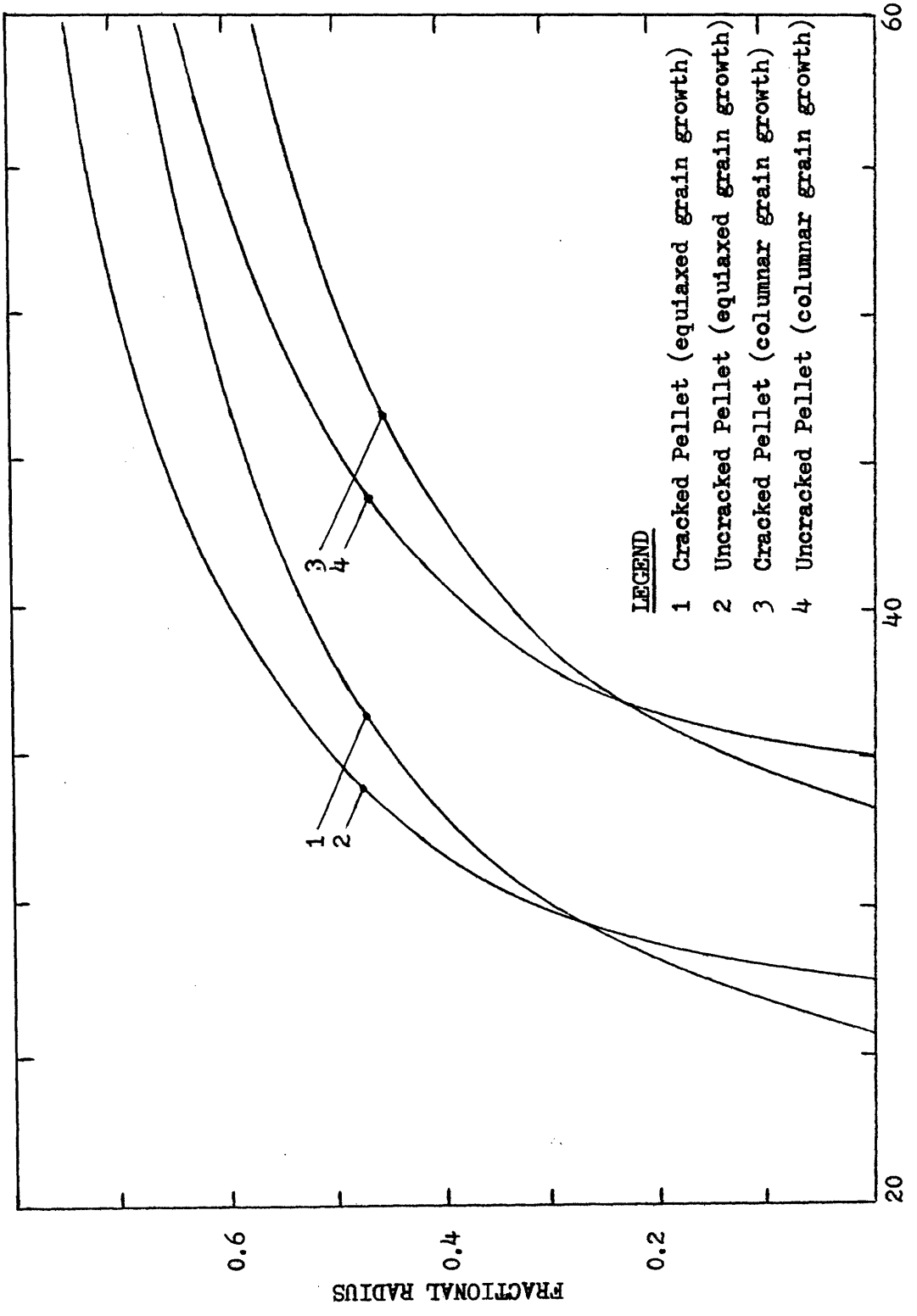

Figure A-8. Comparison of cracked/uncracked fuel pellet fractional radius for the onset of grain growth (cold radial gap width = 115 μm).

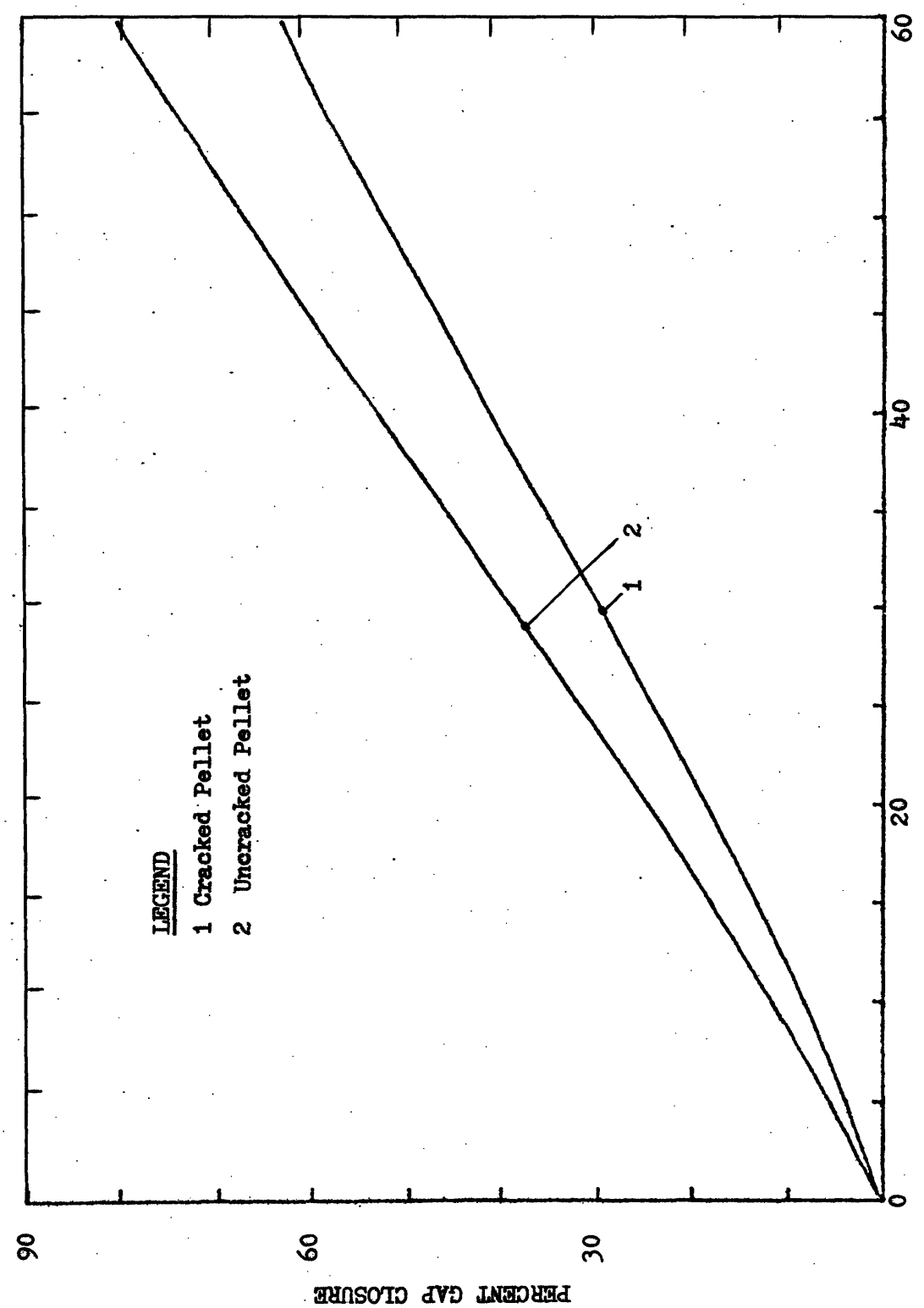

Figure A-9. Comparison of cracked/uncracked fuel gap closure (cold radial gap width = 75 μm).

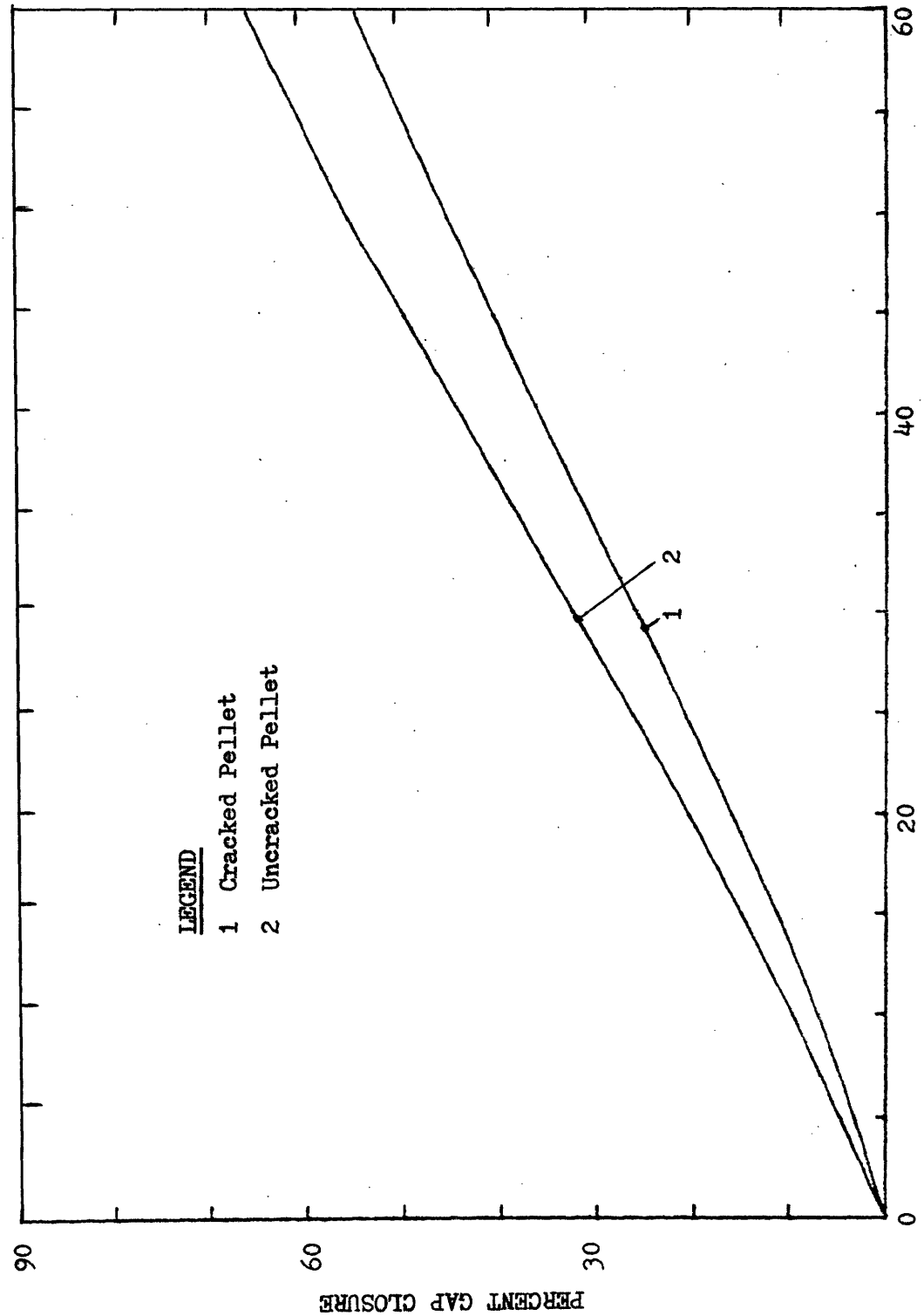

Figure A-10. Comparison of cracked/uncracked fuel gap closure (cold radial gap width = 115 μm).

APPENDIX B
MATERIAL PROPERTIES

This appendix presents the material properties for uranium dioxide, Zircaloy-4, and helium used in this study. In some cases, a comparison between two relations for a particular property, and a discussion concerning the choice of a relation incorporated into the work will be given.

B.1 Fuel Thermal Conductivity

Two relations for the thermal conductivity of uranium dioxide were investigated. The thermal conductivity used by EPRI is (Ref. 15)

$$k_f = PF \left[\frac{3824}{402.4+T} + 6.12 \times 10^{-11} (T+273)^3 \right] \quad \text{(B-1)}$$

$$PF = \frac{1.1316(1-P)}{1+P+10P^2} \quad \text{(B-2)}$$

where k_f = UO_2 thermal conductivity in W/m·K

PF = porosity factor, normalized to 95% theoretically dense fuel (dimensionless);

P = fractional porosity of fuel (dimensionless);

and T = temperature in °C.

MATPRO's version of the UO_2 thermal conductivity correlation for $0°C < T \leq 1650°C$ is (Ref. 6)

$$k_f = PF \left[\frac{4040}{464+T} + 1.216 \times 10^{-2} \exp(1.867 \times 10^{-3} T) \right] \quad \text{(B-3)}$$

for $1650 \leq T < 2840°C$

$$k_f = PF \left[1.91 + 1.216 \times 10^{-2} \exp(1.867 \times 10^{-3} T) \right] \quad \text{(B-4)}$$

$$PF = \frac{1 - (2.58 - 5.8 \times 10^{-4} T)\ (1-D)}{1 - (2.58 - 5.8 \times 10^{-4} T)\ (0.05)} \quad \text{(B-5)}$$

where k_f = UO_2 thermal conductivity in W/m·K;

PF = porosity factor, normalized to 95% theoretically dense fuel (dimensionless);

D = %T.D./100 (dimensionless);

and T = temperature in °C.

The above correlations for 95% T.D. fuel are plotted in Fig. B-1. Both relationships give essentially the same thermal conductivity over the temperature range of primary concern, 300°C to 2000°C. Above this range, the MATPRO version increases more sharply than the EPRI correlation, thus resulting in a 4.5% difference at 2000°C and increasing to a 29% difference at the melting point (∿2800°C).

Figure B-2 presents the porosity factors from EPRI and MATPRO at 500°C and 2000°C. At low temperatures, small differences exist between the two porosity factors. With increasing temperatures, the difference increases. For fuel near 95% T.D., both porosity factors equate quite well for all operating temperatures.

Using the two thermal conductivities, the following conductivity integrals were derived for 95% T.D. fuel with an arbitrarily choosen reference temperature of 0°C. From EPRI:

$$\int_0^T k_f \, dT = 3.824 \, \ell n \left[1 + \frac{T}{402.4} \right] + 1.53 \times 10^{-14} \, (T+273)^4 - 8.5 \times 10^{-5} \quad \text{(B-6)}$$

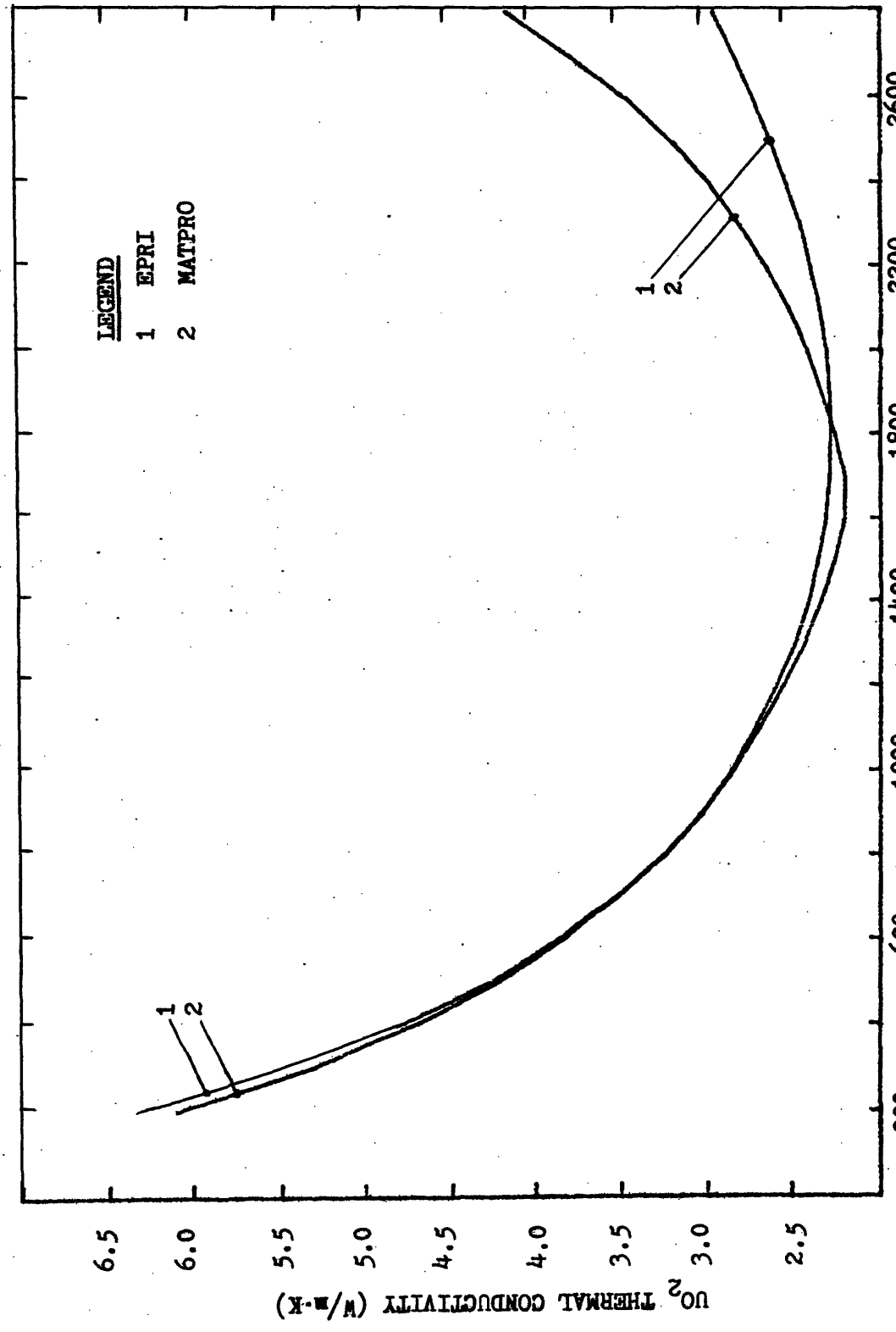

Figure B-1. Comparison of EPRI and MATPRO UO_2 thermal conductivity.

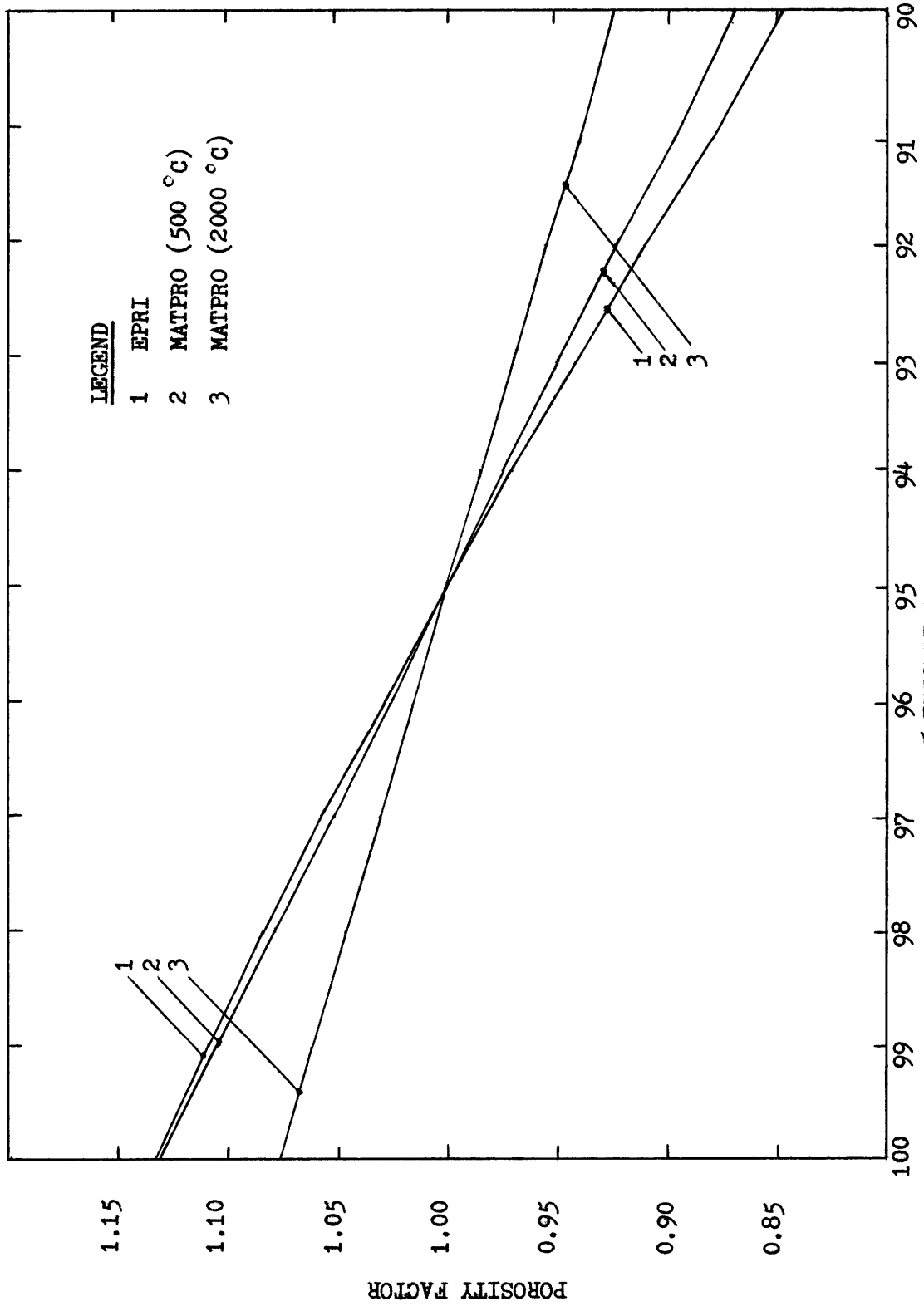

Figure B-2. Comparison of EPRI and MATPRO porosity factors.

where $\int_0^T k_f \, dT$ = conductivity integral in kW/m;

and T = temperature in °C.

From MATPRO for $0°C < T \leq 1650°C$

$$\int_0^T k_f \, dT = 4.040 \, \ell n \left[1 + \frac{T}{464}\right] + 6.513 \times 10^{-3} \exp(1.867 \times 10^{-3} T) - 6.513 \times 10^{-3} \quad \text{(B-7)}$$

for $1650°C \leq T < 2840°C$

$$\int_0^T k_f \, dT = 1.91 \times 10^{-3} T + 6.513 \times 10^{-3} \exp(1.867 \times 10^{-3} T) + 2.974 \quad \text{(B-8)}$$

where $\int_0^T k_f \, dT$ = conductivity integral in kW/m;

and T = temperature in °C.

The values of the above integrals are plotted in Fig. B-3. Over most of the fuel operating temperature range, the difference between the two conductivity integrals is approximately constant. This difference will result in a discrepancy of about 50°C for a fuel centerline temperature calculation.

Due to its greater simplicity and ease of mathematical manipulation, it was decided to use the EPRI version of the UO_2 thermal conductivity in this study. Furthermore, since most fuel operating temperatures are below 2000°C, minute differences would result from cracked pellet

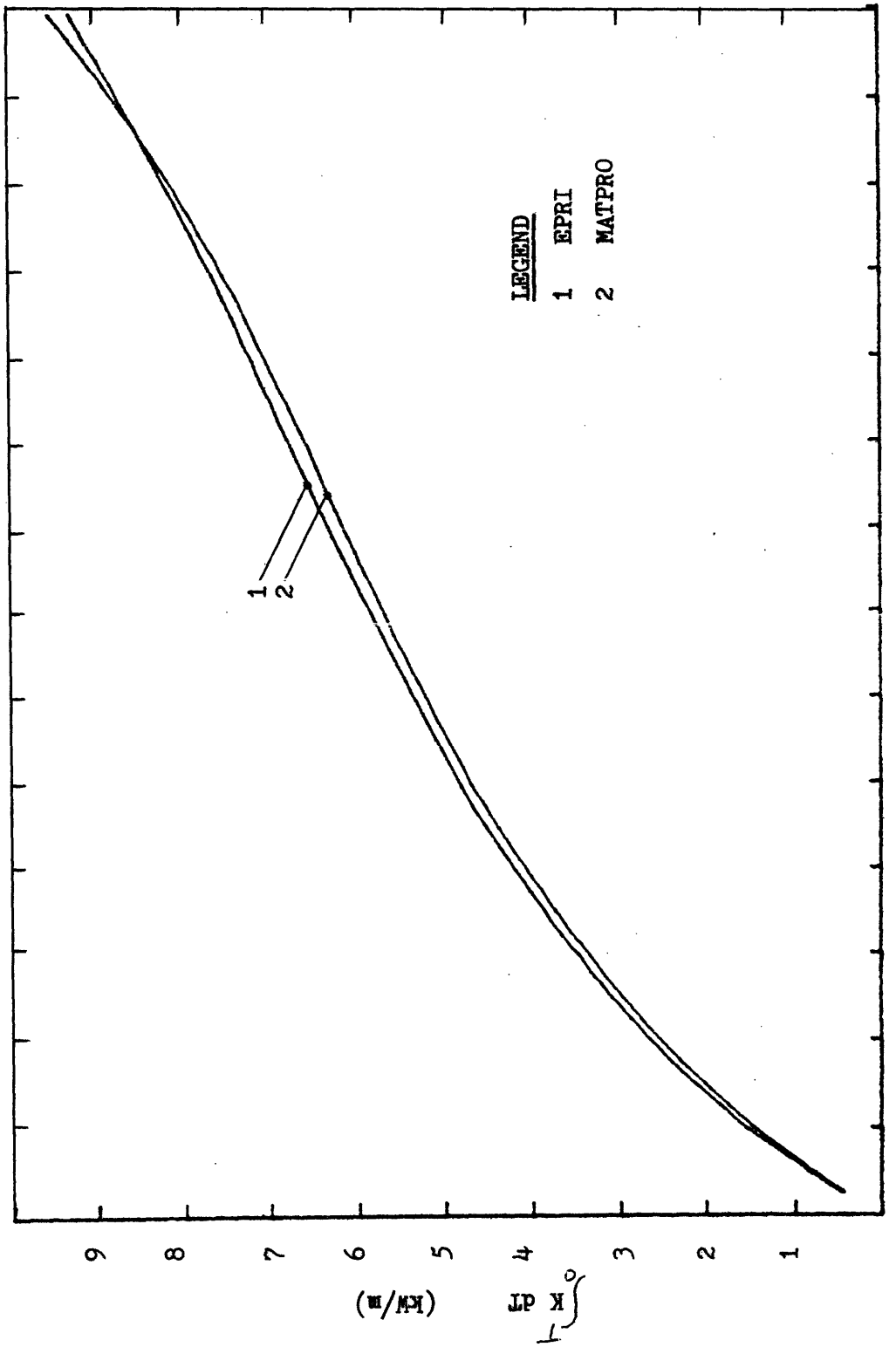

Figure B-3. Comparison of EPRI and MATPRO conductivity integrals.

temperature profile calculations if the MATPRO thermal conductivity were used. If only 95% T.D. fuel were to be considered for uncracked pellet calculations (where the porosity factor is normalized to one), then the MATPRO correlation would have been used. However, to ensure greater flexibility, incorporation of the porosity factor was deemed necessary. Integration of the complete MATPRO relation (with its temperature dependent porosity factor) would have resulted in an exceedingly burdensome equation. Also, a different reference temperature for the conductivity integral (i.e., 200°C) would reduce the calculated pellet centerline temperature differences. Thus, for consistency in the comparative study of cracked and uncracked pellets, the EPRI UO_2 thermal conductivity correlation was employed.

B.2 Fuel Thermal Strain

A relation used for uranium dioxide thermal strain was taken from MATPRO and is presented below

$$\varepsilon_T = -4.972\text{x}10^{-2} + 7.107\text{x}10^{-4}T + 2.581\text{x}10^{-7}T^2 + 1.14\text{x}10^{-11}T^3 \qquad \text{(B-9)}$$

where ε_T = UO_2 thermal strain in %

and T = temperature in °C.

Figure B-4 displays this correlation in graphical form. The root of the thermal strain equation lies at about 65°C.

B.3 Fuel Specific Heat Capacity

For use in stored heat and equivalent fuel rod temperature calculations, a correlation for uranium dioxide specific heat capacity was taken from MATPRO. The following equation is also plotted in Fig. B-5.

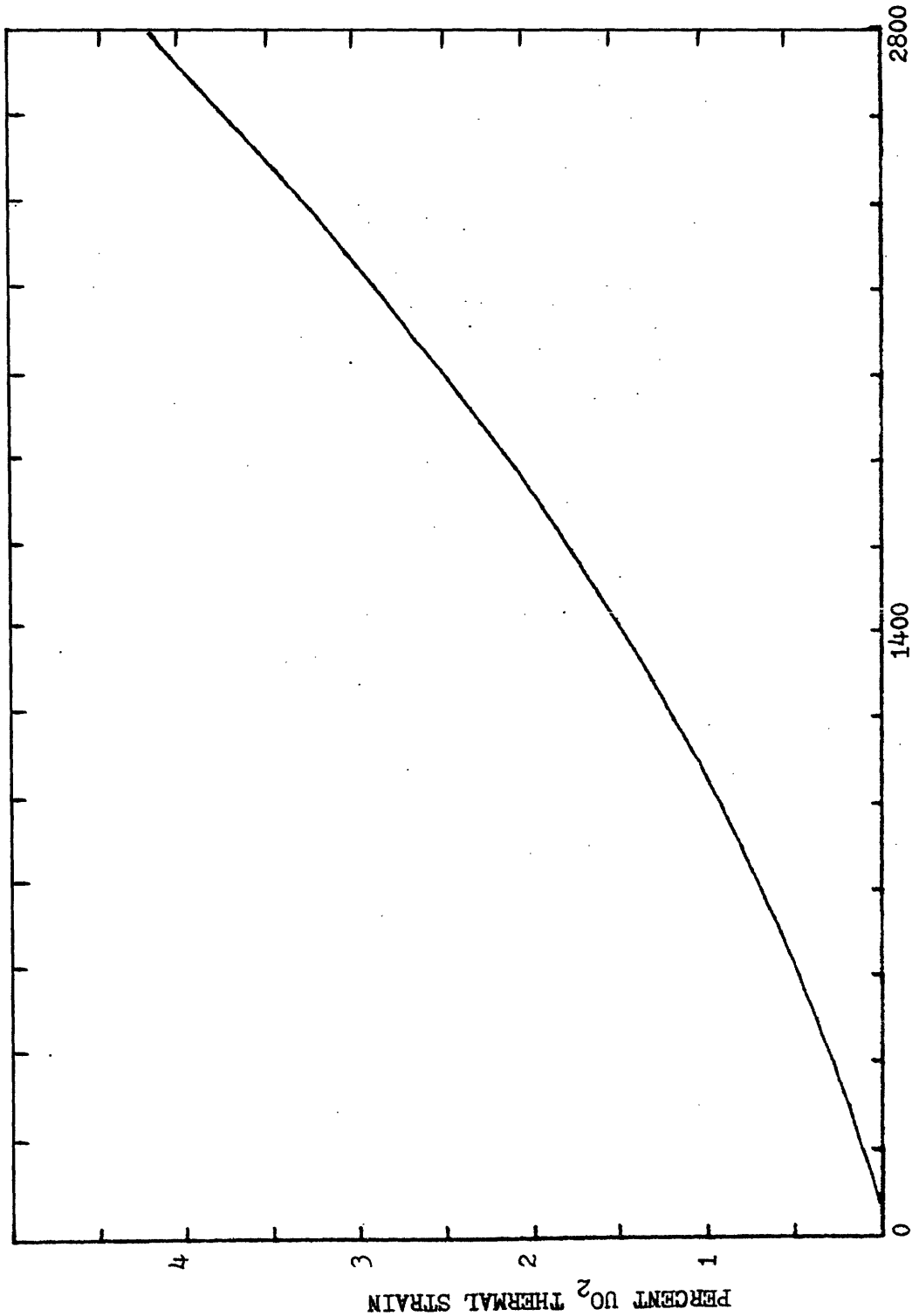

Figure B-4. MATPRO's version of thermal strain for uranium dioxide.

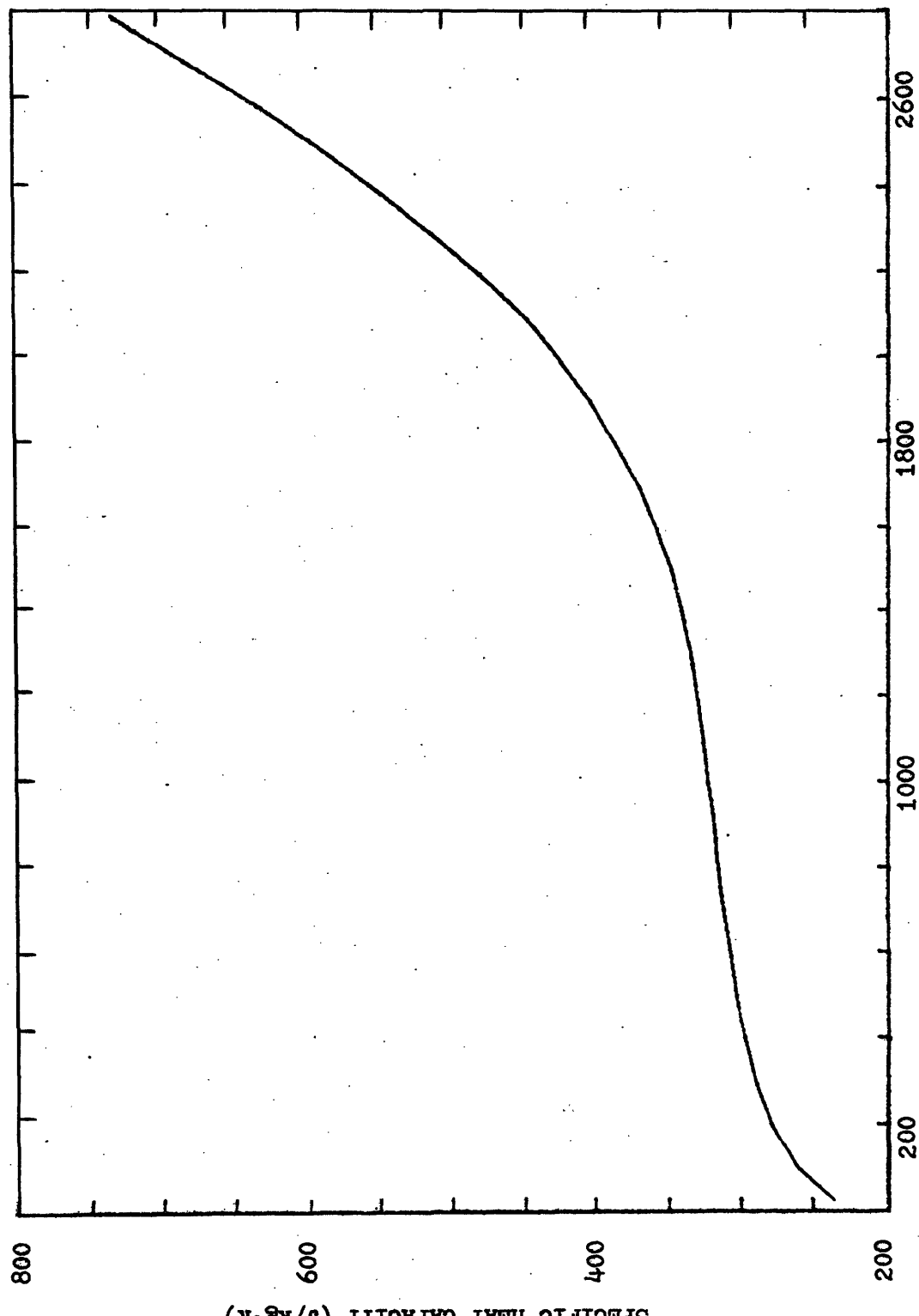

Figure B-5. MATPRO's version of specific heat capacity for uranium dioxide.

$$C_p = \frac{85.005 \exp(\frac{535.285}{T})}{T^2[\exp(\frac{535.285}{T})-1]^2} + 2.432 \times 10^{-8} T$$

$$+ \frac{1.6591 \times 10^6}{T^2} \exp(\frac{-18971}{T}) \qquad \text{(B-10)}$$

where C_p = UO_2 specific heat capacity in MJ/kg·K

and T = temperature in K.

B.4 Enthalpy Change for Fuel

The enthalpy change for UO_2 may be derived from the following equation

$$\Delta H_f(T) = \int_{T_{ref}}^{T} C_p \, dT \quad . \qquad \text{(B-11)}$$

Using the MATPRO specific heat capacity, UO_2 enthalpy is calculated below for a reference temperature of 25°C.

$$\Delta H_f(T) = \frac{.158803}{\exp(\frac{535.285}{T})-1} + 1.216 \times 10^{-8} T^2$$

$$+ 87.455 \exp(\frac{-18971}{T}) - 3.2705 \times 10^{-2} \qquad \text{(B-12)}$$

where $\Delta H(T)$ = UO_2 enthalpy in MJ/kg

and T = temperature in K.

Figure B-6 presents the UO_2 enthalpy change in graphical form.

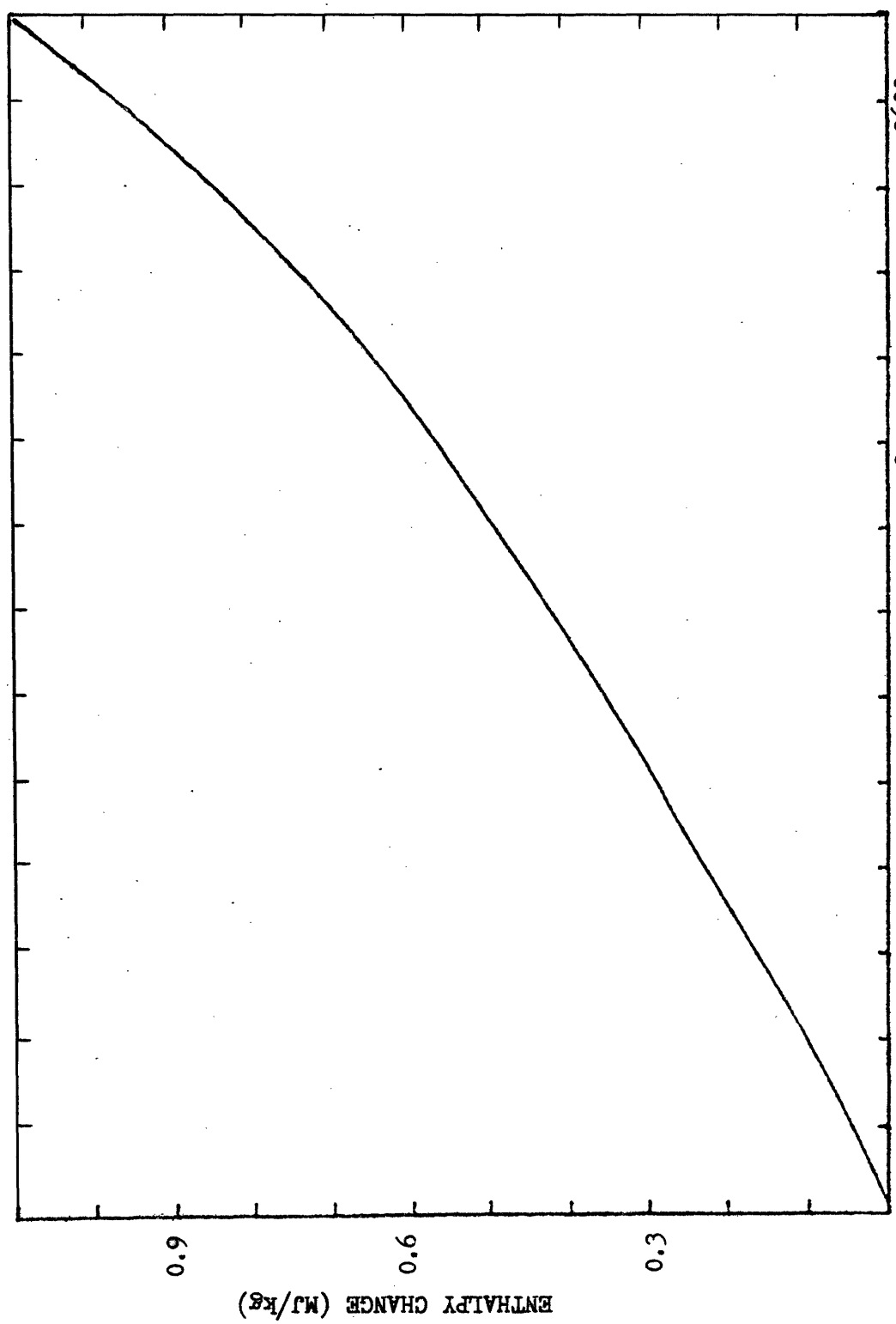

Figure B-6. Enthalpy change correlation for uranium dioxide.

B.5 Cladding Thermal Conductivity

Taken from MATPRO and CENPD-218 (Ref. 16), two correlations for the thermal conductivity of Zircaloy-4 were investigated. MATPRO's version takes the form

$$k_c = 7.51 + 2.09\times10^{-2}T - 1.45\times10^{-5}T^2 + 7.67\times10^{-9}T^3 \qquad \text{(B-13)}$$

where k_c = Zircaloy-4 thermal conductivity in W/m·k

and T = temperature in K.

The relation from CENPD-218 is

$$k_c = 13.959 + 9.8522\times10^{-3}T \qquad \text{(B-14)}$$

where k_c = Zircaloy-4 thermal conductivity in W/m·k

and T = temperature in °C.

The above two conductivities are presented in Fig. B-7. At 300°C the MATPRO conductivity differs by 4.4% from that of CENPD. With increasing temperature, this difference decreases, where at 500°C, the difference is only 1.8%.

To allow for a simple and explicit cladding temperature profile relation, the CENPD thermal conductivity was chosen. The use of the MATPRO thermal conductivity is expected to produce similar results for inside cladding temperature calculations. However, the complexity of the MATPRO relation does not lend itself towards a direct computation of the cladding temperature profile; this made its application unwarranted.

B.6 Cladding Thermal Strain

The correlation used for the cladding thermal strain was taken from MATPRO. For 27 < T < 800°C, the thermal strain relation is

$$\varepsilon_T = -2.373\times10^{-2} + 6.721\times10^{-4}T \qquad \text{(B-15)}$$

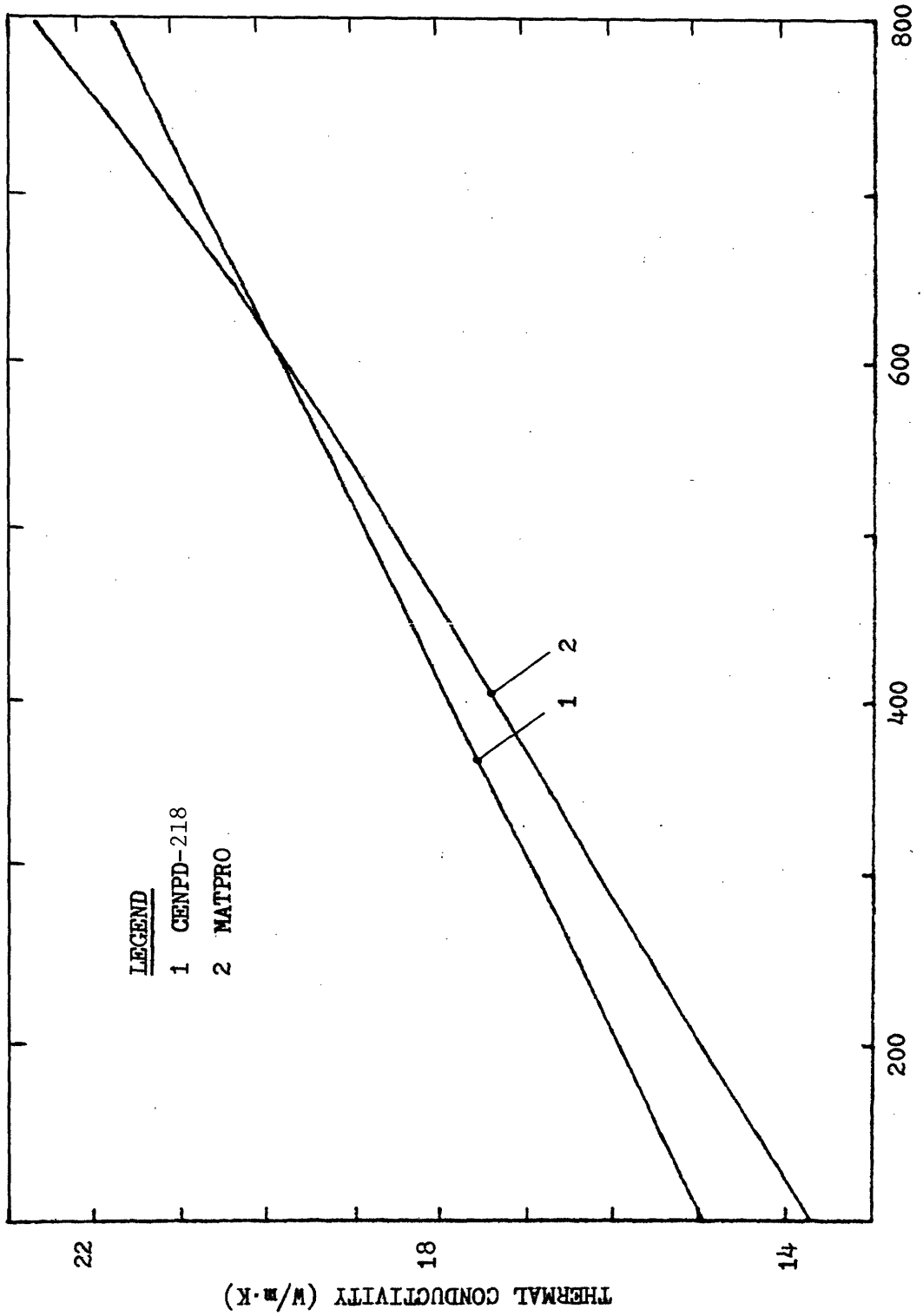

Figure B-7. Comparison of MATPRO and CENPD thermal conductivity for Zircaloy-4.

where ε_T = Zircaloy-4 thermal strain in %

and T = temperature in °C.

The above correlation is presented in Fig. B-8. The root of the thermal strain equation lies at about 35°C.

B.7 Cladding Specific Heat and Enthalpy

From data points supplied by MATPRO, the following equations were derived from linear interpolation for specific heat capacity and enthalpy of Zircaloy-4. These equations may be expressed as

$$(C_p)_c = A + BT \tag{B-16}$$

$$\Delta H_c(T) = C + DT + ET^2 \tag{B-17}$$

where C_p = specific heat capacity of Zircaloy-4 in J/kg·K;

$\Delta H(T)$ = enthalpy change of Zircaloy-4 in MJ/kg;

T = temperature in °C;

and A,B,C,D,E = constant.

The values of A, B, C, D, and E are given in Table B-1. The specific heat of the cladding is plotted in Fig. B-9, and the enthalpy change is presented in Fig. B-10.

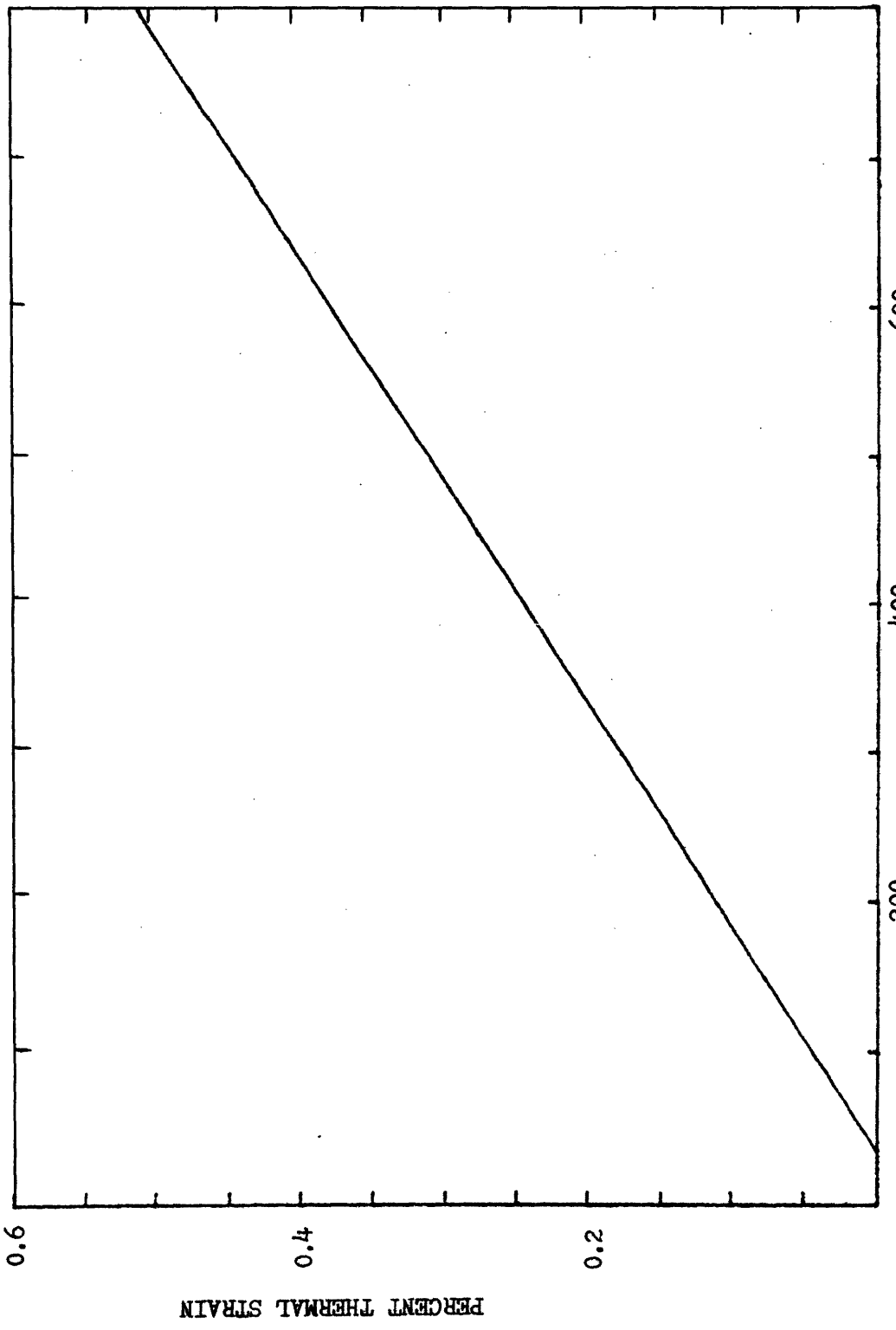

Figure B-8. MATPRO's version of thermal strain for Zircaloy-4.

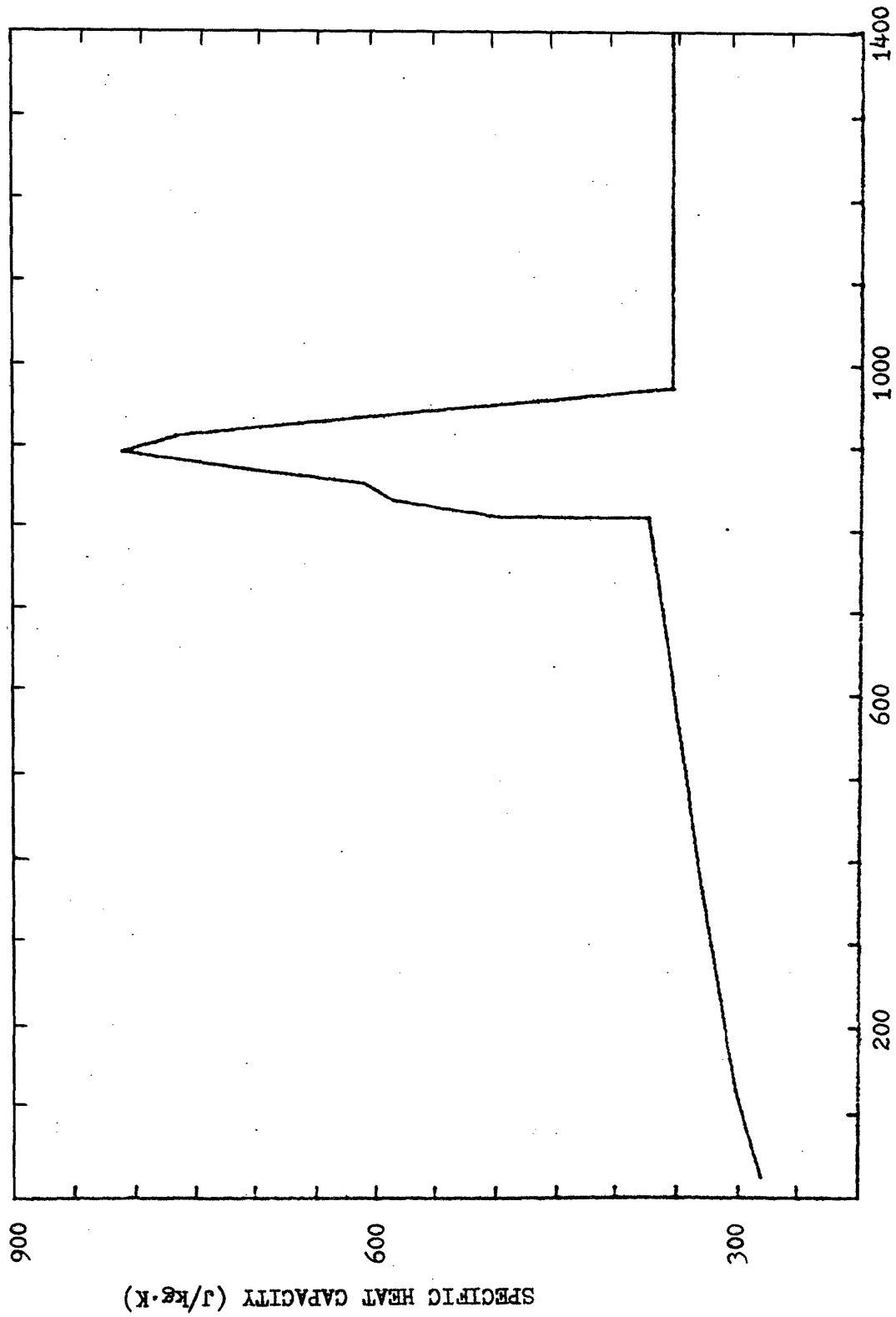

Figure B-9. MATPRO's version of specific heat capacity for Zircaloy-4.

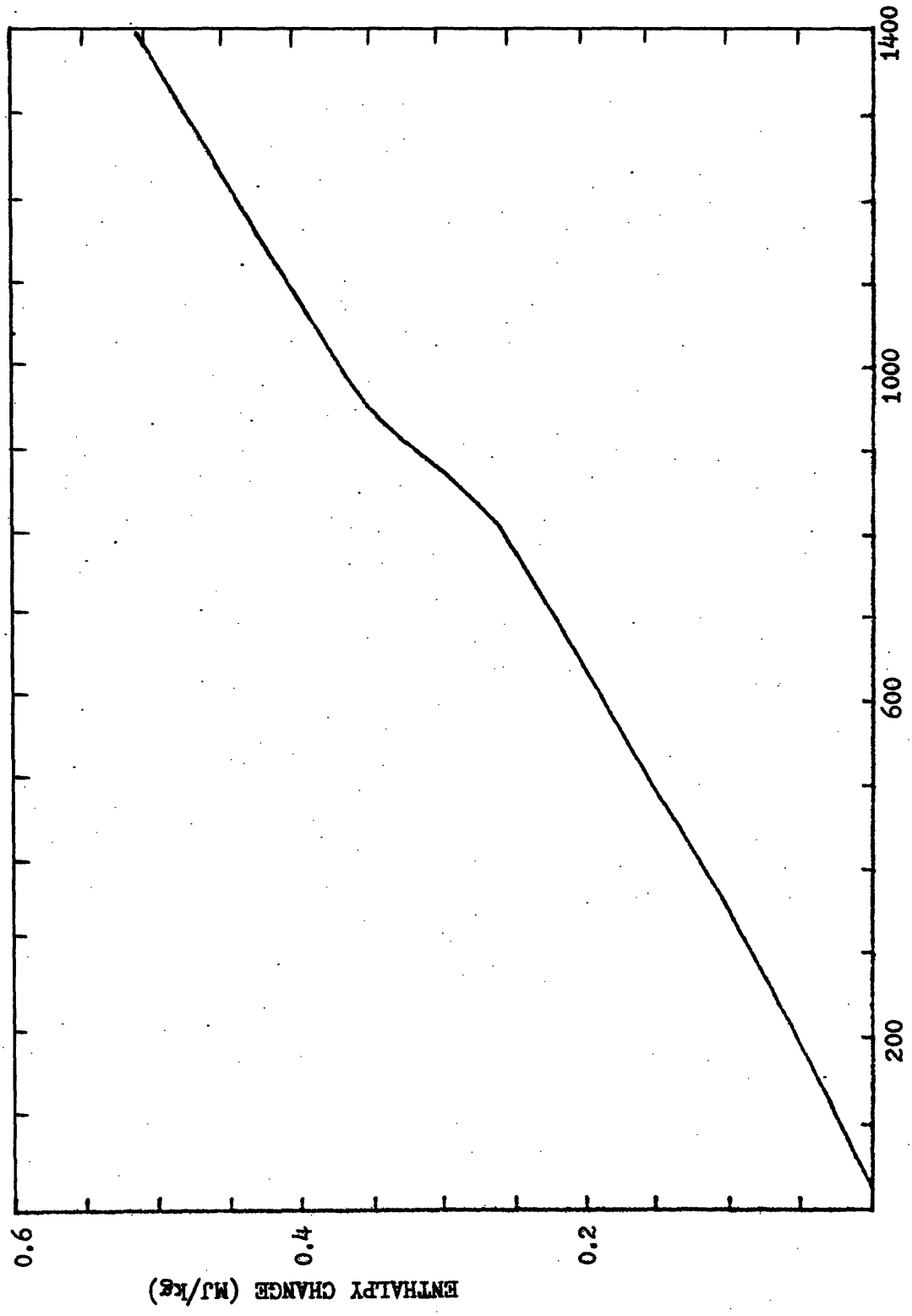

Figure B-10. Enthalpy change correlation for Zircaloy-4.

Table B-1

Constants Used in Specific Heat and Enthalpy Equations for Zircaloy-4 (Eqs. B-16 and B-17)

Range	A	B	C	D	E
$25<T\leq127°C$	275	.21			
$126<T\leq367°C$	287	.121	-7.67×10^{-3}	2.87×10^{-4}	6.04×10^{-8}
$367<T\leq817°C$	295	.0978	-9.23×10^{-3}	2.95×10^{-4}	4.89×10^{-8}
$817<T\leq820°C$	-34200	42.3	14.1	-3.42×10^{-2}	2.12×10^{-5}
$820<T\leq840°C$	- 3110	4.4	1.33	-3.11×10^{-3}	2.2×10^{-6}
$840<T\leq860°C$	- 460	1.25	.222	-4.6×10^{-4}	6.25×10^{-7}
$860<T\leq880°C$	- 3860	5.2	1.68	-3.86×10^{-3}	2.6×10^{-6}
$880<T\leq900°C$	- 3550	4.85	1.55	-3.55×10^{-3}	2.42×10^{-6}
$900<T\leq920°C$	2890	-2.3	-1.35	2.89×10^{-3}	-1.15×10^{-6}
$920<T\leq975°C$	7690	-7.53	-3.56	7.69×10^{-3}	-3.76×10^{-6}
$T\geq975°C$	356	0.0	1.72×10^{-2}	3.56×10^{-4}	0.0

B.8 Thermal Conductivity of Fill Gas

A relation for the thermal conductivity of helium was also taken from MATPRO. The correlation is

$$k_g = 3.366 \times 10^{-3} (T)^{0.668} \qquad \text{(B-18)}$$

where k_g = helium thermal conductivity in W/m·K

and T = temperature in K.

The above equation is plotted in Fig. B-11.

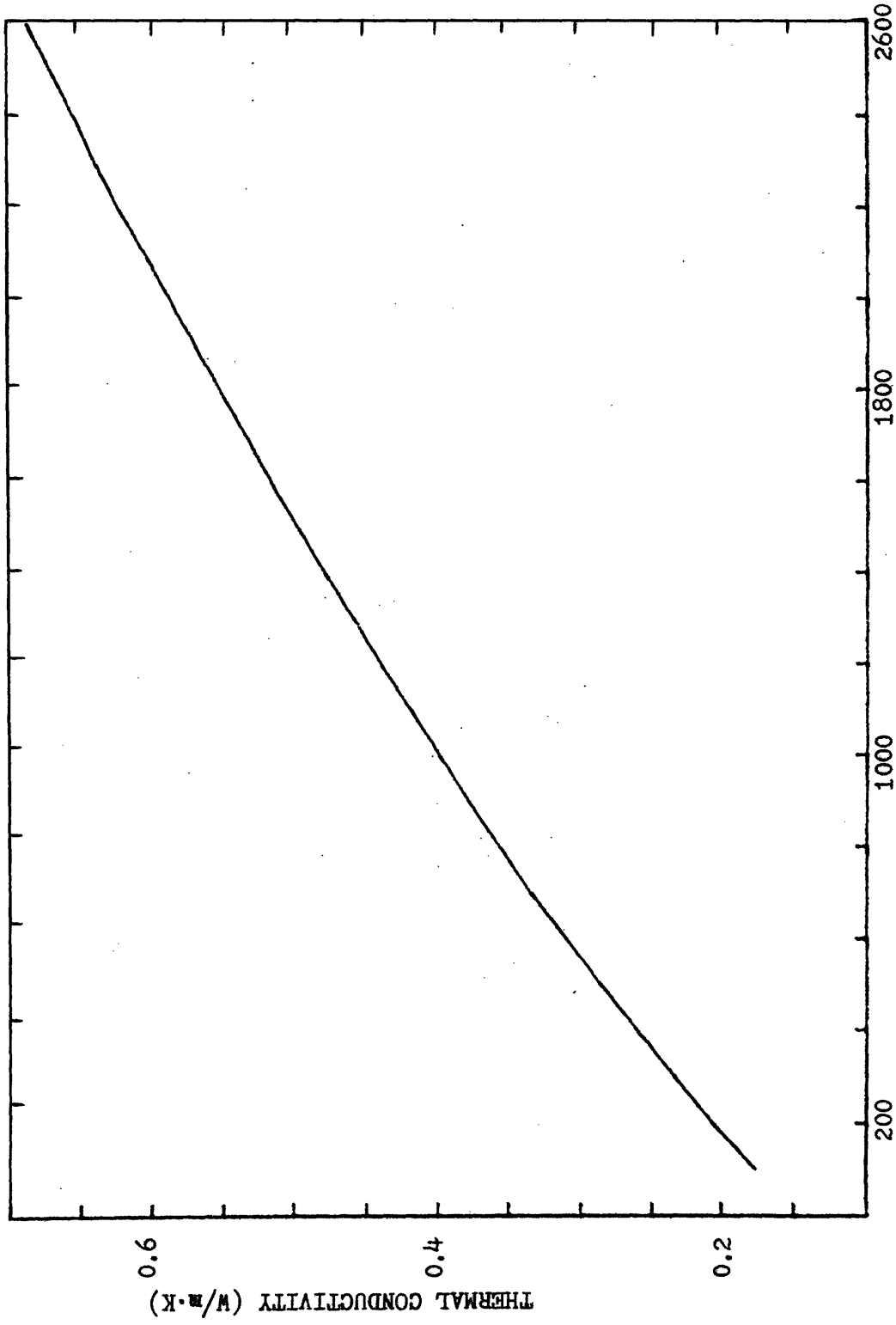

Figure B-11. MATPRO's version of thermal conductivity for helium.

APPENDIX C
INPUT PARAMETERS

The input parameters were supplied by Yankee Atomic Electric Company from base case design and operating data. The data is characteristic of Maine Yankee PWR fuel. However, the conclusions from this study are applicable to other light water reactor fuel.

C.1 General Design Parameters

The following is a list of design features of the Maine Yankee fuel incorporated into this study. In addition, the tolerances on the initial radial gap have been estimated for this study to be ±20 μm (similar to LWBR, Ref. 13, Table 4.2.1-1). Therefore, the nominal and the extreme tolerances are included in the calculations. The diameter of the fuel pellet remained unchanged, whereby the cladding dimensions were altered (at constant thickness) to allow for the differing cold gap widths.

Parameter	Value		
Fuel Density	95% T.D.		
Fill Gas	100% Helium		
Cladding Material	Zircaloy-4		
Fuel-Cladding Surface Roughness (arithmetic mean)	1.5 μm		
Fuel Pellet Radius	4.782 mm		
Cladding Thickness	711 μm	(Nominal)	
Cladding Outside Radius	5.568 mm	5.588 mm	5.608 mm
Cladding Inside Radius	4.857 mm	4.877 mm	4.897 mm
Cold Radial Gap Width	75 μm	95 μm	115 μm

C.2 Outside Cladding Temperature

The following data from Yankee Atomic Electric Company is used in developing an input model for the cladding surface temperature as a function of linear heat generation rate.

Parameter	Value
Active Fuel Length	3.472 m
Core Average LHGR	19.75 kW/m
Average LHGR for Peak Rod (average x 1.45)	28.64 kW/m
Axial Peaking Factor (peak/average)	1.25
Peak LHGR for Peak Rod (28.64x1.25)	35.8 kW/m
System Pressure	15.5 MPa
Fuel Rod Pitch	14.73 mm
Coolant Passage Equivalent Diameter	13.55 mm
Coolant Velocity	4.63 m/sec.
Coolant Inlet Temperature	282°C
Coolant Average Temperature	304°C

Other parameters consistent with the core average temperature at 100% core power are derived below. From enthalpy data which is presented in Fig. C-1, the specific heat capacity of the coolant may be determined (Ref. 17). (All thermodynamic data presented in this Appendix is for water at a pressure of 15 MPa. The error associated with this departure from the system pressure of 15.5 MPa is expected to be insignificant.) Instead of evaluating the specific heat directly at the core average temperature of 304°C, it was decided to make the calculation at the inlet and outlet bulk temperatures. At 100% core power, the temperature rise from the inlet to the core average is equal to the rise from the core average to the bulk outlet temperature for a nominal channel. Thus,

$$(C_p)_w = \frac{\Delta H_w}{\Delta T} \qquad \text{(C-1)}$$

where ΔH_w = H_2O enthalpy rise
= (1.4905 - 1.241) MJ/kg = 0.2495 MJ/kg;

ΔT = H_2O temperature rise
= (326 - 282)°C = 44°C;

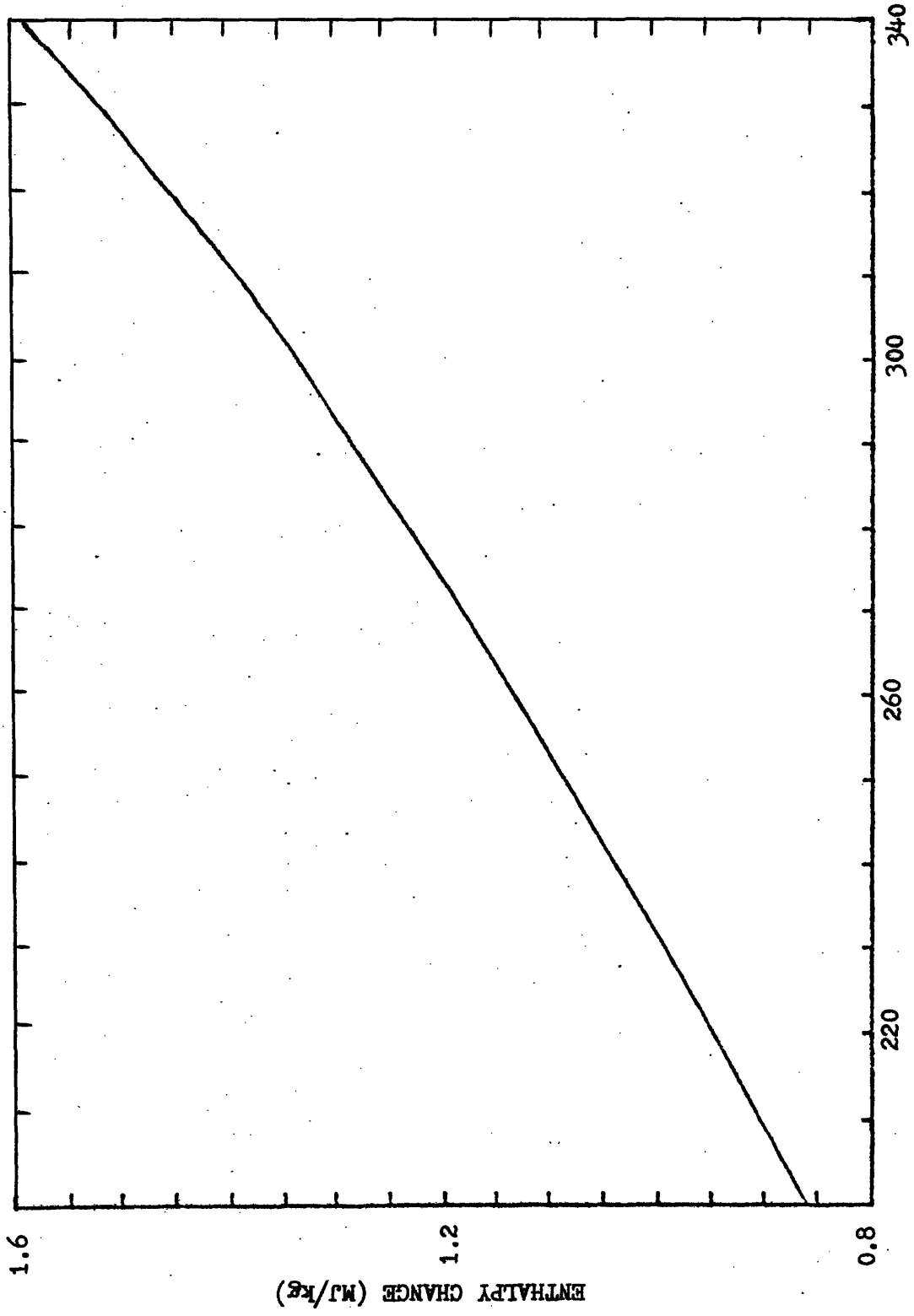

Figure C-1. Correlation for the enthalpy change of water at 15 MPa pressure.

and $(C_p)_w$ = H_2O specific heat = 5.67×10^{-3} MJ/kg·K.

The coolant mass flow rate is also derived for nominal conditions. Here,

$$\dot{m} = \frac{\bar{q}'_{core} \ell}{\Delta H_w} \qquad \text{(C-2)}$$

where $\bar{q}'_{core}$ = core average LHGR = 19.75 kW/m

ℓ = active fuel rod length = 3.472 m;

ΔH_w = H_2O enthalpy rise = 0.2495 MJ/kg;

and $\dot{m}$ = coolant mass flow rate = 0.275 kg/sec.

Using the Dittus-Boelter equation with Maine Yankee and published thermodynamic data, the bulk-cladding heat transfer coefficient may be calculated (Refs. 17,18). Rearranging the Dittus-Boelter equation

$$h = \frac{0.023K^{0.6}}{D_e^{0.2}} (V\rho_w)^{0.8} \left(\frac{(C_p)_w}{(\mu)_w}\right)^{0.4} \qquad \text{(C-3)}$$

for H_2O at 300°C, 15 MPa pressure

where k_w = H_2O thermal conductivity = 0.559 W/m·K;

D_e = equivalent coolant passage diameter = 13.55 mm;

V = coolant velocity = 4.63 m/sec;

ρ_w = H_2O density = 726.2 kg/m^3;

and $(\mu)_w$ = H_2O viscosity = 9.17×10^{-5} kg/m·s results in

h = bulk-cladding heat transfer coefficient = 33.2 kW/m^2·K.

The bulk temperature rise across a coolant channel may be expressed as

$$\Delta T_b = \frac{\bar{q}' \ell}{\dot{m}(C_p)_w} \qquad \text{(C-4)}$$

where $\bar{q}'$ = average LHGR of a fuel rod in the coolant channel
and the other parameters as defined above.
Thus,

$$\Delta T_b = \text{bulk coolant temperature rise} = \left(2.23 \frac{^\circ C}{kW/m}\right) \bar{q}' \qquad \text{(C-5)}$$

The following convention is used for the various linear heat generation rates

$$q'_{hot,max} = 35.80 \text{ kW/m } \left(\frac{\%C.P.}{100}\right) \qquad \text{(C-6)}$$

$$q'_{nominal,max} = 24.69 \text{ kW/m } \left(\frac{\%C.P.}{100}\right) \qquad \text{(C-7)}$$

$$\bar{q}' = q'_{max}/1.25 \qquad \text{(C-8)}$$

where %C.P. = percent core power.

Using Eqs. (C-4) through (C-8), Fig. C-2 displays the coolant behavior as a function of core power with a constant inlet temperature of 282°C and a saturation temperature of 344.8°C.

Correlations for bulk temperature and outside cladding temperature as a function of axial position are given below

$$T_b = T_{b\text{-inlet}} + \tfrac{1}{2} \Delta T_b \left[1 + \frac{\sin\left(\frac{\pi z}{\ell_{ex}}\right)}{\sin\left(\frac{\pi \ell}{2\ell_{ex}}\right)}\right] \qquad \text{(C-9)}$$

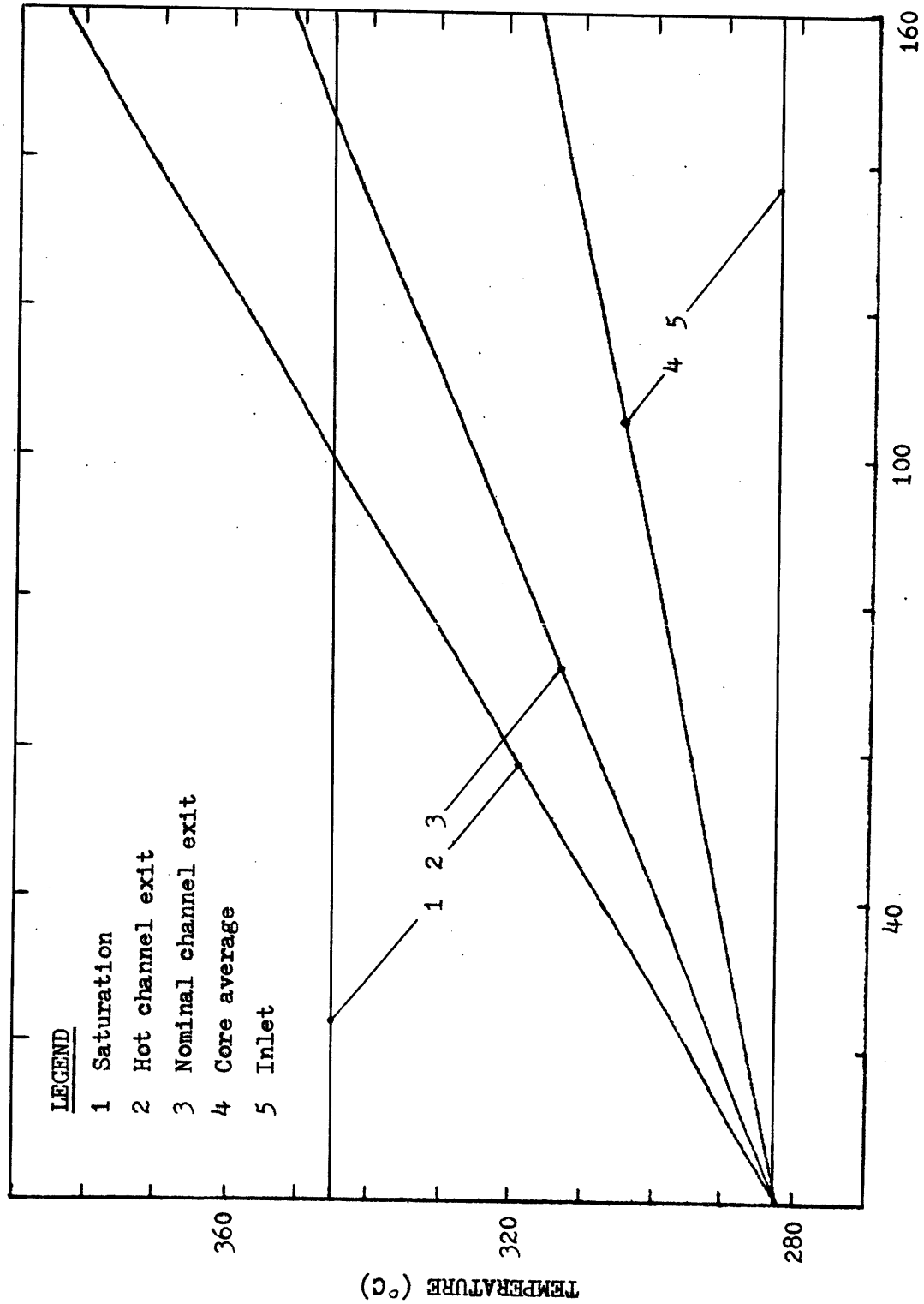

Figure C-2. Behavior of H_2O coolant at a system pressure of 15 MPa.

$$T_o = T_b + \frac{q'_{max}}{2\pi r_o h} \cos\left(\frac{\pi z}{\ell_{ex}}\right) \qquad \text{(C-10)}$$

where z = axial position ($z = 0$ at core midplane);

ℓ = active fuel length;

ℓ_{ex} = extrapolated zero flux fuel length;

h = bulk-cladding heat transfer coefficient;

T_b = bulk coolant temperature;

$T_{b\text{-inlet}}$ = inlet bulk temperature;

ΔT_b = bulk temperature use across channel;

and T_o = cladding outside temperature.

Assuming an axial cosine power distribution and an axial power peaking factor of 1.25, the extrapolated zero flux fuel rod length may be determined by trial and error from the equation

$$\bar{q}' = \frac{q'_{max}}{1.25} = \frac{\int_{-\ell/2}^{\ell/2} q'_{max} \cos\left(\frac{\pi z}{\ell_{ex}}\right) dz}{\int_{-\ell/2}^{\ell/2} dz} \qquad \text{(C-11)}$$

which results in

$$\ell_{ex} = 4.82 \text{ m.}$$

With this value and others previously given, the bulk and outside cladding temperature profiles reduce to

$$T_b = T_{b\text{-inlet}} + \tfrac{1}{2}\,\Delta T_b \left[1 + \frac{\sin(\frac{\pi z}{\ell_{ex}})}{.91}\right] \qquad \text{(C-12)}$$

and

$$T_o = T_b + 0.628\, q'_{max} \cos(\frac{\pi z}{\ell_{ex}}) \qquad \text{(C-13)}$$

where q'_{max} = maximum LHGR of the fuel rod in kW/m.

For conditions when the coolant is undergoing nucleate boiling, the outside cladding temperature is determined by the Jens and Lottes correlation (Ref. 19). For the Maine Yankee Parameters, this relation reduces to

$$(T_o)_{J\&L} = 344.8 + 0.845\, [q'_{max} \cos(\frac{\pi z}{\ell_{ex}})]^{0.25} \qquad \text{(C-14)}$$

where q'_{max} = maximum LHGR in kW/m

and $(T_o)_{J\&L}$ = outside cladding temperature in °C.

Figures C-3 and C-4 show the bulk and outside cladding axial temperature distribution at 100% core power for a nominal fuel rod and a hot fuel rod. At 100% core power, the nominal rod does not undergo nucleate boiling while the hot fuel rod does.

For various core powers, Figs. C-5 and C-6 display the cladding outside temperature as a function of linear heat generation rate for a nominal and hot fuel rod. Superimposed on each figure is the correlation used in the study for the cladding outside temperature. Even though based upon an arbitrary choice, this correlation closely reflects the actual operating conditions. In mathematical terms, the outside cladding temperature correlation is

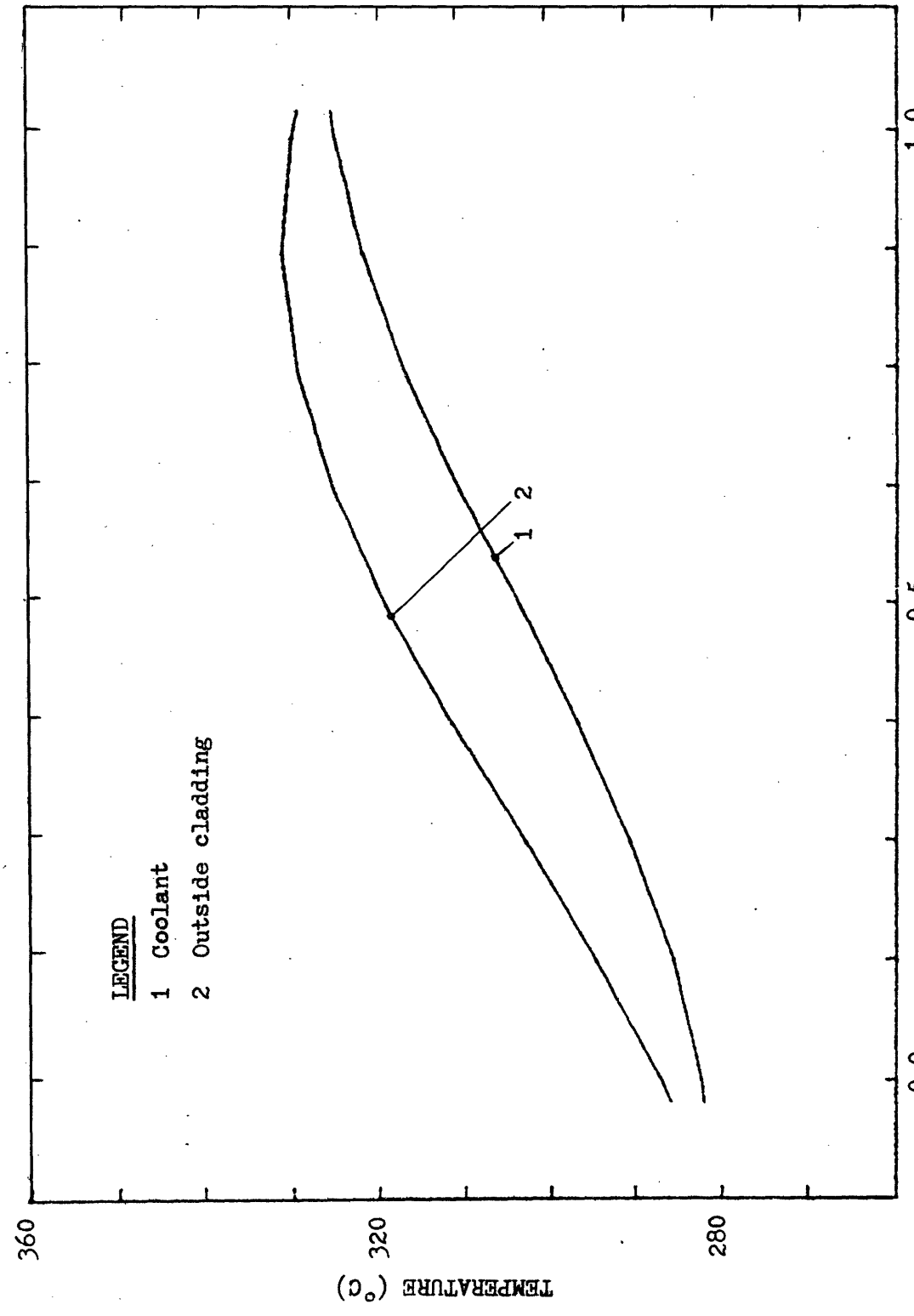

Figure C-3. Behavior of nominal fuel rod at 100% core power.

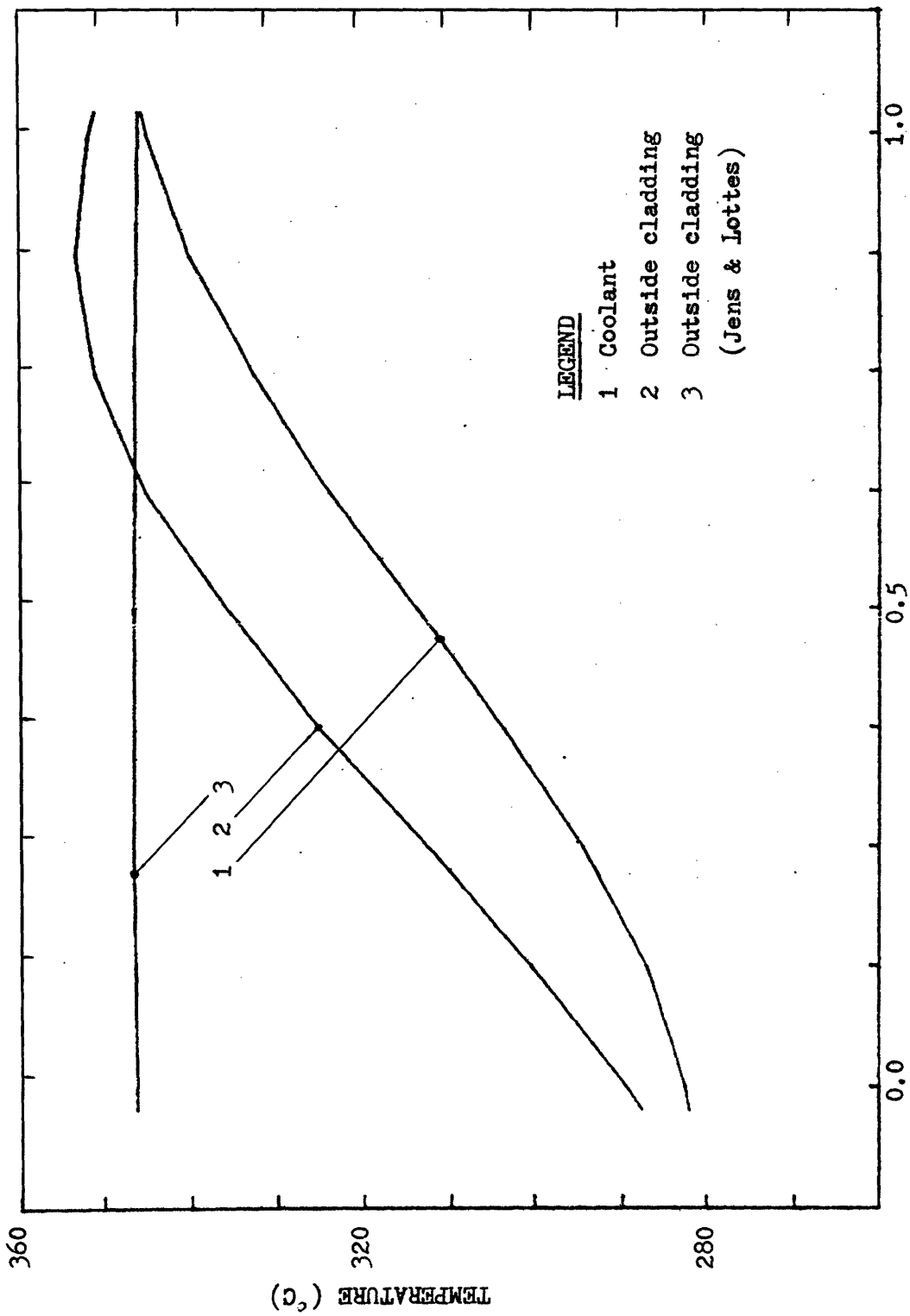

Figure C-4. Behavior of hot fuel rod at 100% core power.

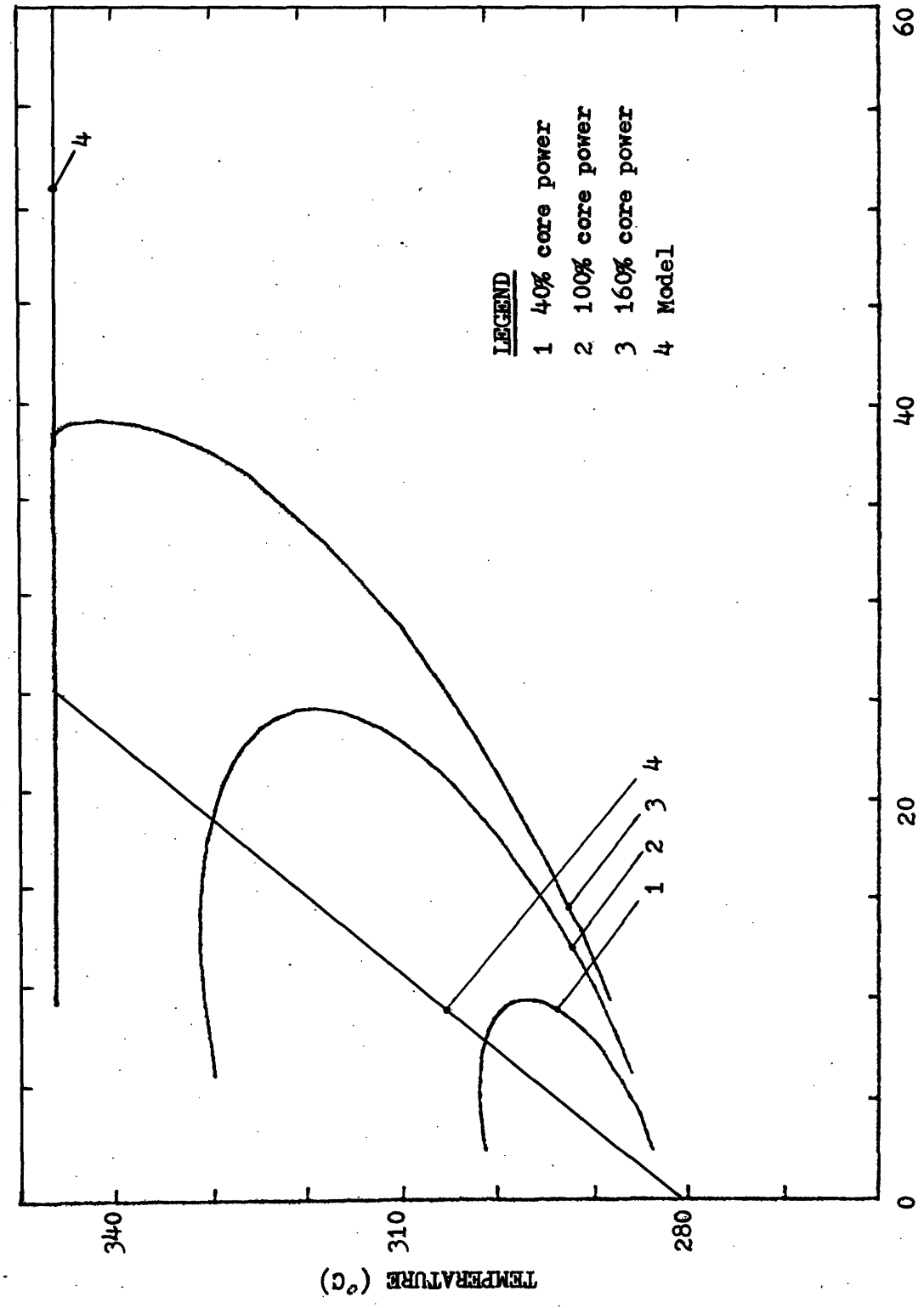

Figure C-5. Comparison of nominal fuel rod outside cladding temperature to modeled outside cladding temperature correlation.

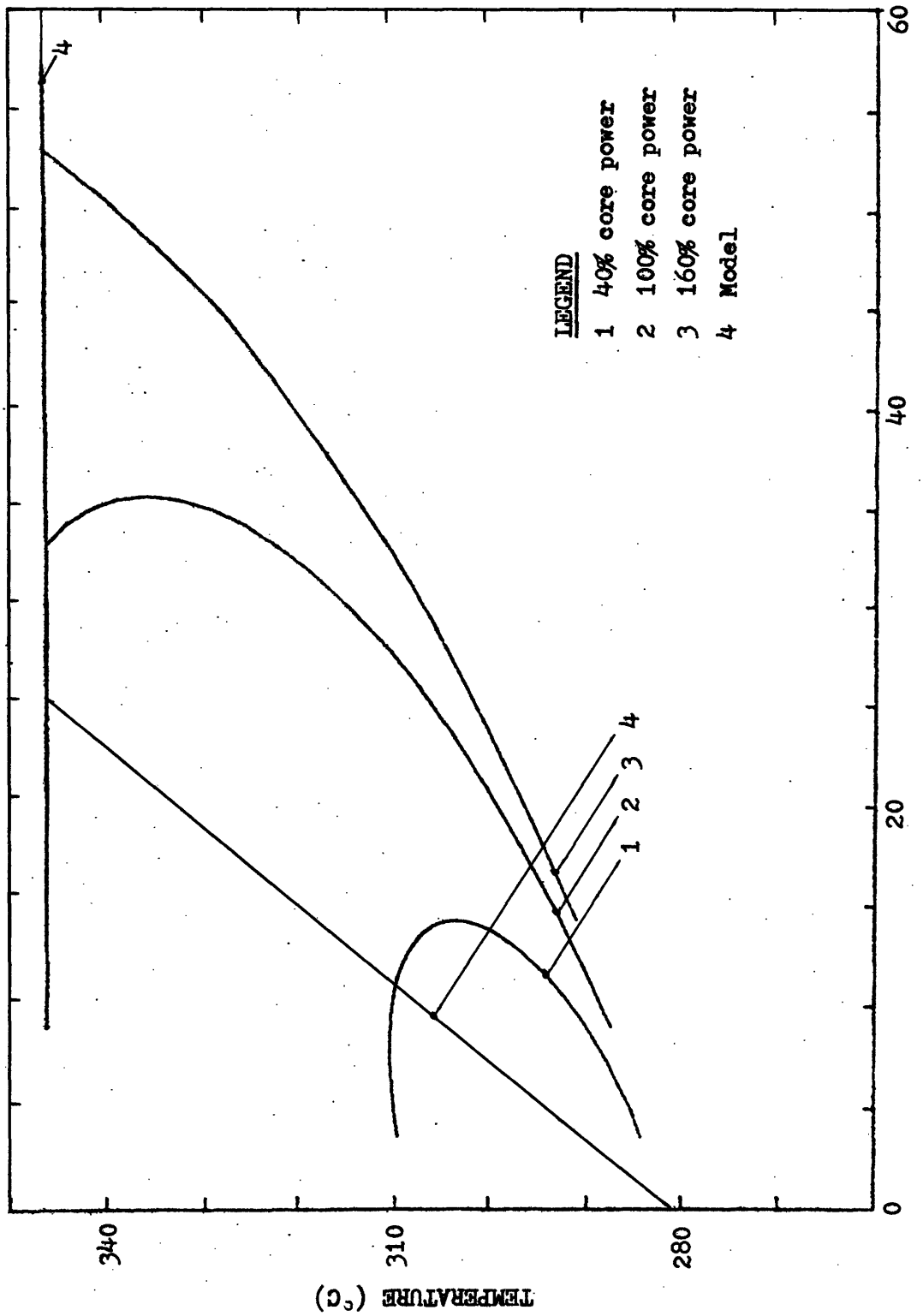

Figure C-6. Comparison of hot fuel rod outside cladding temperature to modeled outside cladding temperature correlation.

$$T_o = 282 + 2.6\ q' \qquad \text{for } 0 \leq q' \leq 25 \text{ kW/m}$$

$$T_o = 347 \qquad \text{for } q' > 25 \text{ kW/m} \qquad \text{(C-15)}$$

where T_o = outside cladding temperature in °C

and q' = LHGR in kW/m.

APPENDIX D
HALDEN FUEL ROD PARAMETERS

This appendix presents the Halden Boiling Water Reactor experimental fuel rod and operating parameters discussed in Chapter 6 (Ref. 20). These parameters also represent the fuel rod conditions inputted to the calculational models.

Parameter	Value
Fuel assembly	IFA-226
Fuel rod	AA
Core active length	1.7 m
Axial power peaking factor	1.2 to 1.7
Coolant	D_2O
System pressure	3.45 MPa
Coolant inlet temperature	237°C
Coolant saturation temperature	240°C
Fill gas	Helium
Fill gas pressure	10.1 kPa
Cladding	Zircaloy-4
Fuel	90.5% UO_2, 9.5% PuO_2
% T.D.	92.1
Cladding outside diameter	10.69 mm
Cladding inside diameter	9.51 mm
Fuel pellet diameter	9.30 mm
Cold radial gap width	105 μm
Burnup	0 - 0.1 MWd/kg U

An outside cladding temperature has again been represented as a two line straight function of linear heat generation rate. Using the Jens-Lottes equation for nucleate boiling (as in Appendix C), the following representation seems reasonable:

$$T_o = 240 + 0.6\ q' \qquad \text{for } 0 \leq q' \leq 25 \text{ kW/m}$$

$$T_o = 255 \qquad \text{for } q' > 25 \text{ kW/m} \qquad \text{(D-1)}$$

where T_o = outside cladding temperature in °C

and q' = LHGR in kW/m.

APPENDIX E

COMPUTER PROGRAM LISTING

A sample listing of input parameters is presented in Table E-1. Not a complete tabulation, this table merely presents an example of the form for inputting data to initialize the computer program. The variable names are explained below.

xmodel = the model designation, 1 being the uncracked model, 2 being the cracked model

den = fractional theoretical density of the fuel

tco = outside cladding temperature in °C

q = linear heat generation rate in kW/m

gapc = cold radial gap width in μm

radco = outside cold clad radius in mm

radci = inside cold clad radius in mm

radfc = cold fuel pellet radius in mm

Table E-2 displays the computer output for one set of input data. The input parameters are listed first which identifies the calculation. These are followed by the parameters computed by the program.

Following Table E-2 is the listing of the Fortran computer program used in this study. For a flow chart of this program see Chapter 2.

xmodel	den	tco	q	gapc	radco	radci	radfc
1.0	0.95	282.0	0.0	115.0	5.608	4.897	4.7815
2.0	0.95	282.0	0.0	115.0	5.608	4.897	4.7815
1.0	0.95	295.0	5.0	115.0	5.608	4.897	4.7815
2.0	0.95	295.0	5.0	115.0	5.608	4.897	4.7815
1.0	0.95	308.0	10.0	115.0	5.608	4.897	4.7815
2.0	0.95	308.0	10.0	115.0	5.608	4.897	4.7815
1.0	0.95	321.0	15.0	115.0	5.608	4.897	4.7815
2.0	0.95	321.0	15.0	115.0	5.608	4.897	4.7815
1.0	0.95	334.0	20.0	115.0	5.608	4.897	4.7815
2.0	0.95	334.0	20.0	115.0	5.608	4.897	4.7815
1.0	0.95	347.0	25.0	115.0	5.608	4.897	4.7815
2.0	0.95	347.0	25.0	115.0	5.608	4.897	4.7815
1.0	0.95	347.0	30.0	115.0	5.608	4.897	4.7815
2.0	0.95	347.0	30.0	115.0	5.608	4.897	4.7815
1.0	0.95	347.0	35.0	115.0	5.608	4.897	4.7815
2.0	0.95	347.0	35.0	115.0	5.608	4.897	4.7815
1.0	0.95	347.0	40.0	115.0	5.608	4.897	4.7815
2.0	0.95	347.0	40.0	115.0	5.608	4.897	4.7815
1.0	0.95	347.0	45.0	115.0	5.608	4.897	4.7815
2.0	0.95	347.0	45.0	115.0	5.608	4.897	4.7815
1.0	0.95	347.0	50.0	115.0	5.608	4.897	4.7815
2.0	0.95	347.0	50.0	115.0	5.608	4.897	4.7815
1.0	0.95	347.0	55.0	115.0	5.608	4.897	4.7815
2.0	0.95	347.0	55.0	115.0	5.608	4.897	4.7815
1.0	0.95	347.0	60.0	115.0	5.608	4.897	4.7815
2.0	0.95	347.0	60.0	115.0	5.608	4.897	4.7815

Table E-1. Sample list of input data for comparative study computer program.

```
  model 1 traditional model 2 cracked this is 2.0
fractional density = 0.9500
outside clad temp =  347.00  c
linear heat generation rate =  40.00  kw per m
cold gap width =  95.00  um
outside cold clad radius =  5.588  mm
inside cold clad radius = 4.877  mm
cold pellet radius = 4.781  mm
inside clad temp = 396.15  c
fuel surface temp = 419.54  c
fuel centerline temp = 1749.62  c
hot fuel radius =  4.829  mm
hot gap width =  58.890  um
percent pellet contact =  30.449
fractional radius for equiaxed grain growth =        0.456752
fractional radius for columnar grain growth =        0.164658
fuel rod equivalent temperature =  891.86  c
```

Table E-2. Sample output from comparative study computer program.

```
c     STEADY STATE UO2 FUEL PELLET TEMPERATURE PROFILE PROGRAM
c
c                        Written by John Maki
c
c                             March 1978
c
c                              M.I.T.
c
c
c        This program calculates clad inside temp,fuel surface temp,
c        fuel centerline temp, hot gap width, hot pellet radius, fractional
c        radius for equiaxed and columnar grain growth, and fuel rod
c        equivalent temperature.
c
c         Two models are used.  Model 1 uses the traditional gap conductance
c         k/GAP,  and UO2 conductivity as the fuel conductivity.
c         Model 2 uses cracked pellet relations for gap conductance
c         and fuel conductivity.
c
c
c
c         Reading in and writing input parameters.
c
       dimension tem2(50)
 100   read(5,110,end=999)xmodel,den,tco,q,gapc,radco,radci,radfc
c
c
c     xmodel is the model number described above
c          1.0 = traditional
c          2.0 = cracked
c     den = fractional fuel  density
c     tco = outside clad temperature in degrees C
c     q = linear heat generation rate in kw/m
c     gapc = cold gap width in um
c     radco = outside cold clad radius in mm
c     radci = inside cold clad radius in mm
c     radfc = cold fuel pellet radius in mm
```

```
c
 110    format(8f10.4)
        write(6,120)xmodel,den,tco,q,sarc,radco,radci,radfc


 120    format("0","  model 1 traditional model 2 cracked this is",f4.1/
     1 "0","fractional density =",f7.4/"0",
     1 "outside clad temp =",f8.2,2x,"c"/"0",
     1 "linear heat generation rate = ",f6.2,2x,"kw per m"/"0",
     1 "cold gap width = ",f6.2,2x,"um"/"0",
     1 "outside cold clad radius = ",f6.3,2x,"mm"/"0",
     1 "inside cold clad radius =",f6.3,2x,"mm"/"0",
     1 "cold pellet radius =",f6.3,2x,"mm")
c
c            Calculating clad inside temp and clad thermal strain.
c
        tci=-1.015e5*(1.3959e-2-sqrt(1.9485e-4+1.9704e-5*
     1(1.3959e-2*tco+4.9261e-6*tco**2.+.159155*q*alog(radco/radci))))
        radcoh=radco
        radcih=radci
 130    radcip=radcih
        delrc=(radcoh-radcih)/25.
        sum0=0.
        do 140 k=1,24
        radc=(25.-k)*delrc+radcih
        elsr=6.721e-6*temcd(q,radcoh,tco,radc)-2.373e-4
 140    sum0=sum0+radc*elsr
        elc=((6.721e-6*tco-2.373e-4)*radcoh+(6.721e-6*tci-
     1  2.373e-4)*radcih+2.*sum0)*(delrc/2.)*(2./(radcoh**2.-
     1  radcih**2.))
        radcoh=radco*(1.+elc)
        radcih=radci*(1.+elc)
        difx=abs(radcih-radcip)
        if(difx .ge. .0005) goto 130
```

```
c
c            Calculating claddins stored heat.
c
        delc=(radcoh-radcih)/25.
        sumc=0.
        do 150 i=1,24
        radc=(25.-i)*delc+radcih
        tempc=temcd(a,radcoh,tco,radc)
        if(tempc .lt. 367.)hc=-7670.+287.*tempc+6.04e-2*tempc**2.
        if(tempc .ge. 367.)hc=-9230.+295.*tempc+4.89e-2*tempc**2.
 150    sumc=sumc+radc*hc
        if(tco .lt. 367.)hco=-7670.+287.*tco+6.04e-2*tco**2.
        if(tco .ge. 367.)hco=-9230.+295.*tco+4.89e-2*tco**2.
        if(tci .lt. 367.)hci=-7670.+287.*tci+6.04e-2*tci**2.
        if(tci .ge. 367.)hci=-9230.+295.*tci+4.89e-2*tci**2.
        hrad=(radcoh*hco+radcih*hci+2.*sumc)*(delc/2.)
        shclad=(1.31e-5)*hrad
c
c             Initalizing outer iterative loop.
c
        tf=tci
        radfuh=radfc
        saph=sapc
        if(xmodel .le. 1.) goto 300
c
c
c     Main program for model 2
c
c
 200    saphp=saph
```

```
c
c              Calculating fuel surface temp for model 2.
c
        call gap2(q,radfuh,gaph,tci,tf)
c
c              Calculating fuel centerline temp and temp profile for model 2.
c
        do 205 i=1,50
 205    tem2(i)=0.
        delr=radfuh/50.
        tn=tf
        rn=radfuh
        do 210 J=1,50
        hek=3.366e-6*(tn+273.15)**.668
        x=(.11316*den)/(2.-den+10.*(1.-den)**2.)
        uo2k=x*(38.24/(402.4+tn)+6.12e-13*(tn+273.)**3.)
        fk=uo2k*(1./((1.0e-3*gaph-3.175e-2)/(radfuh*((.077*hek)/
     1  uo2k+.015))+1.))
        tem2(J)=tn+(q*rn*delr)/(fk*6.2832*radfuh**2.)
        rn=rn-delr
 210    tn=tem2(J)
        tcl=tem2(50)

c
c              Calculating hot fuel radius and hot gap width for model 2.
c
        sum2=0.
        do 215 i=1,49
        radf=(50.-i)*delr
        elst=-4.972e-4+7.107e-6*tem2(i)+2.581e-9*(tem2(i))**2.+
     1  1.14e-13*(tem2(i))**3.
 215    sum2=sum2+radf*elst
        elf=(radfuh*(-4.972e-4+7.107e-6*tf+2.581e-9*tf**2.+
     1  1.14e-13*tf**3.)+2.*sum2)*(delr/2.)*(2./radfuh**2.)
        gaph=gapc+1.0e3*radci*elc-1.0e3*radfc*elf
        if(gaph .lt. 1.5) gaph=1.5
        radfuh=radfc*(1.+elf)
```

```
c
c            Testing for hot gap width convergence in model 2.
c
      diff=abs(gaph-gaphp)
      if(diff .ge. 0.05) goto 200
c
c            Percent of pellet lying against cladding.
c
      perf=30.+100./((100.*((.1*gaph)/radfuh)**4.)+1.429)

c
c            Calculating grain growth regions for model 2.
c
      if(tc1 .lt. 1400.) goto 240
      do 220 k=1,50
      J2=k+1
      a2=J2
      if(tem2(k) .lt. 1400. .and. tem2(J2) .ge. 1400.) goto 225
 220  continue
 225  gge=(50.-a2)/50.+((tem2(J2)-1400.)/(tem2(J2)-
     1 tem2(k)))/50.
      if(tc1 .lt. 1700.) goto 245
      do 230 k2=1,50
      J3=k2+1
      a3=J3
      if(tem2(k2).lt. 1700. .and.tem2(J3).ge. 1700.) goto 235
 230  continue
 235  ggc=(50.-a3)/50.+((tem2(J3)-1700.)/(tem2(J3)-
     1 tem2(k2)))/50.
      goto 250
 240  gge=100.
 245  ggc=200.
 250  continue
```

```
c
c              Calculating fuel stored heat for model 2.
c
        sum=0.
        do 255 i=1,49
        rad=(50.-i)*delr
        temk=tem2(i)+273.15
 255    sum= sum+rad*(1.58803e5*(1./(exp(535.285/temk)-1.))
     1   +1.216e-2*(temk**2.)-3.2705e4+8.7455e7*exp(-1.8971e4/temk))

        tfk=tf+273.15
        trap50=radfuh*(1.58803e5*(1./(exp(535.285/tfk)-1.))
     1   +1.216e-2*(tfk**2.)-3.2705e4+8.7455e7*exp(-1.8971e4/tfk))

        trap=(trap50+2.*sum)*(delr/2.)
        sh=den*2.196e-5*trap
        tmay=tf
        goto 400
c
c
c      Main program for model 1
c
c
 300    saphp=saph
c
c              Calculating fuel surface temp for model 1.
c
        call sap1 (a,radfuh,saph,tci,tf)
c
c              Calculating fuel centerline temp for model 1.
c
        cintcl=cints(tf,den)+a*7.9577e-2
        x=((2.-den+10.*(1.-den)**2.)/(1.1316*den))*cintcl
        tcl=temp1(x)
```

```
c
c               Calculating hot fuel radius and hot gap width for model 1.
c
        del=radfuh/50.
        sum4=0.
        xint=cintg(tf,den)
        do 310 i=1,49
        radf=(50.-i)*del
        gint=g*7.9577e-2*(1.-(radf/radfuh)**2.)+xint
        x=(gint*(2.-den+10.*(1.-den)**2.))/(1.1316*den)
        tin=temp1(x)
        elst=-4.972e-4+7.107e-6*tin+2.581e-9*tin**2.+
     1  1.14e-13*tin**3.
 310    sum4=sum4+radf*elst
        elf=(radfuh*(-4.972e-4+7.107e-6*tf+2.581e-9*tf**2.+
     1  1.14e-13*tf**3.)+2.*sum4)*(del/2.)*(2./radfuh**2.)
        gaph=gapc+1.0e3*radci*elc-1.0e3*radfc*elf
        if(gaph .lt. 1.5) gaph=1.5
        radfuh=radfc*(1.+elf)
c
c               Testing for hot gap width conversence in model 1.
c
        diff=abs(gaph-gaphp)
        if(diff .ge. 0.05) goto 300
```

```
c
c               Percent of pellet lying against claddings.
c
        if(garh .le. 1.5) perf=100.
        if(garh .gt. 1.5) perf=0.0
c
c               Calculating grain growth regions for model 1.
c
        if(tcl .lt. 1400.) goto 320
        gge=sqrt((cintg(tcl,den)-cintg(1400.,den))/(cintg(
     1tcl,den)-cintg(tf,den)))
        if(tcl .lt. 1700.) goto 330
        ggc=sqrt((cintg(tcl,den)-cintg(1700.,den))/(cintg(
     1tcl,den)-cintg(tf,den)))
        goto 340
 320    gge=100.
 330    ggc=200.
 340    continue
c
c
c               Calculating fuel stored heat for model 1.
c
        h=radfuh/50.
        sum=0.
        do 350 i=1,49
        radx=(50.-i)*h
 350    sum= sum+fx1(a,tco,tf,radfuh,den,radx)
        trap=(fx1(a,tco,tf,radfuh,den,radfuh)+2.*sum)*(h/2.)
        sh=den*2.196e-5*trap
```

```
c
c              Calculating fuel rod equivalent temperature.
c
        tmay=tf
 400    tre=tmay
        trek=tre+273.15
        hfuel=(1.098e-5*den)*(158803./(exp(535.285/trek)-1.)+
     1  1.216e-2*trek**2.+8.7455e7*exp(-18971./trek)-3.2705e4)
        cpfuel=(1.098e-5*den)*((8.5005e7*exp(535.285/trek))/
     1  ((trek**2.)*(exp(535.285/trek)-1.)**2.)+2.432e-2*trek+
     1  (1.6591e12*exp(-18971./trek))/(trek**2.))
        if(tre .lt. 367.)hclad=6.55e-6*(-7670.+287.*tre+6.04e-2*tre**2.)
        if(tre .lt. 367.) cpclad=6.55e-6*(287.+.121*tre)
        if(tre .lt. 817. .and. tre .ge. 367.)hclad=6.55e-6*
     1  (-9230.+295.*tre+4.89e-2*tre**2.)
        if(tre .lt. 817. .and. tre .ge. 367.)cpclad=6.55e-6*
     1  (295.+.0978*tre)
        if(tre .lt. 820. .and. tre .ge. 817.)hclad=6.55e-6*
     1  (1.41e7-3.42e4*tre+21.2*tre**2.)
        if(tre .lt. 820. .and. tre .ge. 817.)cpclad=6.55e-6*
     1  (-3.42e4+42.3*tre)
        if(tre .lt. 840. .and. tre .ge. 820.)hclad=6.55e-6*
     1  (1.33e6-3.11e3*tre+2.2*tre**2.)
        if(tre .lt. 840. .and. tre .ge. 820.)cpclad=6.55e-6*
     1  (-3.11e3+4.4*tre)
```

```
      if(tre .lt. 860. .and. tre .ge. 840.)hclad=6.55e-6*
     1(2.22e5-460.*tre+.625*tre**2.)
      if(tre .lt. 860. .and. tre .ge. 840.)cpclad=6.55e-6*
     1(-460.+1.25*tre)
      if(tre .lt. 880. .and. tre .ge. 860.)hclad=6.55e-6*
     1(1.68e6-3.86e3*tre+2.6*tre**2.)
      if(tre .lt. 880. .and. tre .ge. 860.)cpclad=6.55e-6*
     1(-3.86e3+5.2*tre)
      if(tre .lt. 900. .and. tre .ge. 880.)hclad=6.55e-6*
     1(1.55e6-3.55e3*tre+2.42*tre**2.)
      if(tre .lt. 900. .and. tre .ge. 880.)cpclad=6.55e-6*
     1(-3.55e3+4.85*tre)
      if(tre .lt. 920. .and. tre .ge. 900.)hclad=6.55e-6*
     1(-1.35e6+2.89e3*tre-1.15*tre**2.)
      if(tre .lt. 920. .and. tre .ge. 900.)cpclad=6.55e-6*
     1(2.89e3-2.3*tre)
      if(tre .lt. 975. .and. tre .ge. 920.)hclad=6.55e-6*
     1(-3.56e6+7.69e3*tre-3.76*tre**2.)
      if(tre .lt. 975. .and. tre .ge. 920.)cpclad=6.55e-6*
     1(7.69e3-7.53*tre)
      if(tre .ge. 975.)hclad=6.55e-6*(1.72e4+356.*tre)
      if(tre .ge. 975.) cpclad=6.55e-6*356.
      tfun=hfuel*(radfuh**2.)+hclad*(radcoh**2.-radcih**2.)-sh-shclad
      bfun=cpfuel*(radfuh**2.)+cpclad*(radcoh**2.-radcih**2.)
      tmay=tre-(tfun/bfun)
      diffe=abs(tmay-tre)
      if(diffe .ge. 0.05) goto 400
```

```
c
c
c       When fractional radius for equiaxed grain growth equals 100.00
c            the pellet does not exceed 1400.0 C
c
c
c       When fractional radius for columnar grain growth equals 200.00
c              the pellet does not exceed 1700.00 C
c
c
c
c               Writing out calculated values.
c
 410    write(6,420)tci,tf,tcl,radfuh,gaph,perf,gge,ggc,tmay
 420    format("0","inside clad temp =",f7.2,2x,"c"/"0",
     1 "fuel surface temp =",f7.2,2x,"c"/"0",
     1  "fuel centerline temp =",f8.2,2x,"c"/
     1 "0","hot fuel radius =",f8.3,2x,"mm"/
     1"0","hot gap width =",f8.3,2x,"um"/"0",
     1 "percent pellet contact =",f8.3,/"0",
     1 "fractional radius for equiaxed grain growth =",f15.6/"0",
     1 "fractional radius for columnar grain growth =",f15.6/"0",
     1 "fuel rod equivalent temperature =",f9.2,2x,"c",/"0"/"0"/"0"/"0")
```

```
c
c              Returning to read new set of input parameters.
c
       goto 100
 999   continue
       end
c
c
c   Listing of functions and subroutines
c
c
c
c              This function calculates claddins temperature profile.
c
       function temcd(q,radcoh,tco,radc)
       xmo=.159155*q*alog(radcoh/radc)+4.9261e-6*tco**2.
       sre=sqrt(1.9485e-4+1.9704e-5*(1.3959e-2*tco+xmo))
       temcd=-1.015e5*(1.3959e-2-sre)
       return
       end
c
c            This function is used in the fuel stored heat
c            calculation of model 1.
c
       function fx1(q,tco,tf,radfuh,den,rad)
       ere=38.24*alog(1.+(tf/402.4))
       boox=0.1*(ere+1.53e-13*(tf+273.)**4.-8.5e-4)
       booy=q*7.9577e-2*(1.-(rad/radfuh)**2.)
       z=(booy*(2.-den+10.*(1.-den)**2.))/(1.1316*den)+boox
       if(z .le. 3.441) goto 500
       if(z .le. 4.814) goto 510
       if(z .lt. 5.866) goto 520
       if(z .lt. 6.783) goto 530
       if(z .lt. 7.723) goto 540
       goto 550
 500   top=26.68+72.42*z+26.08*z**2.
       goto 560
```

```
 510     tor=126.7+12.82*z+35.01*z**2.
         goto 560
 520     tor=40.26+46.48*z+31.75*z**2.
         goto 560
 530     tor=274.13*z-603.9+12.43*z**2.
         goto 560
 540     tor=604.12*z-1750.15-11.91*z**2.
         goto 560
 550     tor=822.27*z-2589.9-26.08*z**2.
 560     continue
         trad=tor+273.15
         yo=158803./(exp(535.285/trad)-1.)+1.216e-2*trad**2.
     1   +8.7455e7*exp(-1.8971e4/trad)-3.2705e4
         fx1=rad*yo
         return
         end
c
c              This function calculates the conductivity integral
c              for use in model 1.
c
         function cints(t,den)
         pre=(0.11316*den)/(2.-den+10.*(1.-den)**2.)
         cints=pre*(38.24*alog(1.+(t/402.4))
     1   +1.53e-13*(t+273.)**4.-8.5e-4)
         return
         end
c
c              This subroutine calculates the fuel surface temp for model 1.
c
         subroutine sar1 (q,radfuh,saph,tci,tf)
 600     tfp=tf
         hek=3.366e-6*(((tf+tci)/2.+273.15)**.668)
         tf=tci+(1.59155e-4*q*(saph+1.5))/(radfuh*hek)
         diff=abs(tf-tfp)
         if(diff .ge. .05) goto 600
         return
         end
```

```
c
c            This subroutine calculates the fuel surface temp for model 2.
c
      subroutine sap2(q,radfuh,saph,tci,tf)
 700  tfp=tf
      hek=3.366e-6*(((tf+tci)/2.+273.15)**.668)
      f=.3+1./(100.*((.1*saph)/radfuh)**4.+1.429)
      hs=(hek*(1.-f))/(saph+1.5)+(hek*f)/1.5
      tf=tci+(1.59155e-4*q)/(radfuh*hs)
      diff=abs(tf-tfp)
      if(diff .se. .05) soto 700
      return
      end
c
c            This function calculates the fuel temp profile for model 1.
c
      function temp1(x)
      if(x .le. 3.441) soto 800
      if(x .le. 4.814) soto 810
      if(x .lt. 5.866) soto 820
      if(x .lt. 6.783) soto 830
      if(x .lt. 7.723) soto 840
      soto 850
 800  temp1=26.68+72.42*x+26.08*x**2.
      soto 860
 810  temp1=126.7+12.82*x+35.01*x**2.
      soto 860
 820  temp1=40.26+46.48*x+31.75*x**2.
      soto 860
 830  temp1=274.13*x-630.9+12.43*x**2.
      soto 860
 840  temp1=604.12*x-1750.15-11.91*x**2.
      soto 860
 850  temp1=822.27*x-2589.9-26.08*x**2.
 860  continue
      return
      end
```

APPENDIX F

TABLE OF SYMBOLS

Symbol	Quantity	Units	Defining Equation
T	temperature	°C,K	
r	radius	m	
δ	radial gap width	m	
δ'	root mean square cladding-fuel surface roughness	m	
%T.D.	percent theoretically dense UO_2	none	
D	fractional theoretical dense UO_2	none	
P	fractional porosity of fuel pellet	none	
PF	UO_2 porosity factor (normalized to 95% T.D.)	none	(B-2) (B-5)
k	thermal conductivity	W/m·K	
k_e	effective UO_2 thermal conductivity	W/m·K	(4-10)
M	mesh interval	m	(2-5)
ε_T	thermal strain	none	
$\bar{\varepsilon}_T$	average thermal strain	none	(2-4) (2-8)
x	fuel burnup	MWd/kgU	
F_b	burnup factor	none	(4-5)
F	fraction of circumferential cracked pellet to cladding contact	none	(4-5)
h_o	zero contact pressure gap conductance	$W/m^2 \cdot K$	(4-2)
h_c	contact gap conductance	$W/m^2 \cdot K$	(4-2)

h_g	gap conductance	$W/m^2 \cdot K$	(4-2) (3-2)
ρ	density	kg/m^3	
C_p	constant pressure specific heat capacity	$J/kg \cdot K$	
ΔH	enthalpy change	J/kg	
SH	stored heat	J/m	(2-7) (2-9)
$(SH)_{eq}$	constant temperature stored heat	J/m	(2-11) (2-12)
f(T)	equivalent fuel rod temperature function	J/m	(2-13)
f'(T)	derivative of the function f(T) with respect to temperature	$J/m \cdot K$	(2-15)
T_{eq}	equivalent fuel rod temperature	°C	(2-10)
%C.P.	percent core power	none	
q'''	rate of heat deposition per unit volume	W/m^3	
q'(LHGR)	linear heat generation rate	W/m	
D_e	equivalent coolant passage diameter	m	
z	fuel rod axial position	m	
ℓ	active fuel rod length	m	
ℓ_{ex}	extrapolated zero flux fuel rod length	m	
v	coolant velocity along fuel rods	m/s	
$(\mu)_w$	core average H_2O viscosity	$kg/m \cdot s$	
$\dot{m}$	core average coolant mass flow rate	kg/s	(C-2)
h	bulk coolant to cladding heat transfer coefficient	$W/m^2 \cdot K$	(C-3)

ΔT_b	bulk coolant temperature rise across fuel channel	°C	(C-4)
T_b	bulk coolant temperature along fuel rod	°C	(C-9)
$(T_o)_{J\&L}$	outside cladding temperature for the onset of nucleate boiling	°C	(C-14)

Subscripts

w	H_2O
g	fill gas
c	cladding
f	fuel
o	outside cladding
1	inside cladding
2	fuel pellet surface
52	fuel pellet centerline
n	radial increment index

REFERENCES

1. M. Ishida and L. Hosokawa, "Light Water Reactor Fuel Rod Modeling Study at Hitachi, Ltd.", oral presentation at an EPRI sponsored meeting on Fuel Rod Modeling, April 1977.

2. K.P. Galbraith, "Pellet-to-Cladding Gap Closure from Pellet Cracking", XN-73-17, August 1973.

3. N. Fuhrman, V. Pasupathi, D.B. Scott, S.M. Temple, S.R. Pati and T.E. Hollowell, "Evaluation of Fuel Performance in Maine Yankee Core I, Task C", EPRI NP-218, November 1976.

4. T.B. Bailey and M.D. Freshley, "Internal Gas Pressure Behavior in Mixed-Oxide Fuel Rods During Irradiation", Nucl. Appl. Tech. 9, 233-241(1970).

5. R.M. Carroll, "Fission-Product Release from UO_2", Nucl. Safety 4, 35-42(1962).

6. P.E. MacDonald and L.B. Thompson, "MATPRO: Version 09, A Handbook of Materials Properties for Use in the Analysis of Light Water Reactor Fuel Rod Behavior", TREE-NUREG-1005, December 1976.

7. A.S. Bain, "Cracking and Bulk Movement in Irradiated Uranium Oxide Fuel Elements", AECL-1827, September 1963.

8. J.B. Ainscough and F. Rigby, "Measurements of Crack Sintering Rates in UO_2 Pellets", J. Nucl. Matl. 47, 246-250(1973).

9. J.T.A. Roberts and B.J. Wrona, "Crack Healing in UO_2", J. Am. Ceramic Soc. 56, 297-299(1973).

10. W.S. Lovejoy and S.K. Evans, "A Crack Healing Correlation Predicting Recovery of Fracture Strength in LMFBR Fuel", Trans. Am. Nucl. Soc. 23, 174-176(1976).

11. P.E. MacDonald and J.M. Broughton, "Cracked Pellet Gap Conductance Model: Comparison of FRAP-S Calculations with Measured Fuel Centerline Temperatures", CONF-750360-2, March 1975.

12. P.E. MacDonald and J. Weisman, "Effect of Pellet Cracking on Light Water Reactor Fuel Temperature", Nucl. Tech. 31, 357-366(1976).

13. Shippingport Atomic Power Station Preliminary Safety Analysis Report for Light Water Breeder Reactor, 1976.

14. O.R. Olander, "Fundamental Aspects of Nuclear Reactor Fuel Elements", p. 133, ERDA, 1976.

15. H.B. Meieran and E.L. Westermann, "Summary of Phase II of the EPRI LWR Fuel Rod Modeling Code Evaluations Project Using the CYGRO-3, LIFE-THERMAL-1 and FIGRO Computer Programs", ODAI-RP0397-2, RP-397-2, March 1976.

16. M.G. Andrews, H.R. Freeburn, and S.R. Pati, "Light Water Reactor Fuel Rod Modeling Code Evaluation, Phase II, Topical Report", CENPD-218, April 1976.

17. J.H. Keenan, F.G. Keyes, P.G. Hill and J.G. Moore, "Steam Tables, Thermodynamic Properties of Water Including Vapor, Liquid, and Solid Phases", John Wiley and Sons, New York, 1969.

18. M.M. El-Wakil, "Nuclear Heat Transport", p. 243, International Textbook Co., New York, 1971.

19. J.R. Lamarsh, "Introduction to Nuclear Engineering", p. 346, Addison-Wesley Publishing Co., 1975.

20. E.T. Laats, P.E. MacDonald and W.J. Quapp, "USNRC-OECD Halden Project Fuel Behavior Test Program: Experiment Data Report for Test Assemblies IFA-226 and IFA-239", ANCR-1270, December, 1975.